CULATION PROCEDURE FOR VISCOUS INCOMPRESS
BITRARY GEOMETRY AND STUDY OF CONFINED WA
PARTIALLY ENCLOSED BLUFF BODIES

By

ANIRUDDHA MUKHOPADHYAY

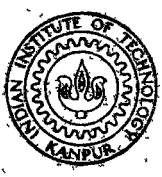

DEPARTMENT OF MECHANICAL ENGINEERIN

INDIAN INSTITUTE OF TECHNOLOGY

March, 1992

PART ALLY ENCLOSED BLUFF BOD ES

A Thesis Submitted
In Partial Fulfilment of the Requirements
for the Degree of

DOCTOR OF PHILOSOPHY

By

ANIRUDDHA MUKHOPADHYAY

to the

DEPARTMENT OF MECHANICAL ENGINEERING
INDIAN INSTITUTE OF TECHNOLOGY KANPU

March, 1992

C E R T I F I C A T E

It is certified that the work contained in the thesis entitled *A Calculation Procedure for Viscous Incompressible Flows in Arbitrary Geometry and Study of Confined Wakes Behind Partially Enclosed Bluff Bodies*, by Aniruddha Mukhopadhyay, has been carried out under our supervision and that this work has not been submitted elsewhere for a degree.

Gautam Biswas
(Dr. Gautam Biswas)
Deptt. of Mech. Engg.
Indian Institute of Technology
Kanpur - 208016, India

T. Sundararajan
(Dr. T. Sundararajan)
Deptt. of Mech. Engg.
Indian Institute of Technology
Kanpur - 208016, India

March, 1992

ACKNOWLEDGEMENTS

I wish to express a deep sense of gratitude to my advisors Dr. Gautam Biswas and Dr. T. Sundararajan for their guidance, support and alround consistent encouragement throughout the course of this research. I feel very fortunate to have the opportunity of getting them as my supervisors. I will always cherish my days of working with them as a potential learning experience and shall always remain obliged to their greatness in devoting such a large share of their valuable time and knowledge to help me complete my work. I would specially acknowledge the great favour of Dr. Biswas in providing me the extra computing facility with his HP9000/340 workstation and the plotter . This has really given me an edge over all odds of the common facilities in the institute.

I would greatfully recall the favour and encouragement I received from Dr. V.K. Garg ,formerly professor of IIT Kanpur during my initial days of this programme.

I would like to Thank my friends at IIT Kanpur especially Mr. Probodh Maji, Mr. Shankar Some, Mr Snehanshu Mandal and Mr. Prasanta Deb for proof reading and valuable suggestions time to time . I would also express my sincere thanks to Mr. B.M. Shukla and Mr. N.V.B. Rao for their cumulative help and support during the entire span of my stay at IIT Kanpur.

Thanks are also due to Mr. Shukla and Mr. Khuswaha for their prompt and efficient drafting work and to Mr. V. Shukla for his equally remarkable typing skill.

Last but not the least, I am extremely thankful to my wife Pamela for her monumental forbearence and perfect understanding during the entire course of this work. Without her cooperation, the present work would have been an impossibility.

(A. Mukhopadhyay)

C O N T E N T S

LIST OF FIGURES

LIST OF TABLES

NOMENCLATURE

A	Area of a control volume
B	Width of the square cylinder
C	a parameter, $Re_B . C_f$
C_f	skin friction coefficient, $2\mu(\partial u/\partial y)/(\rho U_{av}^2)$
C_L	Lift coefficient, $\mathscr{L}/(\frac{1}{2}\rho U_{av}^2 . A)$
D	Diameter of the round cylinder.
f	frequency of vortex shedding
H	channel height
J	jacobian of geometry transformation
ℓ	length of the control volume face
L	length of the channel
$\mathscr{L}$	lift force on the cylinder, $\Sigma \tilde{P}_1 \Delta x - \Sigma \tilde{P}_2 \Delta x$ on the cylinder
M	shape function for pressure variables
n_x, n_y	direction cosines of outward unit normal on control volume faces
N	shape functions for velocity variables
p	pressure
P	non-dimensional pressure, $p/(\rho U_{av}^2)$
$\tilde{P}$	pressure distribution on the cylinder surface
Re_B	Reynolds number based on the cylinder width, $U_{av} B / \nu$
Re_D	Reynolds number based on the cylinder diameter, $U_{av} B/\nu$
s	control volume side index
S	Strouhal number, $f B/U_{av}$
t	time
$\bar{t}$	dimensionless time, $t/(H/U_{av})$
T	time period of oscillation, $1/f$

u	axial component of velocity
U	dimensionless axial velocity u/U_{av}
v	normal component of velocity
V	dimensionless normal velocity. v/U_{av}
w	gauss-point weight for numerical integration
W	upwind-weighted shape function for convective terms
x	axial dimension of the coordinates
X	x/H
y	normal dimension of coordinates
Y	y/H

Greek letters :

α	upwinding factor
μ	dynamic viscosity of the fluid
ν	kinematic viscosity of the fluid
ρ	density of the fluid
ξ, η	coordinates in the computational space
ω	relaxation factor

Subscripts :

1	bottom surface of the obstacle
2	top surface of the obstacle
w	channel wall
av	average
m	mid-plane ($y_m = H / 2$)
n	time level
CS1	boundary of the continuity control volume
CS2	boundary of the momentum control volume
CV1	continuity control volume
CV2	momentum control volume

1 A General Introduction with Historical Perspective

1.1 Role of Computational Fluid Dynamics in Engineering Research

Computational Fluid Dynamics has attained a vital role in fluid mechanics research to the level of having its own standing based on analytical and experimental knowledge of the flow physics as well as the tools of numerical analysis. Analytical solutions, albeit being derived for simplified forms of governing equations, have the distinct advantage of immediately highlighting some of the fundamental features of the flow physics. However, real life situations are usually so complicated that analytical solutions are not available in most of the cases and experiments are too expensive. Due to the rapid growth of efficient and economic computing facilities as well as numerical modelling methods, the predictive procedures support experiments, enrich and even extend the range of analytical solutions and finally contribute actively to product development.

1.1.1 Applications of Computational Fluid Dynamics

Major applications of numerical simulation are related to aerospace research, combustion studies, nuclear reactor control, mechanics of reacting fluid flow, meteorological predictions etc. In these applications, the rapid decrease in the cost of

computations (with the advent of high speed modern-day computers) compared to the staggering cost of performing state of the art experiments, has made numerical simulation an economical alternative. Efficient numerical algorithms are being used and continuously upgraded to substitute rigorous experiments on wind tunnel testing or combustion research. However, the numerically predicted models may further need fine-tuning through final experimental tests. Besides economic advantage, numerical simulation has the potential to depict the detailed flow field information accurately. It can even monitor flow conditions involving fast transients, high temperatures, toxic substances etc., which pose considerable difficulties in experimental measurements.

1.1.2 Salient Features of Numerical Simulation Techniques

Modelling of real life phenomena starts with the basic conservation principles of physical quantities like mass, momentum, energy and species. These fundamental principles are often expressed in terms of algebraic, ordinary or partial differential, or even integral forms of equations. These governing equations along with appropriate boundary and/or initial conditions are mathematically reformatted into equivalent discrete representations of the problem by suitable spatial and/or temporal discretization techniques. The discretized equations are, in turn, solved by appropriate solution procedures. Finally, the numerical solutions thus obtained, are processed further to calculate

quantities of interest

It may be mentioned that the present wide-spread acceptance of the computational methods of simulation as an essential dimension to the studies on mechanics of fluids is the outcome of effective numerical predictions in a variety of applications. In all such studies accuracy of the numerical data largely depends on the correctness of the mathematical approximations in the modelling of the physical situation. This is especially true for turbulent flow predictions, combustion, modelling of reacting fluids, nuclear reactor studies etc. for which rigorous mathematical descriptions are not yet available. However, even for problems in which the mathematical model is well understood, dealing with irregular and complex geometries and selection of the final numerical solution scheme are as much important as the mathematical modelling. In all these cases, very many important and interesting phenomena are often revealed by numerical modelling.

1.2 Complexities Associated with Numerical Modelling of Fluid Flow Problems :

Incorporation of proper flow physics is a very crucial step in the numerical prediction process since the simulation by itself cannot reproduce physics that has not been duly considered. Physical complexities that are often encountered in many flow situations are compressibility, chaos and turbulence, fast

transients in the flow field etc These are usually taken care by suitable constitutive relations or modifications in the basic Navier Stokes and mass conservation equations. Often, heat and mass transfer also occur simultaneously in the flow situations. Many of these problems finally lead to a set of coupled partial differential equations which need to be solved simultaneously. However it is possible to decouple variables like enthalpy or temperature from the solution of the basic velocity and pressure fields in some situations.

While solution of a complicated real life problem can be handled by a set of add-on relations with the basic model of Navier Stokes equations, geometry of the flow domain necessarily requires careful treatment. An orthogonal coordinate frame and a matching set of orthogonal velocity components are always a perfect choice which provide clarity in the adaptation of any numerical scheme, in the solution procedure and during the final flow visualization. However, in real life problems, alignment of the flow variable layouts with respect to a fixed standard coordinate frame may not prevail. Also, the velocity/pressure boundary conditions may be available only at a set of points lying on an irregular boundary so that adoption of a standard coordinate frame turns out to be complicated and often impossible. Many approaches have been tried in the past to handle complex geometries, such as (i) rectangular, axisymmetric or polar coordinates with step wise approximation of curved boundaries (so

called castellated grids), (ii)usage of orthogonal curvilinear coordinate systems, (iii) development of general nonorthogonal body conforming coordinates etc. Each of these approaches has specific usefulness to the respective numerical scheme.

The selection of a numerical scheme for estimating the flow physics is a critical step. This is because of the fact that even the incompressible constant property viscous flows involve nonlinear partial differential equations. The situations are much more complicated in presence of any of the above mentioned physical or geometrical complexities. Aspects which require closer scrutiny in a numerical scheme for incompressible viscous flows are the proper accounting of the nonlinear convective kinematics and the pressure field evaluation. The convection kinematics needs incorporation of the upstream biased modelling, especially, for convection dominated flow situations. Also, in unsteady flows, excepting the explicit schemes, most of the others need iterative velocity evaluation because of nonlinear convection terms. However, getting an acceptable pressure field is a difficult task since there is no direct equation for evaluating pressure, in incompressible viscous flow. The non-zero divergence of an incorrect velocity field is often employed to adjust pressure field till cell wise incompressibility of the fluid is achieved in all cells. Different schemes have so far been developed to optimize this process of preserving incompressibility and simultaneously extracting pressure, corresponding to various flow

situations

1.3 Aim of the Present Work

In this thesis, the task of developing a general calculation procedure for viscous incompressible flows in complex geometries has been undertaken. It has been decided to solve the unsteady Navier Stokes equations for both orthogonal and non-orthogonal grids and follow a time marching procedure to reach a steady state (if the flow field is physically steady) or to reach a particular time level (if the flow field is unsteady periodic). The importance of continuity equation as a constraint on the velocity field has been deployed in solving the pressure field. Finally, the aim of the present thesis is to employ this algorithm for analyzing the wake-zone-aerodynamics behind partially enclosed bluff bodies.

1.4 Development of Computational Methods in Fluid Mechanics - A historical Perspective

1.4.1 Flow Formulations :

The solution of different forms of Navier Stokes equations has been the subject of research for the past three decades. Concurrent attempts have been successfully made with different sets of variables for describing these momentum balance equations.

Two dimensional analysis based on the application of stream function and vorticity variables, has the advantages of removing pressure from the set of solution variables and simultaneously satisfying continuity requirements. However, extension of such a stream function-vorticity approach to three dimensional flows is not possible. Primitive variable formulation involving velocity components and pressure, on the other hand, is used by comparatively a large number of researchers since this is directly extendable to three dimensional geometries. Such a formulation often meets the requirements of prescribed boundary conditions of application problems, in quite a straight forward manner.It may be mentioned that in finite element and other related approaches, the interpolation functions of the stream function and vorticity must have at least continuous first derivatives needing C1 class element. The primitive variable formulation, however, needs only C0 class element, although satisfying zero divergence of velocities over each element sometimes poses serious challenges.

1.4.2 Methods on Regular Geometries

As mentioned earlier, solution of Navier Stokes equations with primitive variables has two basic challenges namely, (i) absence of any obvious equation for solution of pressure and, (ii) the non-linearity of the convection kinematics. Also, the nature of the equation is such that the velocity and pressure solutions may exhibit non-physical oscillations (wiggles) if a collocated grid is used for finite difference formulation of all the variables.

However, this well known problem of 'red - black checker board splitting' of pressure is circumvented through either the implementation of a staggered grid arrangement or with the use of special interpolation techniques on collocated regular grids.

(i) Primitive Variable Based Solvers:

The full Navier Stokes equations in conservative form have been solved by finite difference based explicit transient algorithms such as MAC and SMAC by Harlow and Welch[1] and Harlow and Amsden[2] respectively. In these algorithms the provisional velocities at any instant of time, are first estimated from momentum equations using pressure and velocity values of the earlier time step. These estimated velocities, however, are yet to satisfy continuity requirements. If the cell wise divergence values of these estimated velocity fields are non-zero, then there must be some amount of mass accumulation or annihilation in each cell which is not physically possible. This indicates that the pressure field is incorrect. The non-zero divergence of velocity can be utilized to correct pressure and the velocities in turn, and a Poisson type pressure correction equation can be obtained. The procedures of MAC and SMAC differ in the implementations of this pressure velocity iteration to arrive at zero divergence. These methods use a layer of imaginary cells around the boundary of the physical domain necessitating update of boundary conditions after every change in internal velocity and pressure values. In a related technique of artificial compressibility method developed

by Chorin[3], simultaneous iteration on pressure and velocity components are performed to obtain a converged solution Viecelli[4] has shown the equivalence of all the above mentioned methods. Hirt and Cook[5] have developed a simplified explicit flow solver by making use of the aforesaid pressure-velocity iteration for a wide variety of problems involving three dimensional incompressible flows. While these explicit schemes are quite efficient in the studies of temporal flow development, they have stability restrictions on the time step values. Implicit methods are indeed attractive since they have no such restrictions regarding the choice of time steps. The finite volume method based SIMPLE algorithm of Patankar and Spalding[6] provides an efficient implicit procedure. Enhancement of this basic SIMPLE code has been made by Patankar himself through the version of SIMPLER[7,8] and by Vandoormaal and Raithby through SIMPLEC[9].In SIMPLER, at every iteration level or time step, a first estimate of velocity is obtained from the evaluation of the convection diffusion parts of the momentum equations. The remaining source terms and the pressure terms constitute a pressure equation. The pressure and velocity are iteratively corrected in much the same way as in SIMPLE. Although the changes necessary to incorporate SIMPLEC into a SIMPLE code are minor, the consequences can be great as SIMPLEC eliminates the approximations made in SIMPLE while deriving the pressure velocity corrections. Jang, Jetli and Acharya[10] reported a comparative illustration between the operator splitting

PISO[11] algorithm of Issa and the SIMPLE family of algorithms

(ii) Convection Diffusion Modelling :

Numerical modelling of the convection diffusion phenomena demands as much consideration as deriving a correct pressure solution. Most of the above algorithms and works are quite stable in this regard and have good convergence characteristics corresponding to their ranges of applications. Just as algorithms were generated aiming at proper solution of pressure, parallel developments occurred for the efficient handling of nonlinear convection terms in the flow equations. It is well known that numerical instabilities arise when the flow equations contain dominant first derivative terms. Initial convection discretization models were space-centred second order difference formulae. Instabilities with such formulations were characterized by oscillations (wiggles) in the velocity solutions. It was found that these wiggles could be eliminated by using one-sided (upwind) first order finite difference approximations for the derivatives in the convection terms. Solutions for intermediate Reynolds number flows using such upwind approximations have been published by several investigators[14,15,23]. However, based on detailed studies on the nature of these differencing schemes, Roache[16,17] and several others[18,19] have critisized the idea of introducing 'artificial viscosity' into the physical problem through upwind schemes. DeAllen et al [20], Spalding[21] Raithby et al[22] and others [23] have modified the upstream differencing concept to

blend its advantages with space centred differencing Patankar[7], in his hybrid scheme, has made use of different approximations including this first order differencing to closely follow the one dimensional analytical solution of steady state equation. Many successful usages of similar multiple approximations based on cell Reynolds numbers have been reported in literature [10-14,24-27]. Han et al [39] have used a hybrid differencing scheme in order to solve the flow problem in a lid-driven square cavity for a Reynolds number of $1x10^5$. In the context of high Reynolds number turbulent flows, the upwinding discretization schemes due to Leschziner and Rodi [40] are particularly notable. Roache[16] proved that the truncation error generated due to the use of first order accurate difference formula may become too large to be ignored. He gave a mathematical estimate of this error and showed that as compared to the second order accuracy of all other terms, this error may be fixed with the corresponding truncated term of the Taylor series interpolation of convection. The coefficient of the second derivative in the truncated convection interpolation formula has been identified to introduce a numerical diffusivity for the transported quantity. A similar truncation error arises out of backward first order time differencing in transient studies. As the steady state is approached, this error approaches zero. Restricting the Courant number less than unity, however, takes care of this problem. Raithby[28] has given a host of critical examples to emphasize the

applicability and limitation of first order upwinding Depending on the nature of the problem, several upstream-weighted formulations have been attempted in between. Skew upstream differencing[29] of Raithby, skewed positive influence coefficient upwind procedure of Schneider and Raw[30] , mass-flow-weighted skew upwind procedure due to Hassan et al [31] and the controlled numerical diffusion with internal feedback (CONDIF) scheme of Runchal [32] are a few important efforts in modelling of convection terms.

Another new concept which has been established by Galpin and Raithby[33] is the treatment of the non-linearities in the incompressible Navier Stokes equations by Newton-Raphson linearization . Higher order upstream differencing of convection terms had also been studied widely by Pollard and Siu[34], Davis and Mallinson[35], Leonard [36-38], Han et al [39], Leschziner and Rodi [40], Shyy [41] and Raithby et al [42]. The second order upwind schemes, especially QUICK of Leonard[38], and SUDS of Raithby[29] have received a lot of appreciation for their effective applicability and stability. Tao and Sparrow[43] and the series of communications from Patel et al [44-45] have discussed in detail about the performance characteristics of all the so far available upwind schemes. Vanka[46] has presented a comparison among the second order upwind schemes of Leonard (QUICK)[49], Wilkes and Thompson[47] and Atias et al[48]. Gresho and Lee have demonstrated that the optimal upwind difference scheme with an

effective grid Peclet number of hyperbolic tan function, is unconditionally stable Barrett[50] in his Super upwind scheme has given an estimate of distribution of transported perturbation on both sides of a point of original disturbance.

Zeinkiewicz and co-workers have successfully used upstream asymmetric basis functions[51] and modified function based upwind[52] in corresponding Finite Element formulations. Huyakorn, Taylor, Lee and Gresho[53] compared different mixed interpolation Finite Element methods for fluid flow problems. Sani et al[54] have conducted an exhaustive study on spurious pressure field generated in certain FEM analyses of fluid flow problems and also outlined other aspects of associated difficulties. A higher order convection model in FEM has been suggested by Donea and Giulliani[55]. Kato et al[56] reported to have solved three dimensional cavity flow for large Reynolds numbers using GSMAC FEM algorithm which they have considered optimum on the basis of computational load.

1.4.3 Methods on Complex Geometries :

Finite difference and finite volume based methods have been widely applied to problems in regular geometry whose boundaries fall on the coordinate lines of a simple orthogonal coordinate system. The orthogonality of the coordinate frame makes it possible to decouple the integrands so as to carry out individual line integration products for evaluating the surface integrals. Thus, many researchers have tried to generate orthogonal grids for

complex solution domains while more complex geometries are necessarily modelled with general non-orthogonal curvilinear grids.

(i) Orthogonal Grids:

Usually in engineering problems such regular orthogonal grids may be unsuitable or an analytic coordinate frame may not be available. In order to extend the aforesaid established flow solvers to the complex geometries, use of generalised orthogonal body-conforming coordinate systems have been made in different combinations. While the mathematical utility of such orthogonal grids in fluid mechanical problems is very attarctive, availability of a smooth grid is equally restrictive. Hung and Brown[57] developed an implicit MAC like two-dimensional scheme using grid-oriented orthogonal set of velocity components. However, their formulation was based on non-conservative form of equations. Pope[58] applied the conservative forms of the equations with finite volume method to compute turbulent recirculating flows in diffusers. Gosman and Rapley[59] used a similar procedure for fully developed flows in ducts of arbitrary cross-section. Turbulent flow calculations were done on such grids by Rapley[60], Habib and Whitelaw[61] and Rastogi[62]. Lawal and Majumdar[63] have performed calculations in the entrance region of an arbitrary shaped cross section. Assuming a parabolic flow, collocated cartesian velocity components on orthogonal grids in each cross-sectional plane have been solved along with a Poisson

equation for pressure

(ii) Non Orthogonal Grid

In non-orthogonal systems, general curvilinear coordinates are employed which exactly coincide with the boundaries of the physical domain. The interior also has smooth grids in terms of slope and curvature continuity. The governing partial differential equations are transformed in terms of these curvilinear coordinates and finite difference representations are derived in the transformed domain. Gal-chen and Somerville[64] and Faghri et al[65] used algebraic coordinate transformation. While Gal-chen used a MAC-like grid arrangement coinciding with the grid lines, Faghri et al had used covariant components of velocities. Thompson and coworkers [66,67] have made remarkable contributions to the development of numerical grid generation techniques for solving elliptic partial differential equations related to both external and internal flow problems. Steger and Sorenson [68,69] developed a computer code to solve Poisson equations with grid control near the boundary and with coarse-fine sequential solver. Vanka et al[23], Maliska and Raithby[70], and Shyy et al[71] have extended the available solvers of different flow problems to irregular geometries. The basic flow solvers have been based on the family of SIMPLE algorithms. The adaptive grid procedure of Acharya and Patankar [72] for parabolic flows may be mentioned here for its detailed discussion on the choice of different discretization schemes and their performance in the adaptive grid layout. A new

differencing scheme, the w-tracing scheme, had been suggested here which showed extremely good matching with the corresponding analytical curve. Patel and Briggs[73] used MAC in boundary fitted curvilinear coordinates. Karki and Patankar [74] used a generalised coordinate system with co-variant velocities for flows in complex geometry. In 1981, the first successful application of finite volume methods using non-orthogonal coordinates and collocated grids were reported by Hsu[75]. Concurrent works had also been reported by Prakash[76] and Rhie[77]. Disproving the impracticability of collocated arrangements, several other works had been regularly reported since then. A few of them are due to Rhie and Chow[78], Rhie et al[79], Peric[80], Burns et al[81] and Reggio and Camarero[82]. It may be worthwhile to note from Bernard and Thompson [83] that while staggered grid is a direct solution to avoid pressure split with conventional finite difference interpolations of flow variables, proper interpolation of velocities still remains crucial to avoid oscillatory velocity field even on a staggered grid. An appropriate pressure interpolation avoids pressure splits in these methods of collocated grids. Use of collocated velocity grids has the following obvious advantages (Peric et al[84]):

(a) all velocity variables share the same location implying only one set of velocity control volume;

(b) the convection contribution to the coefficient of the discretized equations is same for all the velocity variables;

(c) for complex geometries cartesian velocity components can be used in conjunction with non-orthogonal coordinates yielding simpler equations than when coordinate oriented velocity components are employed;

(d) there are fewer constraints on the numerical grid, since there is no need to evaluate the so called "curvature terms" , and

(e)treatment of boundary conditions and implementation of higher order differencing are simpler.

Further detailed discussion on these aspects are available in the studies of Hsu[75], Peric[80] and Miller and Schmidt[85]. A finite volume based procedure has been very successfully developed by Majumdar [86] using such collocated velocities and pressure. The concept of "momentum interpolation" of cell face pressures from nodal values has been established showing equivalence in the methods of staggered and collocated arrangements[87]. However, such momentum interpolation needs under relaxation between iterative levels of velocity pressure adjustments. Majumdar [88] has also clarified that a consistent under relaxation will enhance the rate of convergence and at the same time achieve a unique solution that is independent of the under relaxation parameter used.Williams[89] has applied a collocated primitive variable formulation on two dimensional cavity problem where he introduced an amount of intermediate compressibility into a projection scheme to obtain Helmholtz type expression for a pressure variable.

Solution of the Navier Stokes equations on irregular geometries

being the state of-the-art problem, Baliga and Patankar[90] opened a new dimension of the SIMPLER algorithm with the successful proposition of the control volume based finite element method(CVFEM). By discretizing the domain into six noded macro elements each of which consisted of four, three-noded triangular subelements, the discretized equations were obtained by deriving algebraic approximations to integral conservation equations applied to these polygonal control volumes. While pressure variables were stored only at the vertices of the macro elements, all others were stored at nodes of the subelements. Pressure interpolation was linear while other dependent variables were made sensitive to cell Peclet number and the direction of the velocity vectors. Prakash and Patankar[25, 26] used equal order interpolation for pressure and velocity for these CVFEM algorithms. Schneider and Raw[30] introduced special upstream biased convection diffusion model for CVFEM while Muir and Baliga [91] extended them to three dimensional applications. Considerable overall improvement has been reported by Prakash[24] by introducing special shape functions even for the source terms in the transport equations.

For flows in complex geometries, the finite element method appears to be an attractive alternative owing to its intrinsic geometrically additive properties. Application of this method to fluid dynamical problems had been started with Stokes flow. As mentioned earlier, preference is given to primitive variable

formulation over the vector potential (stream function)formulation because of algorithmic suitability. However, as far as concepts of variational calculus are adaptable to FEM, the rigorous theory of extremization subject to (differential) constraints is available only for linear elliptic boundary value problems concerning creeping flow situations. Oden[92], Olson[93], Baker[94] and Taylor and Hood[95] extended the finite element methods successfully to a variety of fluid flow problems. While in structural mechanics problems, the mass conservation is intrinsic because of the Lagrangian description, for flow problems it needs as much attention in FEM as in FDM. Zienkiewicz [96] proposed penalty function method for linear systems, viz., Stokes problem . It was later extended to two dimensional incompressible flows by Reddy[97]. Because of stability and convergence requirements, reduced integrations and corresponding variable layouts had been prescribed by Zienkiewicz et al[98] and Reddy[99]. Tuann and Olson [100] preferred solving the incompressible flow equations in primitive variables using continuity equation to generate the Poisson equation for pressure. However, modelling of convection kinematics remained unresolved until Christie et al [51] used asymmetric linear and quadratic basis functions to overcome the difficulty of significant first derivatives in a one dimensional two-point boundary problem. Heinrich and Zienkiewicz[52] extended this idea to two dimensional applications. A mixed interpolation coupled finite element solution algorithm of the velocity and

pressure for incompressible flow has been discussed in detail by Taylor and Hughes[101]. Comini and Del Guidice [102] have calculated provisional velocity values based on an estimated pressure distribution and momentum interpolation by making use of a Finite Element technique. They have obtained appropriate corrections to the provisional velocities through satisfying continuity requirements. Smith and Brebbia [103] described a method for the solution of transient, incompressible viscous flow in two dimensions. The dependent variables of stream function and vorticity, were approximated over each triangular element using linear interpolation functions. As an application, a study of the vortex street development behind a rectangular obstruction has been described.

In order to use velocity-pressure formulations in FEM, appropriate interpolation functions for velocity and pressure variables are needed. For error consistency reasons, the interpolating functions for pressure should be polynomials of lower degree than those for velocities. Usually, quadratic interpolating shape functions for velocities and linear shape functions for pressure are deployed. To date, two types of mixed-interpolation finite elements have been commonly used. These are eight noded serendipity and six-noded triangular elements. The first type of elements was recommended by Hood and Taylor [104] and the second type of elements are preferred by Kawahara et al. [105]. However, despite valuable contributions

from Baker[106,107], Zienkiewicz and Godbole[108], and Lohmeyer et al [109] finite element algorithms still have some unresolved difficulties such as lack of transportive property in the advective terms.

1.5 Scope and Objective of the Present Work :

Despite several stimulating developments as stated in the earlier sections, a satisfactory answer with regard to the question of computing incompressible flows in complex geometries is still not available. The common difficulties are, namely, derivation of the conservation principles for non-orthogonal control volumes, development of appropriate interpolation schemes and the enormity of book keeping involved with respect to both dependent and independent variables.

In the Present work, a novel algorithm (EXTRA-FLAG) for non-orthogonal geometries using primitive variables is proposed which resolves some of the above mentioned difficulties. Integral forms of conservation equations for finite control volumes in the domain are considered. These forms are particularly appealing because of the potential for using powerful numerical quadratures. Ideas such as element wise interpolation and transformation of non-orthogonal element geometry into a square master element which are commonly used in FEM, have been incorporated. Collocated and Coordinate oriented velocities are used. Pressure nodes are

staggered with respect to the velocity nodes

The proposed EXTRA-FLAG algorithm has been applied to several test problems to establish accuracy, stability and applicability. The problems are basically unsteady isothermal two dimensional incompressible flows in orthogonal and non-orthogonal geometries. The name of the algorithm has been chosen as EXTRA-FLAG which signifies EXplicit TRansient Algorithm for FLows in Arbitrary Geometry. The algorithm has been finally employed to analyze the structure of wakes behind partially enclosed bluff bodies.

Chapter-2

2. Description of the EXTRA-FLAG Algorithm :

This algorithm is based on integral mass and momentum balance applied over non-rectangular control volumes in general. The various steps involved in the algorithm are as follows. The integral flow equations are first converted into algebraic form through numerical quadrature, coupled with spatial interpolation of the velocity and pressure fields in terms of their nodal values. In order to facilitate numerical quadrature, each non-orthogonal (quadrilateral) control volume is mapped into a standard rectangular cell with the help of local curvilinear coordinates. Explicit time-marching is employed for the momentum equations using pressure field corresponding to the previous time level. The satisfaction of the continuity principle on the other hand, is enforced in an implicit fashion by iteratively correcting the velocity and pressure fields. Thus, the proposed algorithm combines the powerful features of interpolation and numerical quadrature used in Finite Element Method with the physical insight of the control-volume approach employed in MAC, SIMPLE and related algorithms. Due to the adoption of non-rectangular control volumes, the present method can be used for solving flow problems

in arbitrary-shaped geometries. The solution procedure (called EXTRA-FLAG because it is an EXplicit TRansient Algorithm for FLows in Arbitrary Geometry) is explained in detail in the following sections

2.1 Derivation of Governing Equations for a Control Volume :

For the illustration of the proposed algorithm, let us consider two-dimensional unsteady incompressible laminar flow inside an arbitrary shaped geometry. As shown in Fig.2.1, the domain is discretized into small curvilinear quadrilateral cells. The velocity nodes are located at the vertices and the pressure nodes are located at the centroids of these cells. In order to determine the values of the velocity and pressure variables , the momentum and continuity principles are applied over the corresponding control volumes which surround the velocity and the pressure nodes respectively. For instance , the continuity control volumes (CV1) are formed by grid lines connecting velocity nodes (Fig.2.2a) . Similarly momentum control volumes (CV2) are formed by curvilinear quadrilaterals whose vertices are pressure nodes (Fig.2.2b) . It is worthwhile to note that in the present algorithm, the velocity components are collocated at a velocity node so that the same momentum control volume can be employed for both x- and y-momentum equations.

Considering a typical control volume for mass continuity, CV1 ,

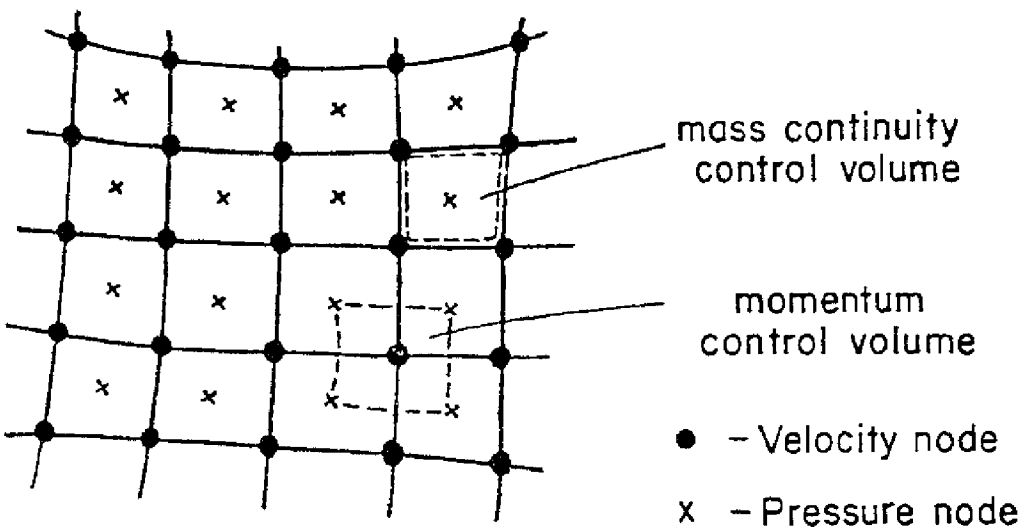

2.1 Schematic representation of grid discretizatio

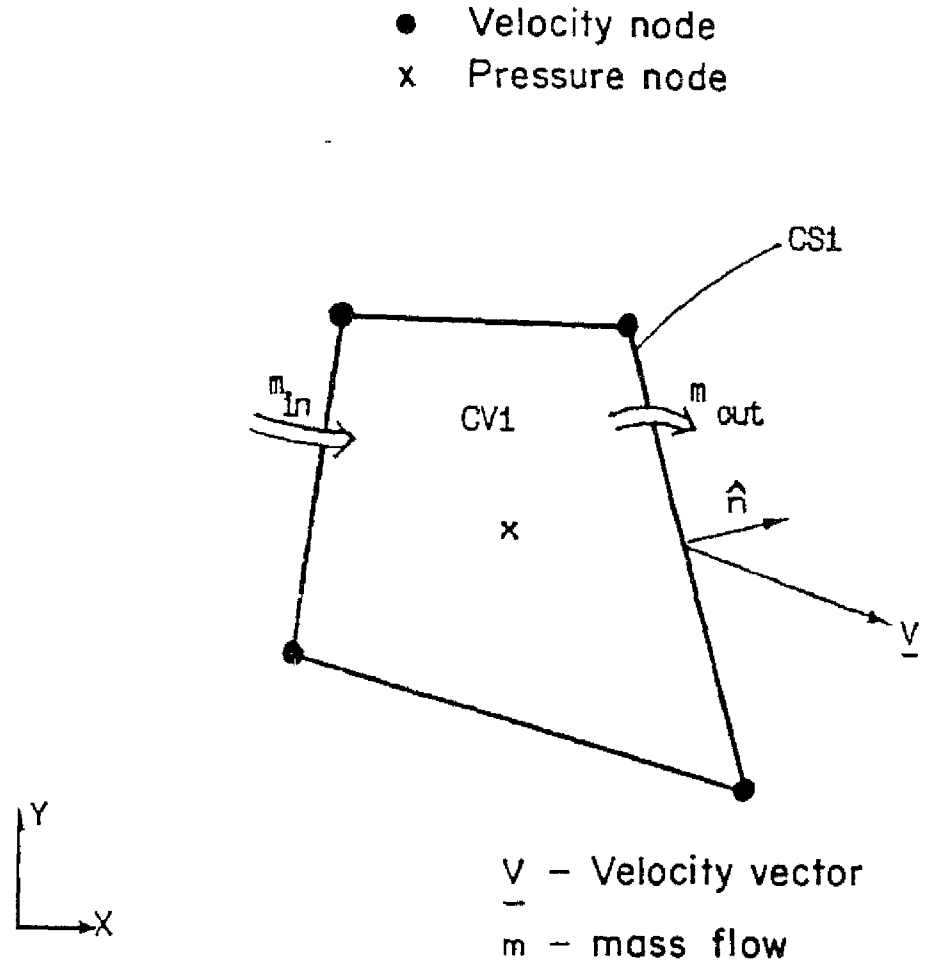

a Mass balance over continuity cell (CVI

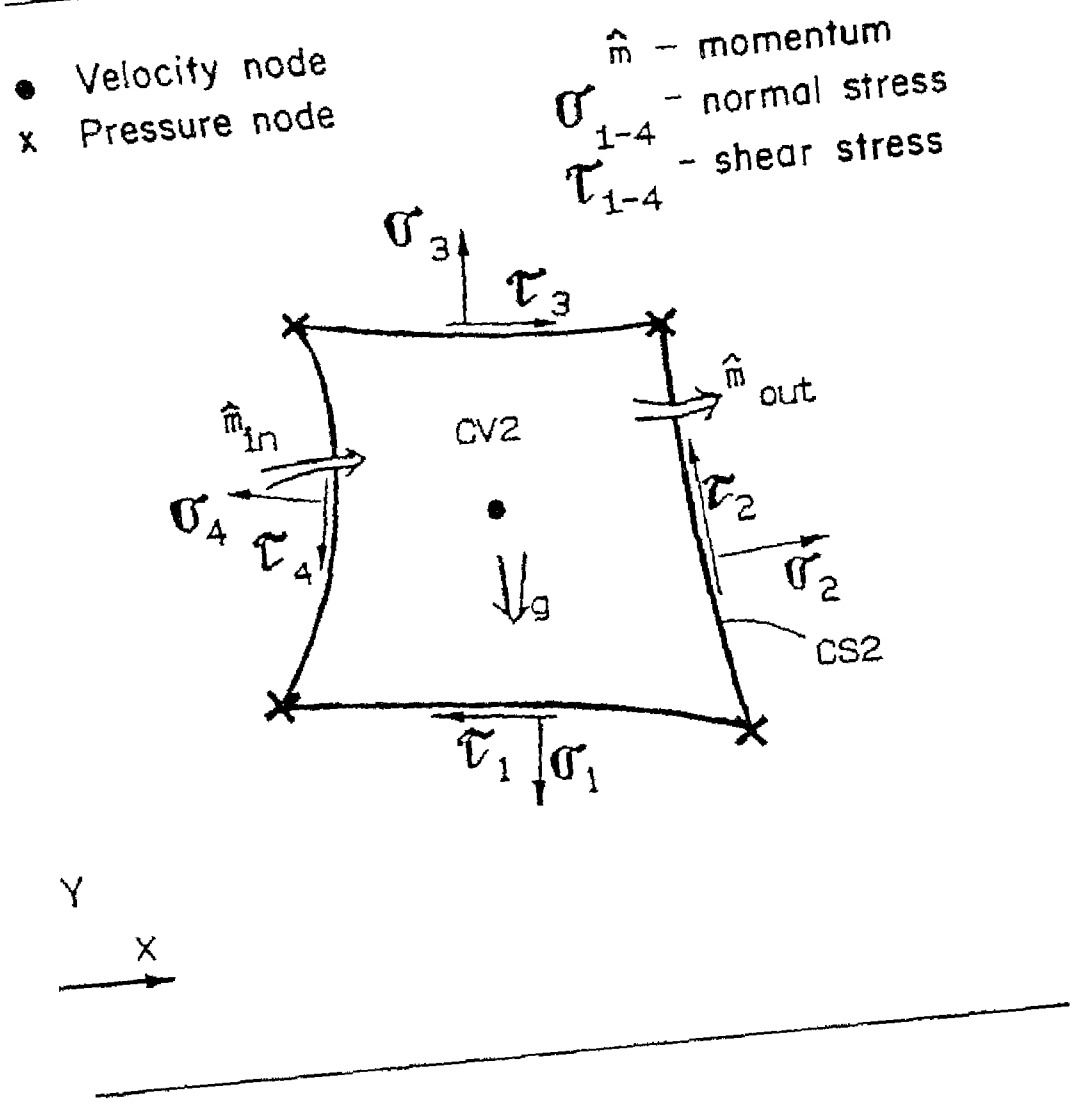

g.2.2b Momentum balance over momentum cel

the integral form of the mass balance equation can be written as

$$\frac{\partial}{\partial t}\iint_{Cv1} \rho dA + \int_{Cs1} \rho \underline{V} \cdot \hat{n}\, d\ell = 0 \qquad (2.1)$$

where $d\ell$ is an elemental length on the boundary (CS1) of the control volume and $\hat{n}$ is the local outward unit normal vector. For incompressible flow, the first term of equation (2.1) is identically zero. Therefore, the equation can be simplified as

$$\oint_{CV1} \underline{V} \cdot \hat{n} d\ell = \oint_{CS1} (u\, n_x + v\, n_y)\, d\ell = 0 \qquad (2.2)$$

where n_x and n_y are the direction cosines of the outward normal $\hat{n}$ on the boundary CS1.

Now considering a typical momentum control volume CV2 , the integral form of x- and y- momentum balance equations can be written as

$$\frac{\partial}{\partial t}\iint_{CV2} u(\rho\, dA) + \oint_{CS2} u(\rho\, \underline{V} \cdot \hat{n}\, d\ell) = F_X \qquad (2.3a)$$

and

$$\frac{\partial}{\partial t}\iint_{CV2} v(\rho\, dA) + \oint_{CS2} v(\rho\, \underline{V} \cdot \hat{n}\, d\ell) = F_Y \qquad (2.3b)$$

In the above equations , $F_X$and F_Y are the components of the resultant forces acting on the control volume in x- and y- directions respectively. These can be evaluated as follows :

$$F_X = \hat{i} \cdot \oint_{CS2} \underline{\underline{\sigma}} \cdot \hat{n}\, d\ell + \hat{i} \cdot \iint_{CV2} \rho\, \underline{g}\, dA$$

$$= \hat{i} \cdot \oint_{CS2} \left\{ -p\underline{\underline{I}} + \mu \left(\underline{\nabla}\,\underline{V} + \underline{\nabla}\,\underline{V}^T \right) - \frac{2}{3}\mu \left(\underline{\nabla}.\underline{V} \right) \underline{\underline{I}} \right\} \cdot \hat{n}\, d\ell$$

$$+ \iiint_{CV2} \rho\, g_x\, dA \qquad (2.4)$$

where $\underline{\underline{\sigma}}$ is the stress and $\underline{g}$ is the acceleration due to gravity. For incompressible flow ,

$$F_x = \oint_{CS2} \left\{ -p\, n_x + 2\mu \frac{\partial u}{\partial x} n_x + \mu \left(\frac{\partial u}{\partial y} + \frac{\partial v}{\partial x} \right) n_y \right\} d\ell +$$

$$+ \iiint_{CV2} \rho\, g_x\, dA \qquad (2.5)$$

similarly,

$$F_y = \hat{j} \cdot \oint_{CS2} \underline{\underline{\sigma}} \cdot \hat{n}\, d\ell + \hat{j} \cdot \iiint_{CV2} \rho\, \underline{g}\, dA$$

$$= \oint_{CS2} \left\{ -p\, n_y + 2\mu \frac{\partial v}{\partial y} n_y + \left(\frac{\partial u}{\partial y} + \frac{\partial v}{\partial x} \right) n_x \right\} d\ell +$$

$$+ \iiint_{CV2} \rho\, g_y\, dA \qquad (2.6)$$

For incompressible flow, the body force contribution in equations (2.5) and (2.6) can be absorbed into the corresponding pressure term. The final expressions for the x and y momentum equations in integral form are :

$$\text{x mom} : \quad \rho \left\{ \frac{\partial}{\partial t} \iiint_{CV2} u\, dA + \oint_{CS2} u\, (u\, n_x + v\, n_y)\, d\ell \right\} =$$

$$\oint_{CS2} \left\{ - p\, n_x + 2\,\mu \frac{\partial u}{\partial x}\, n_x + \mu \left(\frac{\partial u}{\partial y} + \frac{\partial v}{\partial x} \right) n_y \right\} d\ell \qquad (2.7)$$

$$\text{y mom} : \quad \rho \left\{ \frac{\partial}{\partial t} \iint_{CV2} v\, dA + \oint_{CS2} v\, (u\, n_x + v\, n_y)\, d\ell \right\} =$$

$$\oint_{CS2} \left\{ - p\, n_y + 2\,\mu \frac{\partial v}{\partial y}\, n_y + \mu \left(\frac{\partial u}{\partial y} + \frac{\partial v}{\partial x} \right) n_x \right\} d\ell \qquad (2.8)$$

For evaluation of the area and line integrals occurring in the above expressions , it is necessary to define interpolation scheme for the variation of each flow variable over the concerned control volume or control surface. Also, suitable numerical quadratures are to be employed to perform integration over curvilinear areas and lines. These aspects are described in detail in the ensuing sections.

2.2 Interpolation of Flow Variables Within Respective Control Volumes :

Since the order of the momentum equations is higher than that of the continuity equation , the velocity variables have been interpolated using bi-quadratic functions while applying the momentum balance principle ; on the other hand , for the satisfaction of continuity , bilinear interpolation functions have been used to describe the velocity variables over the respective control volume. Mathematically these interpolation schemes can be written as follows.

For the continuity equation :

$$u = \sum_{k=1}^{4} M_k \, u_k \quad ; \quad v = \sum_{k=1}^{4} M_k \, v_k \tag{2.9}$$

and for momentum equations (2.7) and (2.8) :

$$u = \sum_{k=1}^{8} N_k \, u_k \quad ; \quad v = \sum_{k=1}^{8} N_k \, v_k \tag{2.10}$$

The summation in equation (2.9) is performed by making use of the velocities at four vertices of the continuity cell (Fig.2.2a). Similarly the summation in equation (2.10) is accomplished on all the neighboring velocity nodes surrounding the momentum control volume boundary , as shown in Fig.2.3. Also M_k, N_k are respectively bi-linear and bi-quadratic interpolation functions. The expression for these functions are presented in the next section.

The variation of pressure over the momentum control volume is also expressed in the form :

$$p = \sum_{k=1}^{4} M_k \, p_k \tag{2.11}$$

It should be noted , however , that the above-discussed interpolation schemes for the flow variables are based on intuitive reasoning ; alternative schemes are definitely possible which may provide superior handling of specific terms in the flow equations for particular applications. The proposed algorithm is

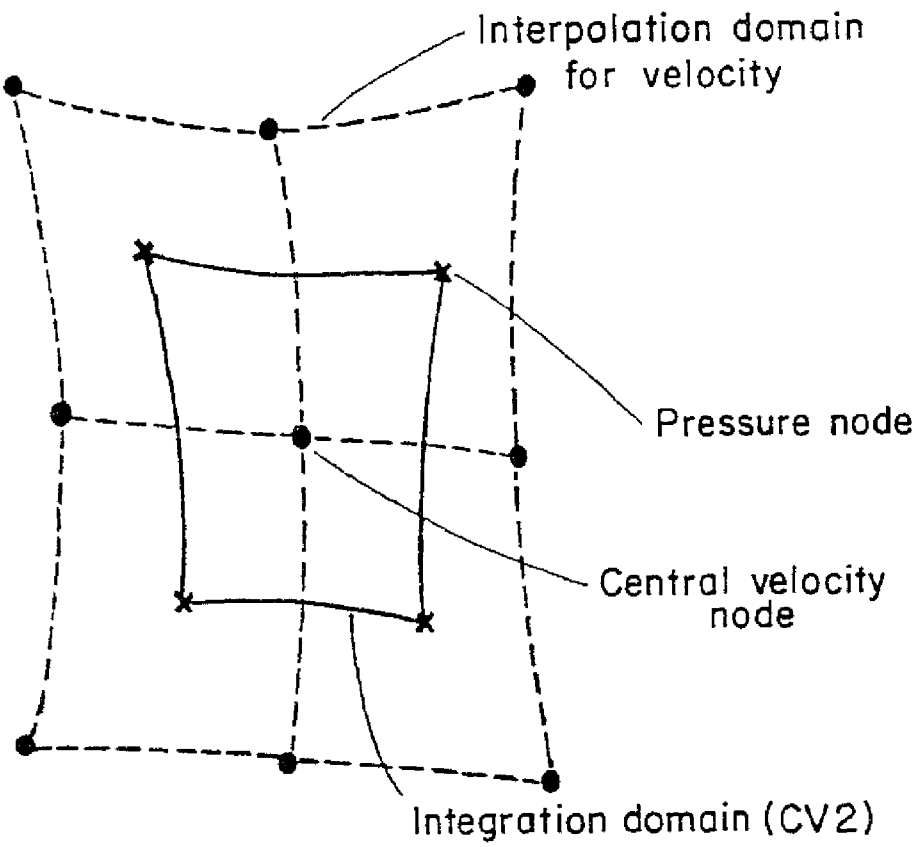

Fig.2.3 Interpolation domain for momentum bal

general in the sense that any such interpolation scheme can be suitably incorporated.

As regards the transient terms in the momentum equations , the lumping concept has been employed for the sake of simplicity and this is easily achieved by setting

$$\rho \frac{\partial}{\partial t} \iint_{CV2} u \, dA = \rho A_{CV2} \dot{u}$$

$$\rho \frac{\partial}{\partial t} \iint_{CV2} v \, dA = \rho A_{CV2} \dot{v} \qquad (2.12)$$

where A_{CV2} is the area of the control volume CV2 and $\dot{u}$, $\dot{v}$ are the time derivatives of the velocity components at the central node of the control volume , CV2.

2.3 Numerical Evaluation of the Area and Line Integrals :

The integrals appearing in equations (2.7) and (2.8) have been evaluated using Gauss-Legendre quadrature , since they are very complex to evaluate analytically . The first step required for the application of such numerical quadratures is the mapping of the non-orthogonal control volume into a master square cell whose coordinates vary from (-1) to (+1) in both the directions (Fig. 2.4). The mapping of the control volume itself can be achieved through what is known as the isoparametric transformation. In this transformation , the coordinates x and y for any point within the non-orthogonal control volume are interpolated in terms of their

1 , 2 _ 9 - Node numbers

①.②_④ - Side numbers

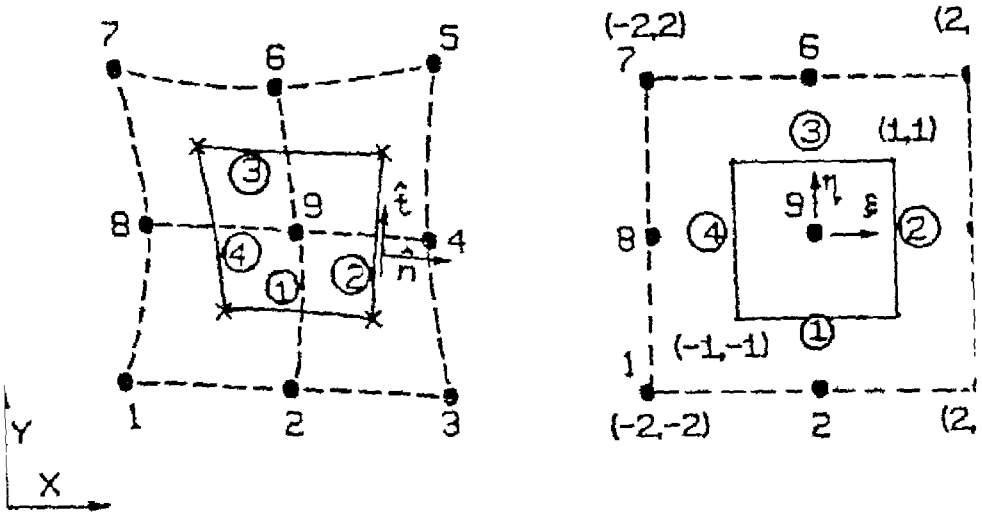

Physical domain Computational doma

ig.2.4 Transformation of a curvilinear contr into a square computational cell.

nodal values in much the same way as the flow variables . When quadratic interpolation functions are used , quadratic curves in the physical domain will be mapped as straight lines in the transformed domain. Therefore a curvilinear control volume bound by quadratic curves will be exactly mapped onto a square computational cell as shown in Fig.2.4. The interpolation scheme for the coordinates of a momentum control volume (CV2) are given by :

$$x = \sum_{k=1}^{8} N_k \, x_k \quad ; \quad y = \sum_{k=1}^{8} N_k \, y_k \tag{2.13}$$

where (x_k , y_k) are the coordinates of the nodes surrounding the control volume as shown in Fig.2.3. For transforming the continuity cells (CV1), linear interpolation is used in the form :

$$x = \sum_{k=1}^{4} M_k \, x_k \quad ; \quad y = \sum_{k=1}^{4} M_k \, y_k \tag{2.14}$$

Equation (2.14) implies that the continuity control volumes are quadrilaterals made up of straight boundaries. Such linear interpolation of coordinates is adequate since velocity components are also interpolated by linear functions for the satisfaction of the continuity principle. The coordinate transformation is isoparametric in this case as well .

The standard square cell in the above-mentioned transformations is represented in terms of local coordinates ξ and η . The range of variation of these coordinates over the cell boundary is from

(-1) to (+1) . Thus , after isoparametric transformation , the limits of all the integrals can be conveniently set as (-1) to (+1). The interpolation functions N_k and M_k are also neatly expressible in terms of the local coordinates ξ and η . These are given by :

$$N_1 = \frac{1}{64}\,\xi\,\eta\,(\xi-2)(\eta-2) \quad ; \quad N_2 = \frac{1}{32}\,\eta\,(4-\xi^2)(\eta-2);$$

$$N_3 = \frac{1}{64}\,\xi\,\eta\,(\xi+2)(\eta-2) \quad ; \quad N_4 = \frac{1}{32}\,\xi\,(\xi+2)(4-\eta^2);$$

$$N_5 = \frac{1}{64}\,\xi\,\eta\,(\xi+2)(\eta+2) \quad ; \quad N_6 = \frac{1}{32}\,\eta\,(4-\xi^2)(\eta+2);$$

$$N_7 = \frac{1}{64}\,\xi\,\eta\,(\xi-2)(\eta+2) \quad ; \quad N_8 = \frac{1}{32}\,\xi\,(\xi-2)(4-\eta^2); \qquad (2.15)$$

$$N_9 = \frac{1}{16}\,(4-\xi^2)(4-\eta^2)$$

and

$$M_1 = \frac{1}{4}\,(1-\xi)(1-\eta) \quad ; \quad M_2 = \frac{1}{4}\,(1+\xi)(1-\eta) \quad ;$$

$$M_3 = \frac{1}{4}\,(1+\xi)(1+\eta) \quad ; \quad M_4 = \frac{1}{4}\,(1-\xi)(1+\eta) \quad .$$

For the completion of the transformation process , it is necessary to convert the arc lengths , areas , surface integrals , derivatives and integrals in the physical coordinate system in terms of the computational coordinates ξ and η. Such conversions for the momentum control volume (CV2) will now be illustrated . Applying the chain rule , the relationships between lengths can be obtained as $x \equiv X(\xi,\eta)$, $y \equiv Y(\xi,\eta)$

$$dx = \frac{\partial x}{\partial \xi}\,d\xi + \frac{\partial X}{\partial \eta} \; ; \; dy = \frac{\partial Y}{\partial \xi}d\xi + \frac{\partial Y}{\partial \eta}\,d\eta$$

or

$$\begin{bmatrix} \frac{\partial x}{\partial \xi} & \frac{\partial x}{\partial \eta} \\ \frac{\partial y}{\partial \xi} & \frac{\partial y}{\partial \eta} \end{bmatrix} \begin{bmatrix} d\xi \\ d\eta \end{bmatrix} = \begin{bmatrix} \sum_{k=1}^{a} \frac{\partial N_k}{\partial \xi} x_k & \sum_{k=1}^{a} \frac{\partial N_k}{\partial \eta} x_k \\ \sum_{k=1}^{a} \frac{\partial N_k}{\partial \xi} y_k & \sum_{k=1}^{a} \frac{\partial N_k}{\partial \eta} y_k \end{bmatrix} \begin{bmatrix} d\xi \\ d\eta \end{bmatrix}$$

lar fashion , the derivatives can be obtained

$$\begin{bmatrix} \frac{\partial x}{\partial \xi} & \frac{\partial y}{\partial \xi} \\ \frac{\partial x}{\partial \eta} & \frac{\partial y}{\partial \eta} \end{bmatrix} \begin{bmatrix} \frac{\partial}{\partial x} \\ \frac{\partial}{\partial y} \end{bmatrix} = \begin{bmatrix} J \end{bmatrix} \begin{bmatrix} \frac{\partial}{\partial x} \\ \frac{\partial}{\partial y} \end{bmatrix}$$

J] is the Jacobian matrix for the transformat

be evaluated using equations (2.13) and (2.15

given above. From equation (2.17), the

can be estimated as :

$$\begin{bmatrix} J \end{bmatrix}^{-1} \begin{bmatrix} \frac{\partial u}{\partial \xi} \\ \frac{\partial u}{\partial \eta} \end{bmatrix} = \begin{bmatrix} J \end{bmatrix}^{-1} \begin{bmatrix} \frac{\partial N1}{\partial \xi} & \frac{\partial N2}{\partial \xi} & \cdots & \frac{\partial N9}{\partial \xi} \\ \frac{\partial N1}{\partial \eta} & \frac{\partial N2}{\partial \eta} & \cdots & \frac{\partial N9}{\partial \eta} \end{bmatrix} \begin{bmatrix} u_1 \\ u_2 \\ \vdots \\ u_9 \end{bmatrix}$$

tives of the interpolation functions appe

.18) can be evaluated using equation (2.15

$\frac{\partial v}{\partial x}$ and $\frac{\partial v}{\partial y}$ can also be evaluated similar

the u- velocity array of equation (2.18

ng v- velocity array .

ction cosines of the local unit normal vector

lengths along each boundary are evaluated

procedure . On the Sth side (s = 1,2,3,

length vector $d\underline{\ell}_s$ at a particular location

written as :

$$d\underline{\ell}_s = dx_s\,\hat{i} + dy_s\,\hat{j} = \left\{ \left(\frac{\partial x}{\partial \xi} \right)_s d\xi + \left(\frac{\partial x}{\partial \eta} \right)_s d\eta \right\} \hat{i} + \left\{ \left(\frac{\partial y}{\partial \xi} \right)_s d\xi + \left(\frac{\partial y}{\partial \eta} \right)_s d\eta \right\} \hat{j} \qquad (2.19)$$

But , for the faces 1 and 3 , η = constant and for the faces 2 and 4 , ξ = constant (see Fig.2.4) . Also , on sides 3 and 4 , the elemental length vector is in the direction opposite to the increasing ξ or η respectively , when an anti-clockwise sense of integration is adopted for all the cyclic boundary integrals. In order to be consistent with the anticlockwise sense of integration, the outward normals at the cell face are considered as positive.

Using the above conditions in equation (2.19) , it can be shown that

$$\hat{t}_1 = \frac{\left(\frac{\partial x}{\partial \xi}\right)_1 \hat{i} + \left(\frac{\partial y}{\partial \xi}\right)_1 \hat{j}}{\left(\frac{\partial \ell}{\partial \xi}\right)_1} \quad ; \quad \hat{n}_1 = \frac{\left(\frac{\partial y}{\partial \xi}\right)_1 \hat{i} - \left(\frac{\partial x}{\partial \xi}\right)_1 \hat{j}}{\left(\frac{\partial \ell}{\partial \xi}\right)_1}$$

$$\hat{t}_2 = \frac{\left(\frac{\partial x}{\partial \eta}\right)_2 \hat{i} + \left(\frac{\partial y}{\partial \eta}\right)_2 \hat{j}}{\left(\frac{\partial \ell}{\partial \eta}\right)_2} \quad ; \quad \hat{n}_2 = \frac{\left(\frac{\partial y}{\partial \eta}\right)_2 \hat{i} - \left(\frac{\partial x}{\partial \eta}\right)_2 \hat{j}}{\left(\frac{\partial \ell}{\partial \eta}\right)_2}$$

$$\hat{t}_3 = \frac{-\left(\frac{\partial x}{\partial \xi}\right)_3 \hat{i} - \left(\frac{\partial y}{\partial \xi}\right)_3 \hat{j}}{\left(\frac{\partial \ell}{\partial \xi}\right)_3} \quad ; \quad \hat{n}_3 = \frac{-\left(\frac{\partial y}{\partial \xi}\right)_3 \hat{i} + \left(\frac{\partial x}{\partial \xi}\right)_3 \hat{j}}{\left(\frac{\partial \ell}{\partial \xi}\right)_3}$$

$$\hat{t}_4 = \frac{-\left(\frac{\partial x}{\partial \eta}\right)_4 \hat{i} - \left(\frac{\partial y}{\partial \eta}\right)_4 \hat{j}}{\left(\frac{\partial \ell}{\partial \eta}\right)_4} \quad ; \quad \hat{n}_4 = \frac{-\left(\frac{\partial y}{\partial \eta}\right)_4 \hat{i} + \left(\frac{\partial x}{\partial \eta}\right)_4 \hat{j}}{\left(\frac{\partial \ell}{\partial \eta}\right)_4}$$

where $\hat{t}_s$, $\hat{n}_s$ ($s = 1,2,3,4$) are respectively the local unit tangential vector and the unit outward normal vector on the sth side . Also , the denominators of the above expressions can be calculated as

$$\left.\begin{aligned} \left(\frac{d\ell}{d\xi}\right)_s &= \sqrt{\left(\frac{\partial x}{\partial \xi}\right)_s^2 + \left(\frac{\partial y}{\partial \xi}\right)_s^2} \\ \left(\frac{d\ell}{d\eta}\right)_s &= \sqrt{\left(\frac{\partial x}{\partial \eta}\right)_s^2 + \left(\frac{\partial y}{\partial \eta}\right)_s^2} \end{aligned}\right\} \qquad (2.20)$$

The elemental length , $d\ell$, along each side can be represented as :

$$\left.\begin{aligned} d\ell_s &= \left(\frac{\partial \ell}{\partial \xi}\right)_s d\xi \quad , \quad \text{for} \quad s = 1 \text{ and } 3 \ ; \\ d\ell_s &= \left(\frac{\partial \ell}{\partial \eta}\right)_s d\eta \quad , \quad \text{for} \quad s = 2 \text{ and } 4 \ ; \end{aligned}\right\} \qquad (2.21)$$

Lastly , the elemental area , dA, appearing in the transient terms of the equation (2.7) and (2.8) can be expressed as :

$$dA = | J | \, d\xi \, d\eta \qquad (2.22)$$

where the $| J |$ is the determinant of the Jacobian matrix [J]

defined in equation (2.17) . Now all the integrals appearing in equations (2.7) and (2.8) can be rewritten in terms of the transformed coordinates ξ and η . The Gauss-Legendre quadrature can be easily adopted for evaluating these integrals since the limits are (-1) to (+1). The quadrature formula for the area integrals is given by

$$\int_{-1}^{+1}\int_{-1}^{+1} F(\xi,\eta)\, d\xi\, d\eta = \sum_{k=1}^{m}\sum_{l=1}^{m} F(\xi_k,\eta_l)\, w_k\, w_l \qquad (2.23)$$

where (ξ_k,η_l) are the Gauss sampling points and w_k , w_l are the corresponding weights . The coordinates of the sampling points (known as Gauss points) are the zeros of the m th degree Legendre polynomials , where m is the total number of Gauss points used in a particular direction. The line integrals can be similarly evaluated as :

$$\int_{-1}^{+1} F(\xi)\, d\xi = \sum_{k=1}^{m} F(\xi_k)\, w_k \quad \text{and} \quad \int_{-1}^{+1} F(\eta)\, d\eta = \sum_{l=1}^{m} F(\eta_l)\, w_l \qquad (2.24)$$

In the present work , 3- point quadrature has been employed for evaluating the momentum equations . The corresponding Gauss point coordinates and weights are provided in Table 2.1 .

Gauss Point Location and Weights for 3-point G

Gauss point	Co-ordinate location (ξ or η)	Weight
1	$-\sqrt{0.6}$	0.5555555556
2	0.0	0.8888888889
3	$-\sqrt{0.6}$	0.5555555556

the application of the above quadrature formul

u , v and p , their x- and y- derivative

cosines n_x , n_y of the local outward

t of jacobian $|J|$, elemental length $d\ell$

area dA are evaluated at each Gauss point

boundary or control volume and all such Gau

ons are summed up according to equations (2

Eventually , matrix equations are obtained

olume which represent the x- and y- momentu

. The solution of the equations is describe

on . For the continuity equation (2.2) , i

to employ the numerical quadrature since the

simpler and the velocity interpolation is lin

tion of the continuity equation is also discuss

section.

x Equations for Momentum and Mass Balance :

The final discretized momentum equations in matrix form are :

$$\underset{2\times1}{\begin{Bmatrix} \dot{u} \\ \dot{v} \end{Bmatrix}} = \underset{2\times18}{\left[[C] + [D] \right]} \underset{18\times1}{\begin{Bmatrix} (u) \\ (v) \end{Bmatrix}_{CV2}} + \underset{2\times4}{[\ S\ ]} \underset{4\times1}{\{\ p\ \}_{CV2}} \qquad (2.25)$$

The convective coefficient matrix in the momentum equations can be expressed as :

$$\underset{2\times18}{[\ C\ ]} = \left[\begin{array}{c|c} \underset{1\times9}{(C1_j)} & \underset{1\times9}{0} \\ \hline 0 & (C2_j) \end{array}\right] \qquad (2.26a)$$

where

$$\underset{1\times9}{(C1_j)} = \underset{1\times9}{(C2_j)} = \oint \frac{1}{\rho\, A_{CV2}} N_j \left(u\, n_x + v\, n_y \right) d\ell \qquad (2.26b)$$

Applying Gauss-Legendre quadrature ,

$$(C1_j) = (C2_j) = \frac{1}{\rho A_{CV2}} \sum_{s=1}^{4} \sum_{k=1}^{3} \left[N_j \sum_{q=1}^{9} (u_q\, n_x + v_q\, n_y)\, N_q \right] w_k\, \Delta\ell_s \qquad \ldots\ldots\ldots (2.26c)$$

where $A_{CV2} = \sum_{l=1}^{3} \sum_{k=1}^{3} |\ J\ |\ w_k\ w_l$

The diffusion matrix can be expressed as follows

$$\underset{2\times18}{[\ D\ ]} = \left[\begin{array}{c|c} \underset{1\times9\ \text{each}}{(DU_{1j})} & (DV_{1j}) \\ \hline (DU_{2j}) & (DV_{2j}) \end{array}\right] \qquad (2.27a)$$

where

$$
\left.
\begin{aligned}
(DU_{1j}) &= \frac{1}{\rho A_{cv2}} \oint_{cs2} \left[2\,\mu \frac{\partial N_j}{\partial x} n_x + \mu \frac{\partial N_j}{\partial y} n_y \right] d\ell \\
(DV_{1j}) &= \frac{1}{\rho A_{cv2}} \oint_{cs2} \left[\mu \frac{\partial N_j}{\partial x} n_y \right] d\ell \\
(DU_{2j}) &= \frac{1}{\rho A_{cv2}} \oint_{cs2} \left[\mu \frac{\partial N_j}{\partial y} n_x \right] d\ell \\
(DV_{2j}) &= \frac{1}{\rho A_{cv2}} \oint_{cs2} \left[\mu \frac{\partial N_j}{\partial x} n_x + 2\,\mu \frac{\partial N_j}{\partial y} n_y \right] d\ell
\end{aligned}
\right\} \quad (2.
$$

Applying Gauss-Legendre quadrature ,

$$
(DU_{1j}) = \frac{1}{\rho A_{cv2}} \sum_{s=1}^{4} \sum_{k=1}^{3} \left[2\,\mu\, n_x \frac{\partial N_j}{\partial x} + \mu\, n_y \frac{\partial N_j}{\partial y} \right]_{k,s} w_k\, \Delta\ell_s
$$

$$
(DV_{1j}) = \frac{1}{\rho A_{cv2}} \sum_{s=1}^{4} \sum_{k=1}^{3} \left[\mu\, n_y \frac{\partial N_j}{\partial x} \right]_{k,s} w_k\, \Delta\ell_s
$$

$$
(DU_{2j}) = \frac{1}{\rho A_{cv2}} \sum_{s=1}^{4} \sum_{k=1}^{3} \left[\mu\, n_x \frac{\partial N_j}{\partial y} \right]_{k,s} w_k\, \Delta\ell_s
$$

$$
(DV_{2j}) = \frac{1}{\rho A_{cv2}} \sum_{s=1}^{4} \sum_{k=1}^{3} \left[\mu\, n_x \frac{\partial N_j}{\partial x} + 2\,\mu\, n_y \frac{\partial N_j}{\partial y} \right]_{k,s} w_k\, \Delta\ell_s .
$$

The pressure matrix also can be expressed in a similar way :

$$\underset{2 \times 4}{[\ S\ ]} = \underset{1 \times 4 \text{ each}}{\begin{bmatrix} (S_{1j}) \\ (S_{2j}) \end{bmatrix}} \qquad (2.28a)$$

where

$$\left.\begin{aligned} (S_{1j}) &= -\frac{1}{\rho A_{CV2}} \oint_{CS2} M_j\, n_x\, d\ell \\ (S_{2j}) &= -\frac{1}{\rho A_{CV2}} \oint_{CS2} M_j\, n_y\, d\ell \end{aligned}\right\} \qquad (2.28b)$$

Applying Gauss-Legendre quadrature ,

$$\left.\begin{aligned} (S_{1j}) &= -\frac{1}{\rho A_{CV2}} \left[\sum_{s=1}^{4} \sum_{k=1}^{3} (M_j\, n_x)_{k,s}\, w_k\, \Delta\ell_s \right] \\ (S_{2j}) &= -\frac{1}{\rho A_{CV2}} \left[\sum_{s=1}^{4} \sum_{k=1}^{3} (M_j\, n_y)_{k,s}\, w_k\, \Delta\ell_s \right] \end{aligned}\right\} \qquad (2.28c)$$

The mass balance equation (2) can be rewritten as :

$$\oint_{CS1} (u\, n_x + v\, n_y)\, d\ell = 0$$

or,
$$\sum_{s=1}^{4} (\bar{u}_s\, n_{xs} + \bar{v}_s\, n_{ys})\, \Delta\ell_s = 0 \qquad (2.29)$$

where $\bar{u}_s$, $\bar{v}_s$ are respectively the average values of x and y velocity components on the sth side and n_{xs} , n_{ys} are the direction cosines of the outward normal for that side . The appropriate evaluation of $\bar{u}_s$ and $\bar{v}_s$ on each face of the continuity cell is somewhat intricate and this is discussed in the subsequent section .

2.5 Derivation of Pressure Correction Equation

As the name of the algorithm (EXTRA-FLAG) suggests , the velocities are evaluated explicitly at each momentum control volume for the next time step by making use of the momentum equations (2.25) . The pressure , however , is evaluated implicitly in conjunction with the continuity equation . Equation (2.25) can be rewritten as

$$\begin{Bmatrix} u^{n+1} \\ v^{n+1} \end{Bmatrix} = \begin{Bmatrix} (u)^n \\ (v)^n \end{Bmatrix} + \Delta t \left[[C]^n + [D] \right] \begin{Bmatrix} (u)^n \\ (v)^n \end{Bmatrix} + \Delta t \, [S] \begin{Bmatrix} p \end{Bmatrix}^{n+1} \quad (2.30)$$

where the superscripts n and n+1 denote time levels .

In the implementation of the algorithm , only those velocity and pressure values which satisfy both the momentum and the continuity equations are given the superscript n+1. The provisional values which have been obtained through the explicit calculations of equation (2.25) (and not satisfying continuity) are represented with the superscript * . Thus, equation (2.25) can be rewritten as:

$$\begin{Bmatrix} u^* \\ v^* \end{Bmatrix} = \begin{Bmatrix} (u)^n \\ (v)^n \end{Bmatrix} + \Delta t \left[[C]^n + [D] \right] \begin{Bmatrix} (u)^n \\ (v)^n \end{Bmatrix} + \Delta t \, [S] \begin{Bmatrix} p \end{Bmatrix}^{n} \quad (2.31)$$

Note that in equation (2.31) , the pressure is still at the nth level since it has not been so far updated via the compliance of continuity equation. Equation (2.31) can be expressed in a

slightly more general form as :

$$\begin{Bmatrix} u^* \\ v^* \end{Bmatrix} = \begin{Bmatrix} (u)^n \\ (v)^n \end{Bmatrix} + \Delta t \left[[C]^n + [D] \right] \begin{Bmatrix} (u)^n \\ (v)^n \end{Bmatrix} + \Delta t \, [S] \begin{Bmatrix} p^* \end{Bmatrix} \quad (2.32)$$

It is conjectured that after satisfying the continuity equation in each cell , provisional values (values with * superscripts) for the dependent variables will be transformed into final converged values for that time step . Thus the accomplishment of $u^* \longrightarrow u^{n+1}$ $v^* \longrightarrow v^{n+1}$ and $p^* \longrightarrow p^{n+1}$ is performed through an iterative procedure which will be discussed herein .

Subtracting equation (2.32) from equation (2.30) the expressions for the velocity corrections can be obtained as

$$\underset{2 \times 1}{\begin{Bmatrix} u^{n+1} - u^* \\ v^{n+1} - v^* \end{Bmatrix}} = \underset{2 \times 1}{\begin{Bmatrix} \delta u \\ \delta v \end{Bmatrix}} = \Delta t \underset{2 \times 4}{[S]} \underset{4 \times 1}{\begin{Bmatrix} \delta p \end{Bmatrix}} \quad (2.33)$$

where the δu , δv are the velocity corrections and δp is the pressure correction. Equation (2.33) can be used to calculate the velocity corrections, if the pressure corrections are known .

The evaluation of the pressure corrections is carried out through an implicit satisfaction of the continuity equation as described below. Assuming that the mass balance principle is satisfied by the converged values of velocity components at both the time levels of n and n+1, one can write

$$\sum_{s=1}^{4} \left(\bar{u}_s^n \, n_{xs} + \bar{v}_s^n \, n_{ys} \right) \Delta \ell_s = 0 \quad (2.34a)$$

$$\sum_{s=1}^{4} \left(\bar{u}_s^{n+1} n_{xs} + \bar{v}_s^{n+1} n_{ys} \right) \Delta\ell_s = 0 \qquad (2.34b)$$

The unconverged velocities , however , do not satisfy continuity and therefore leave a non-zero residue . Thus ,

$$\sum_{s=1}^{4} \left(\bar{u}_s^{*} n_{xs} + \bar{v}_s^{*} n_{ys} \right) \Delta\ell_s = R \qquad (2.34c)$$

Subtracting equation (2.34c) from equation (2.34b) , we obtain :

$$\sum_{s=1}^{4} \left(\delta\bar{u}_s n_{xs} + \delta\bar{v}_s n_{ys} \right) \Delta\ell_s = R \qquad (2.35)$$

where $\delta\bar{u}_s$ and $\delta\bar{v}_s$ are the average velocity corrections on the sth side , so as to satisfy continuity principle in the control volume . From equation (2.34c) and (2.34a) , the residue can be written as :

$$R = \sum_{s=1}^{4} \left\{ \left(\bar{u}_s^{*} - \bar{u}_s^{n} \right) n_{xs} + \left(\bar{v}_s^{*} - \bar{v}_s^{n} \right) n_{ys} \right\} \Delta\ell_s$$

$$= \sum_{s=1}^{4} \left(\delta\bar{u}_{mom,s} n_{xs} + \delta\bar{v}_{mom,s} n_{ys} \right) \Delta\ell_s \qquad (2.36)$$

where $\delta\bar{u}_{mom,s}$ and $\delta\bar{v}_{mom,s}$ are the average velocity modifications in the sth side of the continuity cell arising from the explicit time increment calculation of the momentum equation (2.31) . Combining equations (2.35) and (2.36) ,

$$\sum_{s=1}^{4} \left(\delta\bar{u}_s n_{xs} + \delta\bar{v}_s n_{ys} \right) \Delta\ell_s = \sum_{s=1}^{4} \left(\delta\bar{u}_{mom,s} n_{xs} + \delta\bar{v}_{mom,s} n_{ys} \right) \Delta\ell_s$$

.....(2.37)

By substituting for the velocity corrections in the LHS of equation (2.37) in terms of pressure corrections , equation (2.37)

can be converted into a pressure correction equation . The crucial step in this process , however , is the estimation of the average velocity corrections $\delta\bar{u}_s$ and $\delta\bar{v}_s$ in terms of the nodal velocities of the sth side . Referring to Fig.2.5 , the obvious choice for the average which may arise in one's mind is :

$$\left.\begin{aligned} \delta u_1 &= (\delta u_I + \delta u_{II}) / 2 \quad ; \quad \delta v_1 = (\delta v_I + \delta v_{II}) / 2 \\ \delta u_2 &= (\delta u_{II} + \delta u_{III}) / 2 \quad ; \quad \delta v_2 = (\delta v_{II} + \delta v_{III}) / 2 \end{aligned}\right\} \quad (2.38)$$

and so on . The nodal velocity corrections δu_I , δv_I etc. , can in turn , be written in terms of the pressure corrections via equation (2.33) . It was found that such a simple averaging procedure leads to a pressure correction equation which exhibits decoupling between the pressures of odd and even continuity cells. This pressure splitting has also been observed by Majumdar, Rodi and Vanka [87] and it has to be avoided since it introduces numerical oscillations in the pressure field .

The pressure splitting can be avoided by a proper definition of the average corrections δu_s and δv_s on each side . Defining face-centre velocity corrections $\delta u_{f,s}$ and $\delta v_{f,s}$, the average corrections can be calculated as follows . On the east side of CV1 (refer Fig. 2.5)

$$\left.\begin{aligned} \delta u_e &= \frac{1}{6}\,\delta u_{II} + \frac{1}{6}\,\delta u_{III} + \frac{2}{3}\,\delta u_{f,e} \\ \delta v_e &= \frac{1}{6}\,\delta v_{II} + \frac{1}{6}\,\delta v_{III} + \frac{2}{3}\,\delta v_{f,e} \end{aligned}\right\} \quad (2.39)$$

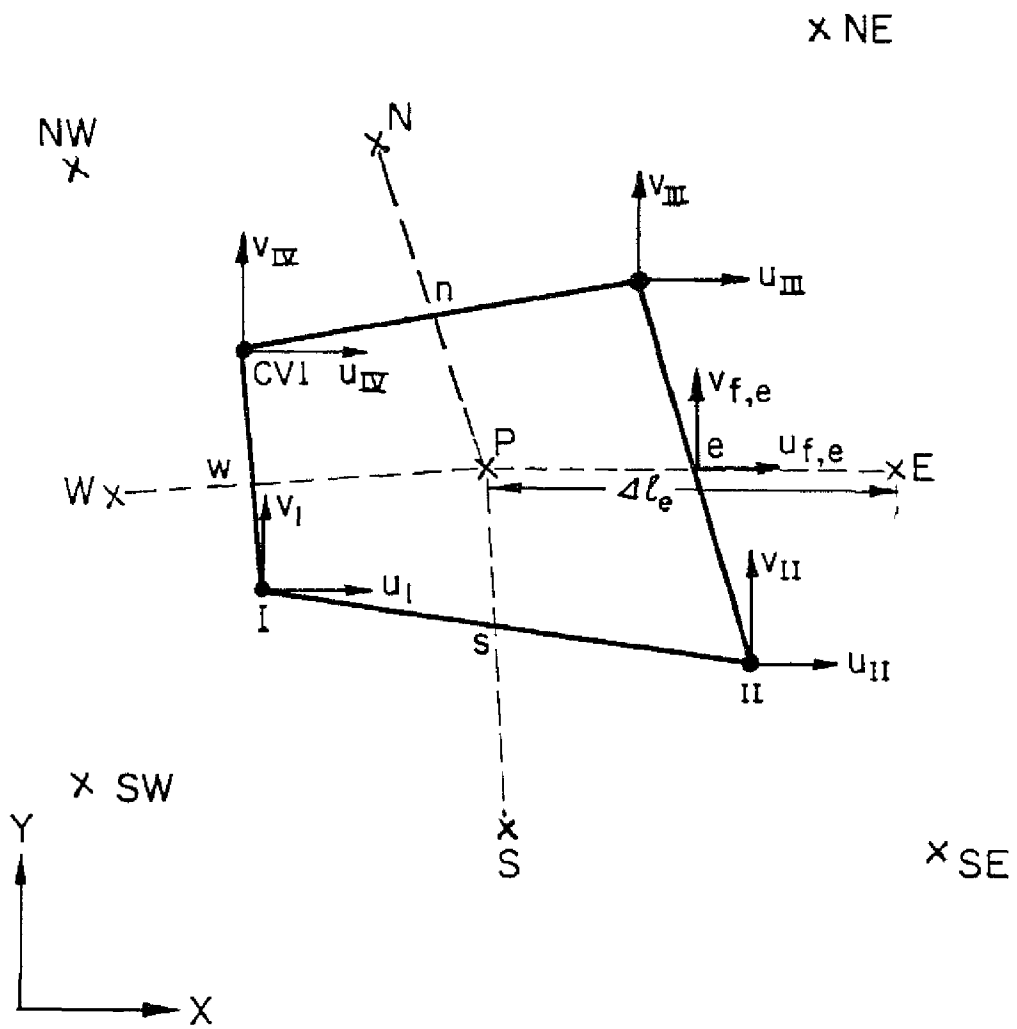

2.5 Pressure-velocity coupling for a continuity cor
volume.

similarly , the average corrections on the sides (n , w , s) can also be estimated in terms of the corresponding nodal and face-centre values of velocity corrections . Note that equation (2.39) amounts to the application of Simpson's rule along the boundaries of the continuity control volume CV1 .

It now remains to link this face-centre velocity corrections with the pressure corrections . A close look at equation (2.33) provides the key to resolve this issue . Equation (2.33) can be viewed as an expression relating the correction in the velocity vector , $\delta\underline{V}$ to the gradient of pressure correction $\underline{\nabla}(\delta p)$. Indeed , this simplified momentum equation can be rewritten as :

$$\delta\underline{V} = - \frac{\Delta t}{\rho} \underline{\nabla} (\delta p) \qquad (2.40)$$

Now , the face-centre velocity corrections on the east face $\delta u_{f,e}$ and $\delta v_{f,e}$ are given by :

$$\delta u_{f,e} = (\hat{i} \cdot \delta\underline{V})_{f,e} = - \frac{\Delta t}{\rho} \hat{i} \cdot \left\{ \hat{e} \frac{\delta p_E - \delta p_P}{\Delta \ell_E} \right\}$$

or ,
$$\delta u_{f,e} = \frac{\Delta t}{\rho} \left\{ \frac{x_E - x_P}{\Delta \ell_E} \right\} \left\{ \frac{\delta p_P - \delta p_E}{\Delta \ell_E} \right\} \qquad (2.41a)$$

similarly ,
$$\delta v_{f,e} = \frac{\Delta t}{\rho} \left\{ \frac{y_E - y_P}{\Delta \ell_E} \right\} \left\{ \frac{\delta p_P - \delta p_E}{\Delta \ell_E} \right\} \qquad (2.41b)$$

In the above equations $\hat{e}$ is the unit vector connecting the central node P within the control volume to the pressure node E of the eastern neighbouring continuity cell (see Fig. 2.5). Also, $\Delta \ell_E$ is the distance between the nodes P and E . In a similar

fashion , the face-centre velocity corrections for the north , west and south sides of the control volume can be obtained as :

$$\delta u_{f,(n,w,s)} = \frac{\Delta t}{\rho} \frac{\left(x_{(N,W,S)} - x_P \right)}{\Delta \ell_{(N,W,S)}} \left\{ \frac{\delta p_P - \delta p_{(N,W,S)}}{\Delta \ell_{(N,W,S)}} \right\} \quad (2.42a)$$

$$\delta v_{f,(n,w,s)} = \frac{\Delta t}{\rho} \frac{\left(y_{(N,W,S)} - y_P \right)}{\Delta \ell_{(N,W,S)}} \left\{ \frac{\delta p_P - \delta p_{(N,W,S)}}{\Delta \ell_{(N,W,S)}} \right\} \quad (2.42b)$$

where the subscripts within the brackets may be chosen appropriately for the side under consideration .

These relationships can be used in the derivation of the pressure correction equation in the following way . The mass residue contribution R_e to the east face is given by :

$$\Delta \ell_e (\delta u_e \, n_{xe} + \delta v_e \, n_{ye}) = - R_e \quad (2.43a)$$

substituting for δu_e , δv_e from equation (2.39) ,

$$\Delta \ell_e \left\{ \frac{1}{6} \delta u_{II} + \frac{1}{6} \delta u_{III} + \frac{2}{3} \delta u_{f,e} \right\} n_{xe} +$$

$$\Delta \ell_e \left\{ \frac{1}{6} \delta v_{II} + \frac{1}{6} \delta v_{III} + \frac{2}{3} \delta v_{f,e} \right\} n_{ye} = - R_e \quad (2.43b)$$

Now , from equation (2.33) , the nodal velocity corrections are given by :

$$\begin{Bmatrix} \delta u_{II} \\ \delta v_{II} \end{Bmatrix} = \Delta t \; [\, S \,]_{II} \begin{Bmatrix} \delta p_S \\ \delta p_{SE} \\ \delta p_E \\ \delta p_P \end{Bmatrix} \quad (2.44a)$$

$$\text{and} \quad \begin{Bmatrix} \delta u_{III} \\ \delta v_{III} \end{Bmatrix} = \Delta t \; [\, S \,]_{III} \begin{Bmatrix} \delta p_P \\ \delta p_E \\ \delta p_{NE} \\ \delta p_N \end{Bmatrix} \qquad (2.44b)$$

as can be seen from Fig. 2.5. In equations (2.44a) and (2.44b) the subscripts II and III refer to quantities corresponding to nodes II and III . Thus, substituting equations (2.41a), (2.41b), (2.44a), and (2.44b) into equation (2.43b), the residue contribution of the east face R_e can be calculated in terms of pressure corrections. Similarly for the other faces (n , w , s) also, the velocity corrections at nodes and face-centres can be written in terms of appropriate pressure corrections. The final expression for the pressure correction equation can be then derived from the mass residue equation (37), in a form :

$$\underset{1 \times 9}{[\, CP \,]} \underset{9 \times 1}{\{ \delta P \}} = -\sum_{s=1}^{4} \left\{ \delta \bar{u}_{mom,s} \, n_{xs} + \delta \bar{v}_{mom,s} \, n_{ys} \right\} \Delta \ell_s = - R_{mom} \qquad (2.45)$$

where CP is the coefficient matrix corresponding to the pressure correction array and R_{mom} is the mass residue generated after the explicit evaluation of the momentum equations through equation (2.31). The left hand side of equation (2.45) has a strong diagonally dominant structure , with the δp of the concerned continuity cell linked to the pressure corrections of all the eight neighbouring cells (see Fig.2.5) .

The pressure correction equations written using equation

(2.45) for all the continuity cells can be solved together by matrix inversion technique , line-by-line sweeping or by point-by-point method . In the present work , point-by-point iteration has been employed for the sake of simplicity . It may be mentioned that after the explicit momentum evaluations , only changes which have taken place in the nodal velocity values are available . The changes in the face-centre velocities are not available . To start with , these may be estimated by simple averaging as given in equation (2.38) and the approximate value of the residue R_{mom} can be evaluated . As pressure values get modified during the continuity iterations , the corresponding changes in the nodal or face-centre velocities are also calculated using equation (2.33) and (2.41) respectively . The change in the mass residues due to the changes in the velocities are again evaluated and used in equation (2.45) . In this fashion , the pressure and velocity corrections are iteratively improved until the corrections to the mass residues decrease below a pre-defined small value ($\approx 10^{-6}$ to 10^{-7}) for all the continuity cells . The (n+1)th level velocity and pressure values at each node are then calculated as :

$$\left.\begin{aligned} p^{n+1} &= p^{n} + \delta p \\ u^{n+1} &= u^{n} + \delta u \\ v^{n+1} &= v^{n} + \delta v \end{aligned}\right\} \qquad (2.46)$$

where δp , δu and δv are the overall pressure and velocity corrections accumulated iteratively over the time step Δt . Thus by explicit momentum evaluation and implicit satisfaction of continuity , time marching of nodal velocities and pressures are continued until steady state is reached from given initial conditions .

An important point to be noted is that in the present algorithm , the domain boundaries always contain velocity nodes . Since known velocity conditions are more often prescribed (through no-slip or given flow velocity) at the domain boundaries , the velocity corrections for the corresponding nodes and face-centres can be set equal to zero . Therefore , the contributions to mass residue (or correction in the mass residue) will be zero for these boundaries .

2.6 Non dimensional Form of Governing Equations and Definition of Problems Under Investigation

The equation of continuity (2.2) and the momentum equations (2.7) and (2.8) are expressed in nondimensional forms as

$$\oint_{CS1} (U n_x + V n_y) \, d\ell = 0 \qquad (2.47)$$

$$\left\{ \frac{\partial}{\partial t} \iint_{CV2} U \, dA + \oint_{CS2} U \, (U n_x + V n_y) \, d\ell \right\} =$$

$$\oint_{CS2} \left\{ - P\, n_x + \frac{2}{Re} \frac{\partial U}{\partial X} n_x + \frac{1}{Re} \left(\frac{\partial U}{\partial Y} + \frac{\partial V}{\partial X} \right) n_y \right\} d\ell \qquad (2.48)$$

$$\left\{ \frac{\partial}{\partial t} \iint_{CV2} V\, dA + \oint_{CS2} V\, (U\, n_x + V\, n_y)\, d\ell \right\} =$$

$$\oint_{CS2} \left\{ - P\, n_y + \frac{2}{Re} \frac{\partial V}{\partial Y} n_y + \frac{1}{Re} \left(\frac{\partial U}{\partial Y} + \frac{\partial V}{\partial X} \right) n_x \right\} d\ell \qquad (2.49)$$

respectively. In the above equations, the velocities have been nondimensionalized with respect to the characteristic velocities of the problems concerned, all lengths have been nondimensionalized with respect to the characteristic lenghts of the respective problems and the nondimensional pressures have been obtained with respect to $\rho(U_{char})^2$.

We have applied the EXTRA-FLAG algorithm to five problems, namely, (i) Lid-driven square cavity (ii) Lid-driven oblique cavity (iii) Developing flow in a channel (iv) Investigation of confined wakes behind a square cylinder in a channel and (v) Investigation of confined wakes behind a circular cylinder in a channel. The characteristic velocity, length and the definition of Reynolds number are presented in Table 2.2

Table 2.2 Characteristic Velocity, Length and Definitic Reynolds number for the Problems Under Consideration

Problem Studied	Characteristic Velocity	Characteristic Length
(i) Lid-driven square cavity	Lid velocity ULID	Height H
(ii) Lid-driven oblique cavity	Lid velocity ULID	Oblique height H
(iii) Developing flow in a channel	Average velocity at the channel inlet U_{av}	Channel height H
(iv) Investigation of confined wakes behind a square cylinder in a channel	Average velocity at the channel inlet U_{av}	Cylinder height B
(v) Investigation of confined wakes behind a circular cylinder in a channel	Average velocity at the channel inlet U_{av}	Cylinder Diameter D

The proposed EXTRA-FLAG algorithm has been embodied in a computer code to envisage the objectives enumerated above. The computations were done on the CONVEX C-220 computer while pre-and post processing were done on a HP 9000 (M-340) Workstation.

The results obtained by using the proposed algorithm have been discussed in the subsequent chapters. Code validation has been accomplished by comparing our results with available results in open literature.

Chapter-3

3. Testing of the Algorithm on Model Problems

The EXTRA-FLAG algorithm is tested on three flow configurations: driven cavity flow in square and oblique cavities and developing flow in a channel . In this section, the results obtained by the present algorithm are reported and further discussed how they compare with the results available in literature.

3.1 Flow in a Lid-driven Square Cavity:

The numerical domain consists of a two dimensional lid-driven square cavity with no-slip and impervious boundary conditions at the bottom and side walls except at the top , where u is a non-zero constant and equal to ULID. In the governing equations , the velocities have been nondimensionalized with respect to ULID. All lengths have been scaled with respect to cavity height H, and the Reynolds number is defined as Re = (ULID.H)/ν. A large number of numerical bench-mark solutions on this domain are available in open literature.

The streamline patterns using a 41 x 41 grid and a 81 x 81 grid

for the aforesaid two dimensional cavity at Re = 400 are shown in Fig.3.1(a) and 3.1(b) respectively. The numerical solution of Ghia et al [110] compares favourably with the present solution calculated with 81 x 81 grid . As stated in the earlier chapter, a time-marching scheme was deployed and the flow became steady when the maximum deviation of each flow variable between consecutive time steps is below 5×10^{-4} . In Fig.3.2 u velocity components at the vertical mid plane are plotted for 41 x 41 and 81 x 81 grids and compared with the results obtained by Ghia et al [110] and cited by Peyret and Taylor [111] . It may be mentioned that Ghia et al employed a 129 x 129 grid via a multigrid technique . However, Fig.3.2 shows reasonably good agreement between Ghia et al's result and the present computation with a 81 x 81 grid . Even otherwise, the positions and values of the minimum u velocity in position and value of all the computations agree with each other on an overall assessment . The v velocity components at the horizontal mid plane of the cavity for the same Reynolds number (Re = 400) are shown in Fig.3.3. It is evident that the present computation with 81 x81 grid demonstrates extremely good agreement with that of Guj and Stella [112] for both the maximum and the minimum v velocity positions and values . However, the minor discrepancy with Ghia et al's result (with respect to maximum v velocity 7.5 percent, and with respect to

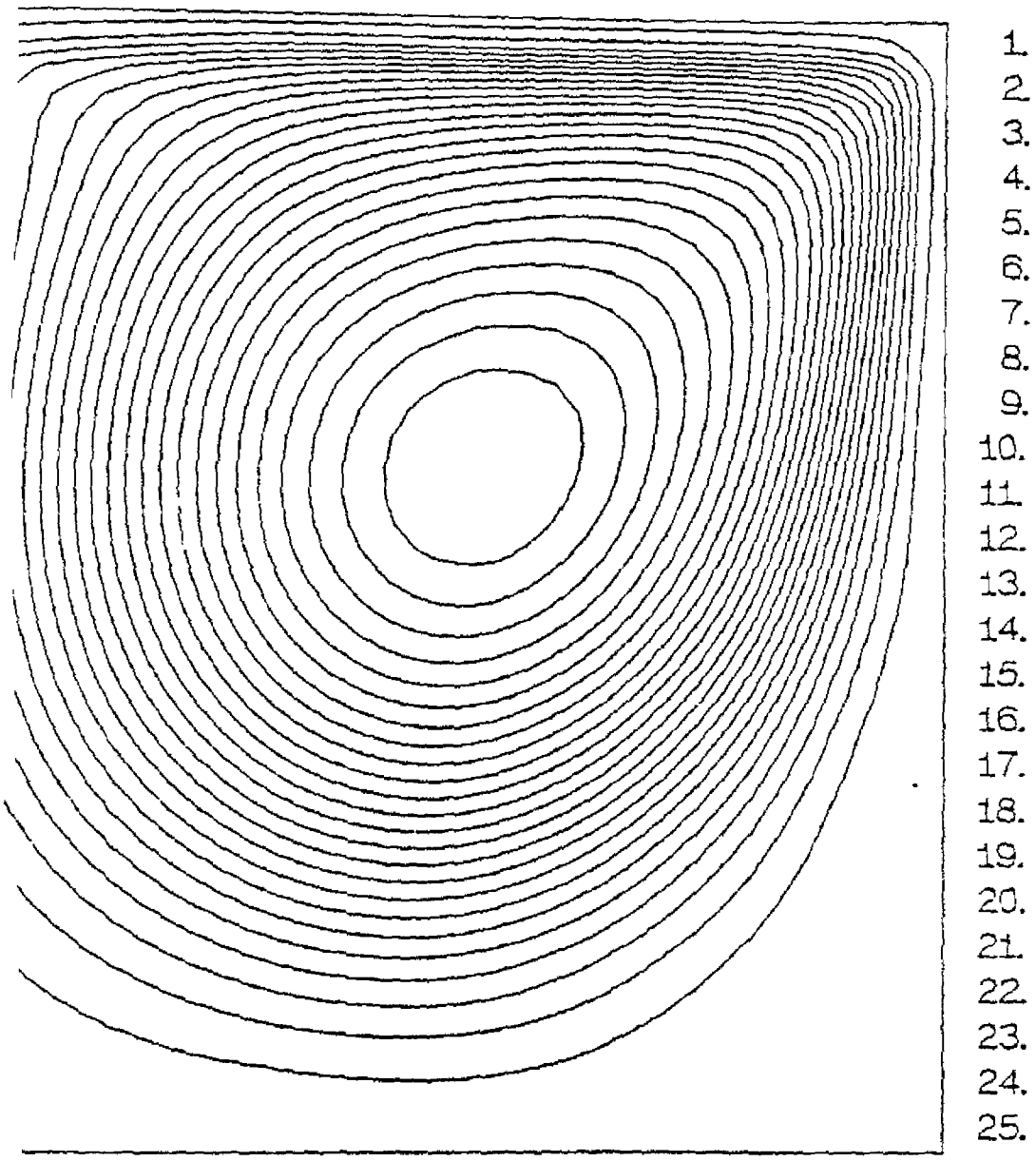

Streamlines in a lid driven cavity for Re = 400 (41 X 41 grids).

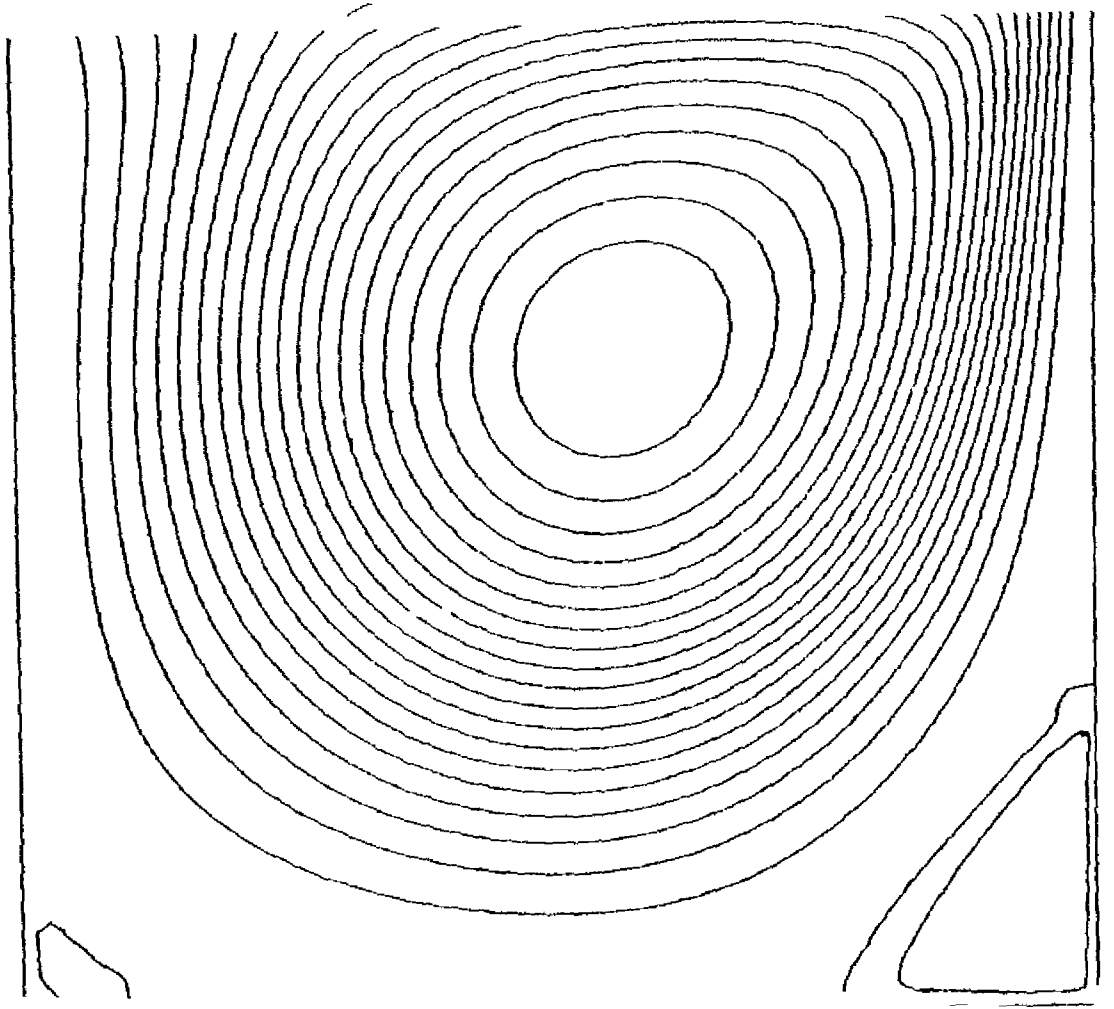

3.	-.08587
4.	-.08082
5.	-.07577
6.	-.07072
7.	-.06567
8.	-.06062
9.	-.05556
10.	-.05051
11.	-.04546
12.	-.04041
13.	-.03536
14.	-.03031
15.	-.02526
16.	-.02021
17.	-.01515
18.	-.01010
19.	-.00505
20.	.00000
21.	.00188
22.	.00197
23.	.00206
24.	.00215
25.	.00224

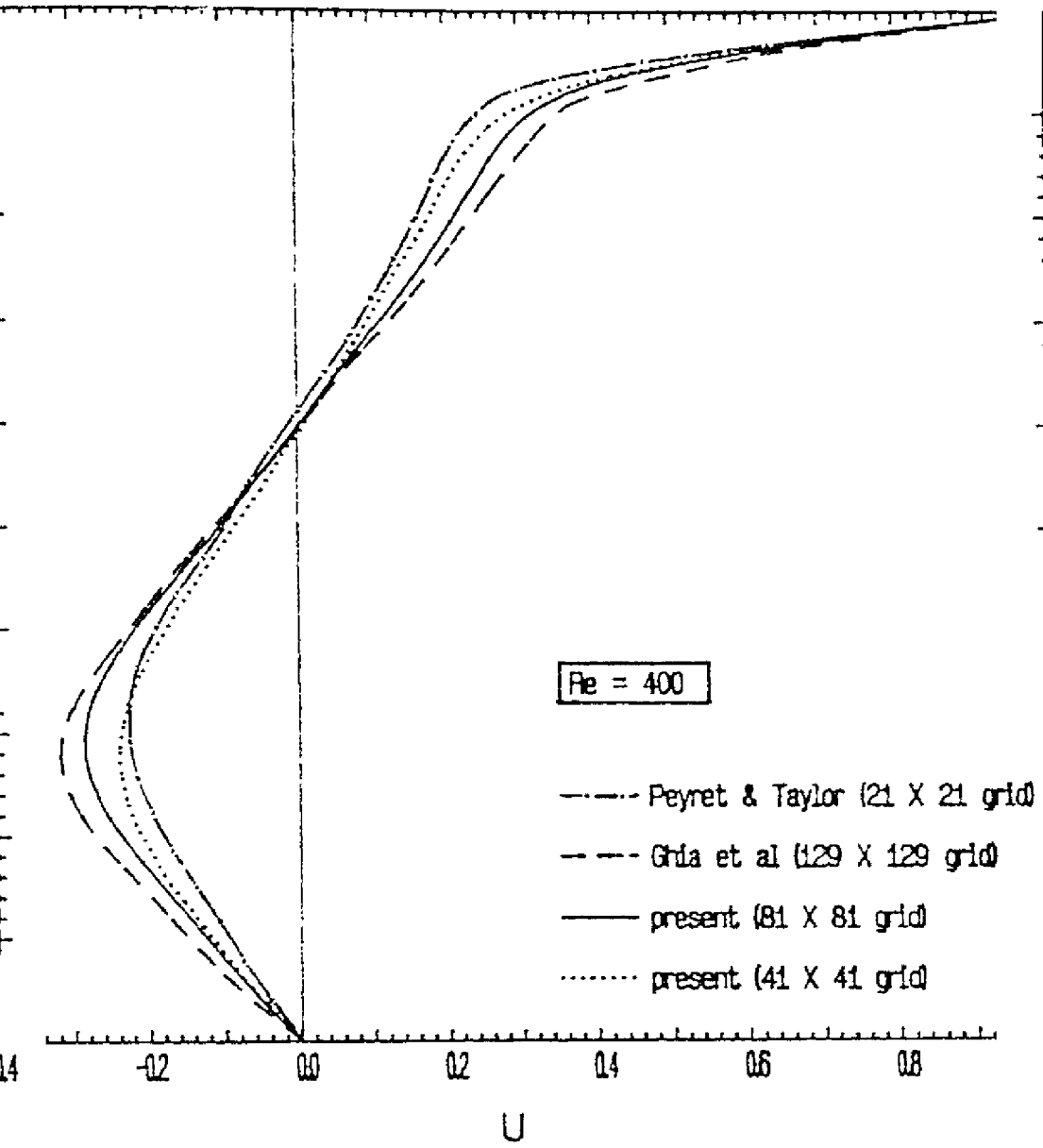

Variation of U velocity along the vertical mid p

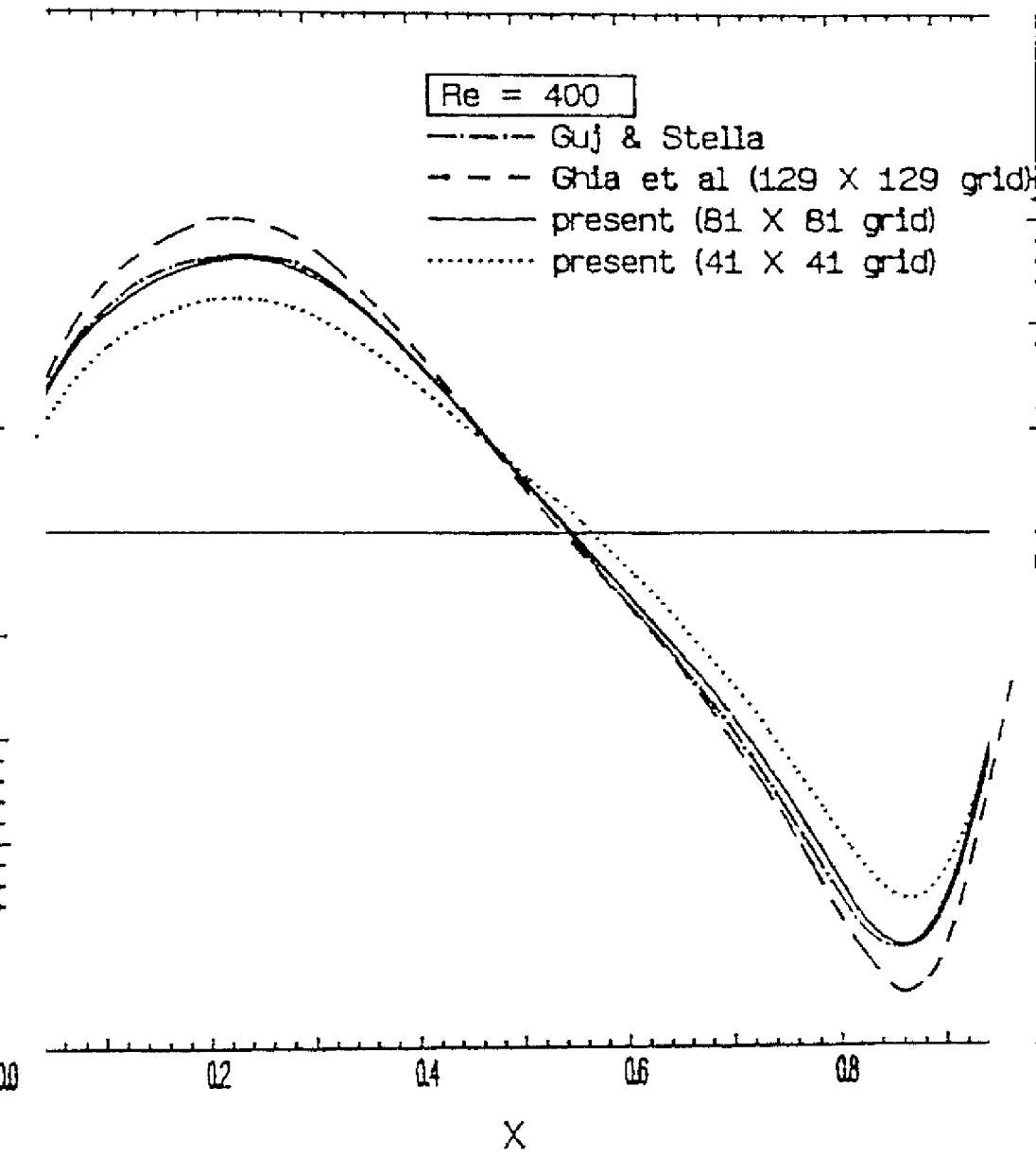

3 Variation of V velocity along the horizontol

locity 8 percent) can be attributed to the r
ion of grids used by us . In order to dis
information on the velocity field, the
the above mentioned flow field have been
For a better clarity , the right hand bott
gnified in Fig.3.4(b) . Main vortical flo
ting corner eddies which is clearly depicte
ctor plot .

nolds number of 1000 , a 41 x 41 grid is use
ues of velocities were compared with th
Ghia et al [110] and Wang et al [113]. The
wn in Table 3.1.

Extremes in Velocity for the Driven Cavity

u_{min} at x = 0.5		v_{min} at y = 0.5		v_{max} at
u_{min}	y	v_{min}	x	v_{max}
-0.388	0.172	-0.516	0.906	0.371
-0.135	0.240	-0.300	0.930	0.138
-0.244	0.175	-0.361	0.925	0.227

x 41 grid , streamlines for Reynolds numbe
Fig. 3.5. It may be mentioned that our resu
th the result of Perng and Street [114] .

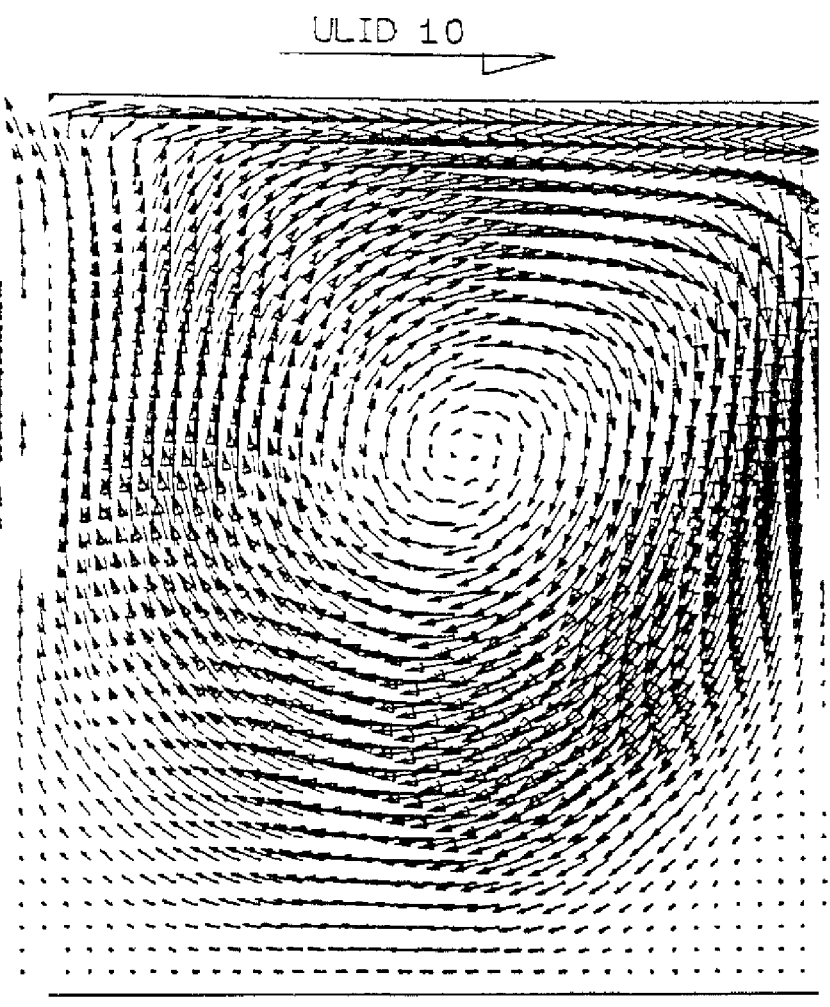

(a) Velocity vectors in a lid driven cavity f
Re = 400 (81 X 81 grid)

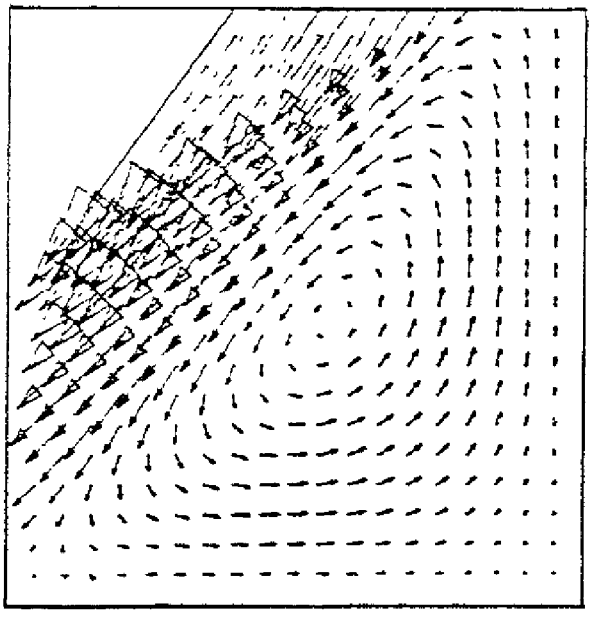

(b) Magnified view of the right bottom cor
of the cav ty shown n F g 3 4(a)

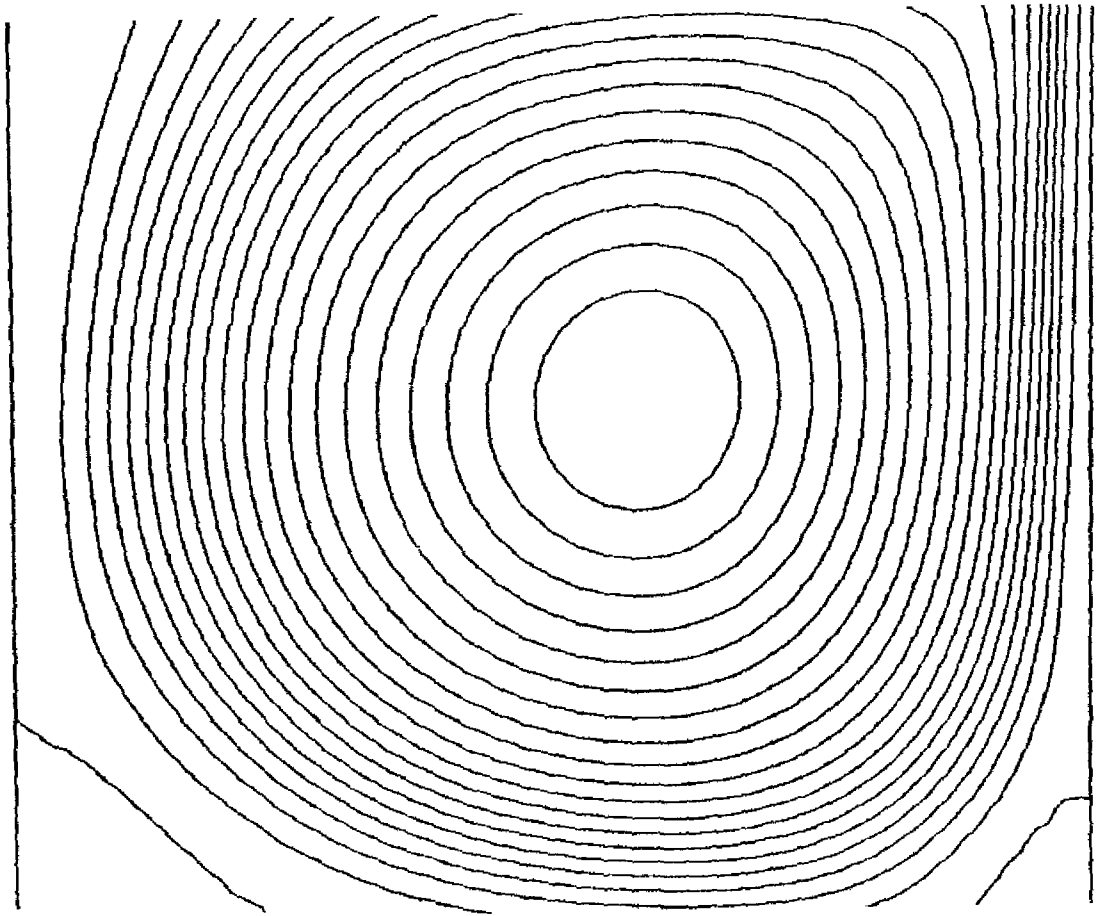

4.	-.04009
5.	-.03758
6.	-.03508
7.	-.03257
8.	-.03007
9.	-.02756
10.	-.02506
11.	-.02255
12.	-.02004
13.	-.01754
14.	-.01503
15.	-.01253
16.	-.01002
17.	-.00752
18.	-.00501
19.	-.00251
20.	.00000
21.	.00142
22.	.00149
23.	.00156
24.	.00163

3.2 Flow in Lid-driven Oblique Cavity

Laminar flow in an oblique-cavity with moving lid at different Reynolds numbers is chosen as another important test case for which a non-orthogonal grid has been used. Fig.3.6(a) shows the grid and the boundary conditions. Fig.3.6(b) shows the velocity vectors in the cavity at a Reynolds number of 100 with a 21 x 21 grid. The u-velocity distribution along the mid-plane for Reynolds numbers of 100, 400 and 1000 have been shown in Fig.3.7. The positions and values of minimum u-velocity for all the Reynolds numbers appear to be physically meaningful. Fig.3.8 shows the velocity vectors in an oblique cavity at a Reynolds number of 1000. It is to be noted that our results for oblique cavity compare favourably with results of Peric [115]. Basically, these computations were done in order to test the ability of the algorithm in tackling non-orthogonal geometry. Due to sparse numerical or experimental data base on oblique cavity, rigorous comparison was not possible. However, this particular aspect of the algorithm has been tested on a complex geometry in a subsequent chapter.

3.3 Developing Flow in a Channel

Developing flow in a rectangular channel was calculated in an

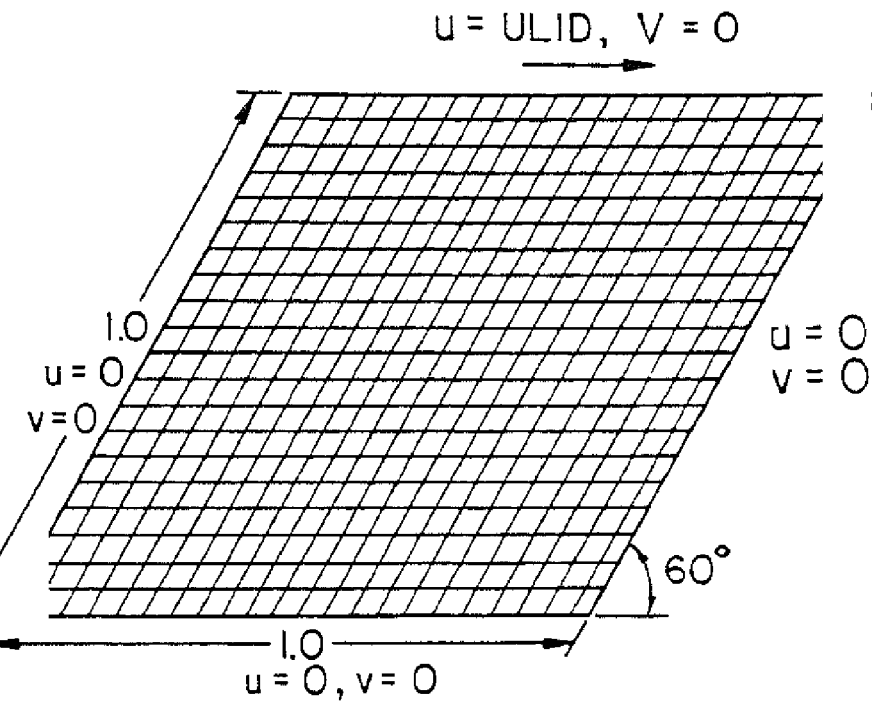

Non-orthogonal grid in an oblique cav

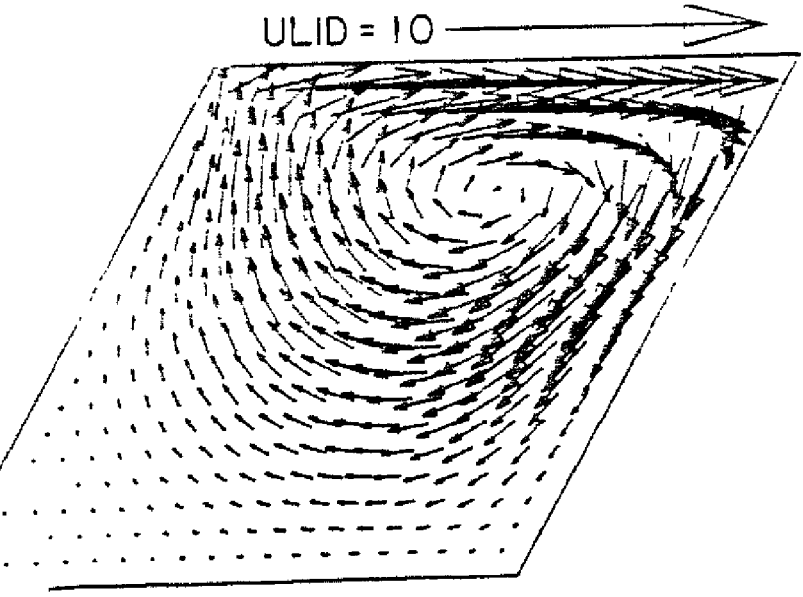

b Velocity vectors in an oblique cavity f
Re = 100

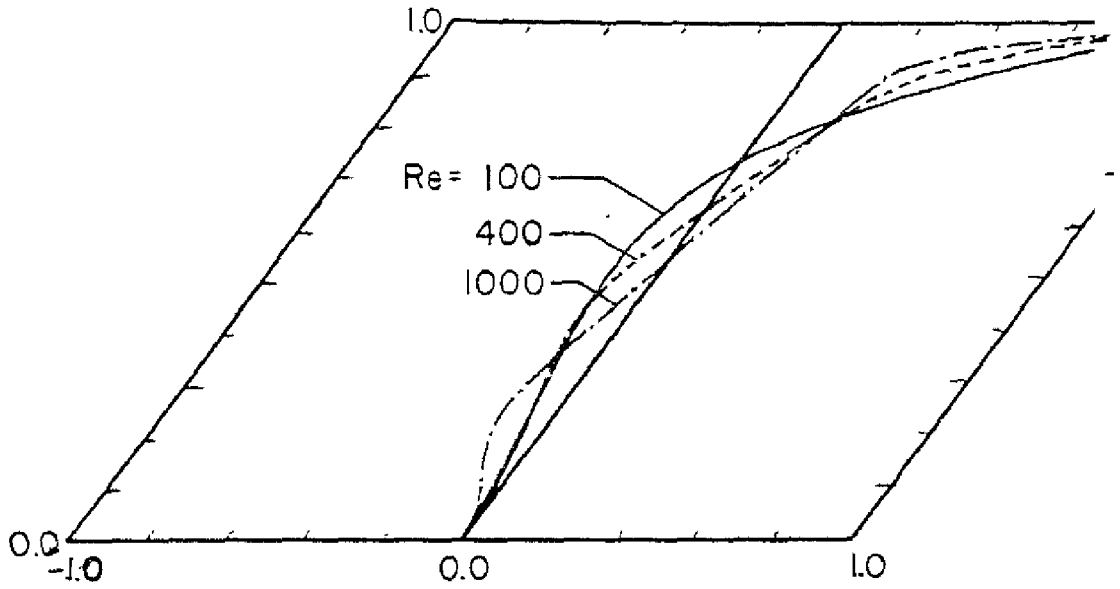

Fig.3.7 Variation of U velocity along the mid plane in an oblique cavity.

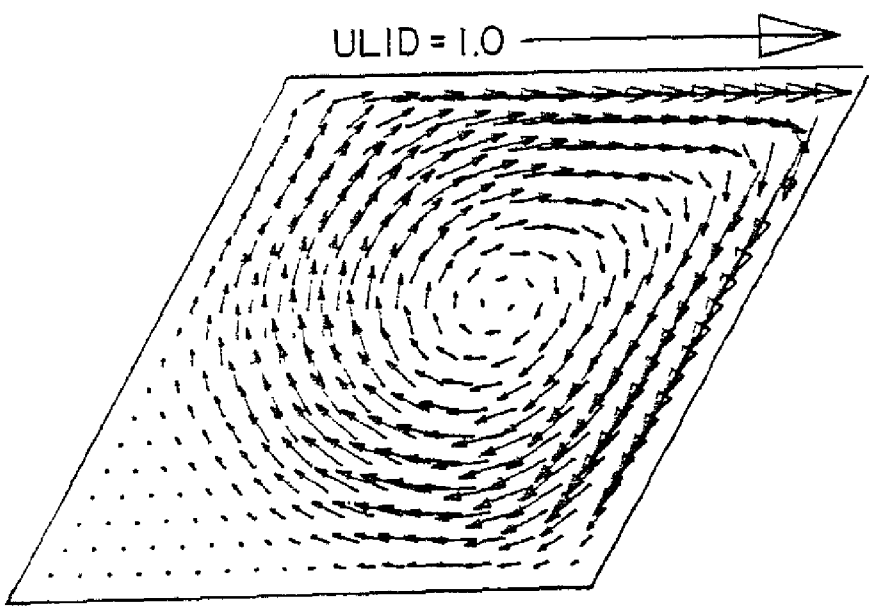

Fig.3.8 Velocity vectors in an oblique cavity for Re = 1000

effort to find out the hydrodynamic entrance length in a two dimensional channel flow . In the governing equations , the velocities have been nondimensionalized with respect to the average incoming velocity U_{av} at the channel inlet, all lengths have been nondimensionalized with respect to the channel height H and the Reynolds number is defined as Re = (U_{av}.H) / ν . No slip and impervious boundary conditions for the axial and normal components of velocity are applied on the top and the bottom walls (u=0, v=0). At the inlet, the normal component of velocity is zero (v=0) and a uniform axial velocity profile ($u=U_{av}$) is deployed.At the exit of the channel, the second derivatives of the dependent variables in the flow direction are set equal to zero ($\frac{\partial^2 u}{\partial x^2} = \frac{\partial^2 v}{\partial x^2} = 0$) in order to ensure smooth transition through the outflow boundary. The problem of laminar flow in the entrance region of ducts has been studied extensively by several investigators . We shall examine whether our results corroborate the results available in literature .

Fig.3.9 shows the velocity profiles at the entrance region of a two dimensional rectangular channel for a Reynolds number of 50. In the immediate downstream of the inlet , the profile has a local minimum on the axis of symmetry and a pair of maxima located symmetrically on either side of the axis . In the farther downstream , the boundary layers grow in size ; consequently the

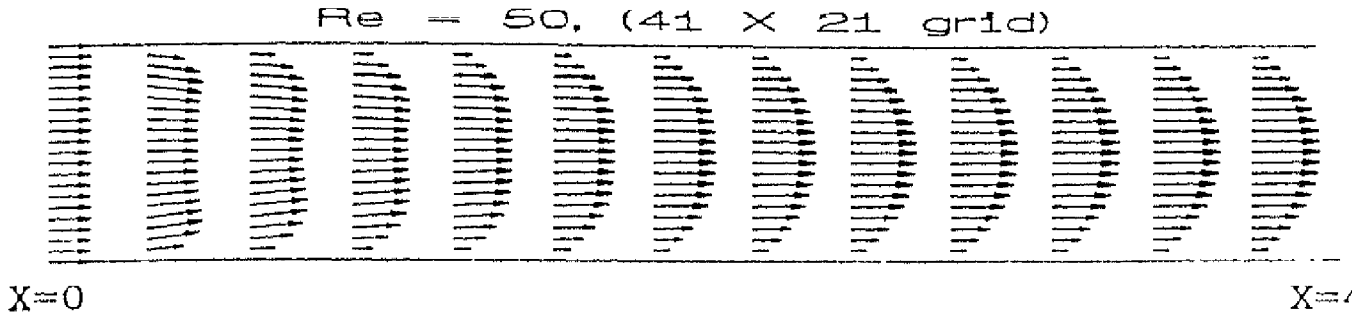

Fig.3.9 Velocity profiles for devoloping flow in a two dimensional rectangular channel.

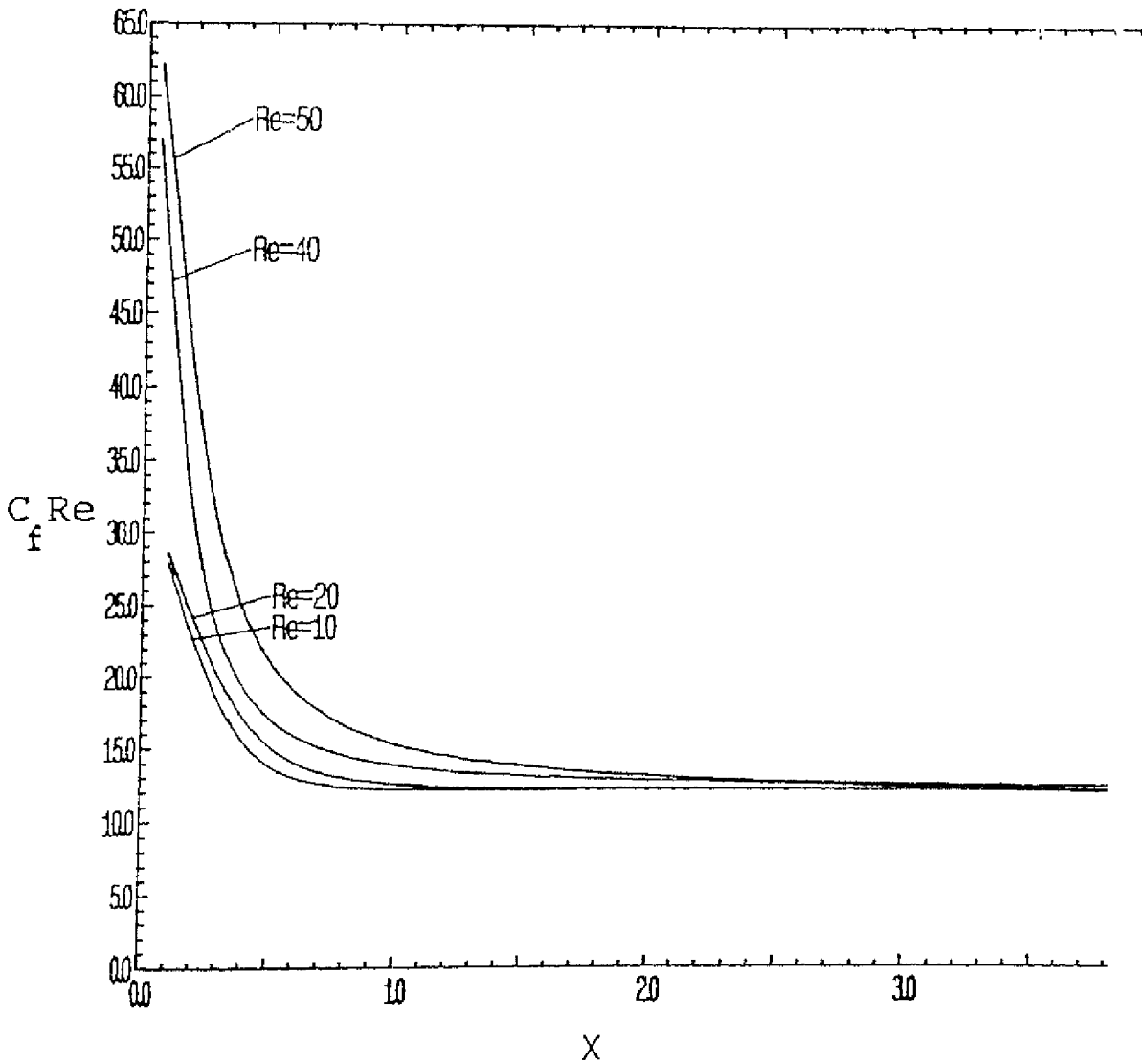

Fig.3.10 Variation of $C_f Re$ in a two dimensional channel.

velocity profiles tend to become fully developed and after a distance (entrance length) it remains unchanged . Convexity is induced in the velocity profile and finally it culminates as a parabolic profile . However , this trend of variation of velocity profile can be corroborated and expatiated by comparing the results of Abarbanel , Brandt et al [116].

Variation of skin friction ($C_f Re$) along the channel walls for different Reynolds numbers has been shown in Fig. 3.10. It may be mentioned that the distributions of skin friction ($C_f Re$) along the channel walls are exactly same for the top and the bottom walls . As expected , the skin friction values ($C_f Re$) for all the Reynolds numbers are very high near the inlet . Thereafter , they take a sharp plunge and asymptotically reach a constant value of 12 (which is the value corresponding to the fully developed Poiseuille flow) . However , from our results it is quite evident that the entry length (the length at which fully developed velocity profile culminates) is a function of Reynolds number and this functional relationship may be summarized as

$$(x / H) \approx 0.055 \, Re$$

It may also be mentioned that here we have considered attainment of the 99 % of velocity profile as the index of fully developed condition . If we consider that the entry length is made up of inlet and filled regions , the estimation of entry length

will be somewhat more (see Mohanty and Das [117]) . However , we are not estimating the value of entrance region to a very high degree of correctness in this analysis . Our purpose is to examine the overall validation of the proposed numerical algorithm . Within the framework of 99 % attainment of Poiseuille profile as definition of fully developed condition and corresponding entry length , our prediction of the same corroborates the results available in literature (see Wang and Longwell [118]) .

Chapter 4

4. Study of Confined Wakes Behind a Square Cylinder in a Channel

4.1 Introduction

The oscillation of chimney stacks and other structures in transverse flows is caused by vortex shedding. An initially smooth and steady flow across a bluff body may bring about damaging deflection of the body in case the natural frequency of the obstacle is close to the shedding frequency of the vortices. If we concentrate on the wake region where Karman vortex street has been formed behind a bluff body, we shall observe that the wake zone undulates like a flag from side to side. This alternating deflections of the wake induce periodicity in the entire flow field. As a result the forces on the bluff body become periodic which culminate in vibration that can be detected from the oscillation of the bluff body. If this excitation frequency synchronizes with the natural frequency of the bluff body, the phenomenon of resonance is the obvious outcome. Hence the unsteady flows about the bluff bodies are of direct relevance to design of structures, road vehicles, heat exchangers and where ever the flow induced vibration is important.

In this chapter, the numerical investigation of the structure of confined wakes behind a square cylinder is presented. Details of the vortex-shedding phenomenon are simulated through numerical

flow visualization. We have used the well known MAC (Marker And Cell) algorithm of Harlow and Welch [1] to analyse the basic flow features of the problem. Subsequently the proposed EXTRA-FLAG algorithm has also been applied, in order to look into the similar aspects of the problem and compare the results with those obtained by MAC algorithm.

It has been known from both experimental and numerical studies that at moderate Reynolds numbers vortex shedding behind the cylinder introduces periodicity in the flow field. The unsteady periodic wake can be characterized by the Strouhal number which varies with Reynolds number and blockage-ratio of the channel. The periodicity of the flow is, however, damped in the downstream of a long duct. This damping may be attributed to the influence of side walls on the flow structure. In the present study, such fundamental flow features as well as the non-dimensional releationships characterizing the vortex-shedding frequency, have been analysed in detail.

4.2 Previous Work

Vortex structure in the wake of a circular cylinder has been investigated both experimentally [119,120] and numerically [121,122]. These investigations have shown that vortex shedding behind a circular cylinder in an unbounded medium starts around a Reynolds number of 40 and periodicity is induced in the flow field [123]. Study of vortex shedding behind rectangular / square cylinders has also been the subject of investigation for many researchers. A systematic study of eddies behind a rectangular

cylinder has been undertaken by Okajima [124] His experimental results show how Strouhal number varies with the aspect ratio of cylinders in the range of Reynolds number between 70 and 2 x 10^4. A recent work of Okajima [125] presented the variation of lift and drag forces, base pressure and Strouhal number of rectangular cylinders with Reynolds number. His computations by finite difference method showed good agreement with experimental results and it was possible to detect a critical range of Reynolds number where the value of Strouhal number changes followed by a drastic change in flow pattern . Kelkar and Patankar [126] have computed steady two dimensional flow around a square cylinder at different Reynolds numbers and determined the onset of unsteadiness through a linear stability analysis of steady flow. Stability of the steady flow to small perturbations is examined by computing the evolution of these perturbations.Davis, Moore and Purtell [127] reported results of a numerical and experimental study of flow around a rectangular cylinder in a horizontal channel. Strouhal numbers obtained from their computations are in good agreement with their measurements. Baba and Miyata [128] have studied the vortical structures of the flow around a rectangular cylinder by numerical integration of Navier-Stokes equations and explained some features of nonlinear interaction between vortical motions of different scales. However, if the square cylinder is confined in a channel , irrespective of shedding of vortices in the near wake, a parabolic velocity profile will evolve again at the exit of a long channel [129]. Biswas, Laschefski, Mitra and Fiebig [129] studied structure of laminar wake and heat transfer in the presence of

thermal buoyancy in a horizontal channel with a built in square cylinder. Based on these investigations carried out on related topics, it can be said that the channel walls exert damping effects on periodic flow. But concrete inferences about the relationship between the wake-zone aerodynamics and the channel walls have not been drawn so far. The purpose of the present work is to perform numerical investigation of the influence of Reynolds number and the channel walls on the structure of wakes behind a square cylinder in a two dimensional duct.

4.3 Statement of the problem

The system of interest is a horizontal channel with an obstacle in the form of a square cylinder placed inside it (Fig. 4.1). The dimensionless equations for continuity and momentum may be expressed in the following conservative form

$$D = \frac{\partial U}{\partial X} + \frac{\partial V}{\partial Y} = 0 \qquad (4.1)$$

$$\frac{\partial U}{\partial t} + \frac{\partial U^2}{\partial X} + \frac{\partial (UV)}{\partial Y} = - \frac{\partial P}{\partial X} + \frac{1}{Re} \left(\frac{\partial^2 U}{\partial X^2} + \frac{\partial^2 U}{\partial Y^2} \right) \qquad (4.2)$$

$$\frac{\partial U}{\partial t} + \frac{\partial (UV)}{\partial X} + \frac{\partial V^2}{\partial Y} = - \frac{\partial P}{\partial Y} + \frac{1}{Re} \left(\frac{\partial^2 V}{\partial X^2} + \frac{\partial^2 V}{\partial Y^2} \right) \qquad (4.3)$$

Boundary conditions of interest in this investigation are :
At the top and bottom surfaces of the channel

$$u = v = 0 ,$$

at the entrance to the channel

$$\frac{u}{U_{av}} = 1.5 \left[1 - \left(\frac{y_m - y}{y_m} \right)^2 \right]$$

$$v = 0.$$

At the exit of the channel, the continuity boundary condition is used by setting

$$\frac{\partial^2 u}{\partial x^2} = \frac{\partial^2 v}{\partial x^2} = 0.$$

This ensures smooth transition through the outlet. No-slip boundary conditions are used for the velocity components on the obstacle. The differential form of governing equations presented above have been employed for solving the problem by the MAC procedure. While obtaining the predictions of EXTRA-FLAG for the sake of comparison, the integral equations (2.47-2.49) described in chapter 2 have been used.

4.4 Method of Solution

In order to solve the problem with EXTRA-FLAG algorithm the computational domain is divided into cartesian cells. The velocity nodes are located at the vertices and the pressures are located at the centre of the cells. The continuity control volumes and the momentum control volumes are shown in Fig.4.2. The solution procedure through the EXTRA-FLAG algorithm has already been discussed in Chapter-2. This is not being elaborated here for the sake of brevity. For high Reynolds number situation, however, a minor modification has been introduced in the solution procedure for providing upwind bias. This modification in the algorithm is described below.

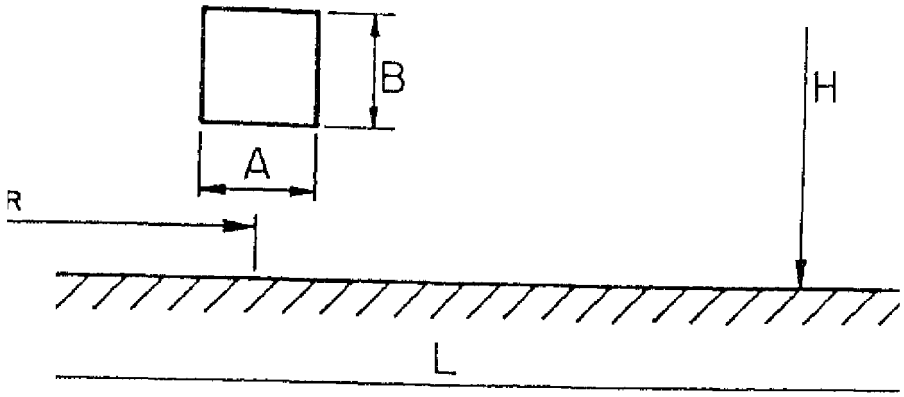

in a horizontal channel with built-in obstacle

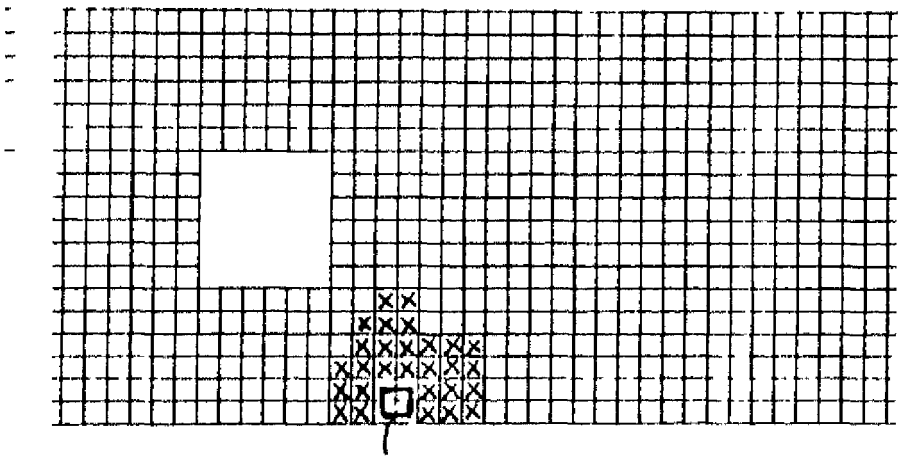

y control volume Momentum control volume

Pressure • ≡ Velocity

2 Grid layout in the comutational domain for EXTRA-FLAG algorithm

4 4 1 Implementation of Upwinding in EXTRA-FLAG

In the study of flow around a square cylinder, it was observed that almost upto a cell Reynolds number of 6, no upwinding was needed for EXTRA-FLAG. However, for very high flow Reynolds numbers (with a cell Re of the order of 10 or more), an upwind bias was necessary to obtain numerically stable results. In the present work, an elementary attempt has been made to introduce upwind bias in the convective terms (refer equations (2.25) and (2.26)). The scheme implemented is as follows. Considering the convective contribution to the x-momentum equation, it is redefined for upwinding purposes as

$$[C_{ij}]\,[u_j] = \frac{1}{\rho\, A_{cv2}}\,[\oint W_j\,(u\,n_x + v\,n_y)dl]\,[u_j] \qquad (4.4a)$$

where the interpolation functions W_j are given extra bias in the flow direction. There are calculated by the expression

$$\sum_{j=1}^{9} W_j\,u_j = \sum_{j=1}^{9} (1-\alpha)\,N_j\,u_j + \alpha\,u_r \qquad (4.4b)$$

where the subscript r corresponds to the node situated upstream of the concerned face. The weight α lies between 0 and 1.

Using the above approach, for instance, on the east face of the control volume (see, Fig.2.4), if the mass flow is outwards r=2 (central node) and if the mass flow is inwards r = 4 (east side mid-node). In a similar fashion, for all the faces of the control volume, upwind-weighted interpolation has been applied for both the x-momentum and 4-momentum equations.

Admittedly, the above implementation is only a first step towards a scientific way of accounting for dominant convective effects. More elaborate study is required to develop proper

upwinding strategies for high Reynolds number flows. As mentioned earlier, we have also solved the problem with the MAC algorithm to validate the EXTRA-FLAG algorithm on one hand and to highlight some intricate flow physics of the problem on the other. In the subsequent section, we shall discuss in brief, the MAC algorithm.

4.4.2 Solution Procedure by MAC Algorithm

A modified version of Marker and Cell (MAC) method [1,5] is used to obtain the numerical solution of equations (4.1) - (4.3). The computational domain is divided into cartesian cells. Staggered grid arrangements are used, in which velocity components are defined at midpoints of the cell sides on which they are normal (Fig.4.3). The pressure is defined at the centre of the cell.

To start a computational cycle, guess-fields for velocity and pressure are used. From these fields, corrected pressure and velocity fields are obtained by pressure and velocity iteration through continuity equation, as discussed in the following paragraph in detail. The corrected velocity and pressure fields are, in turn, used in the Navier-Stokes equations (4.2) and (4.3) to evaluate velocities for the next time increment.

In each cycle, solutions for velocities are obtained in two folds. First, the velocity components are advanced in time using the previous state of flow to calculate the accelerations caused by convection, viscous stresses, and pressure gradients over a time step of duration $\delta\bar{t}$. The explicit time increment may not necessarily lead to a velocity field with a zero mass

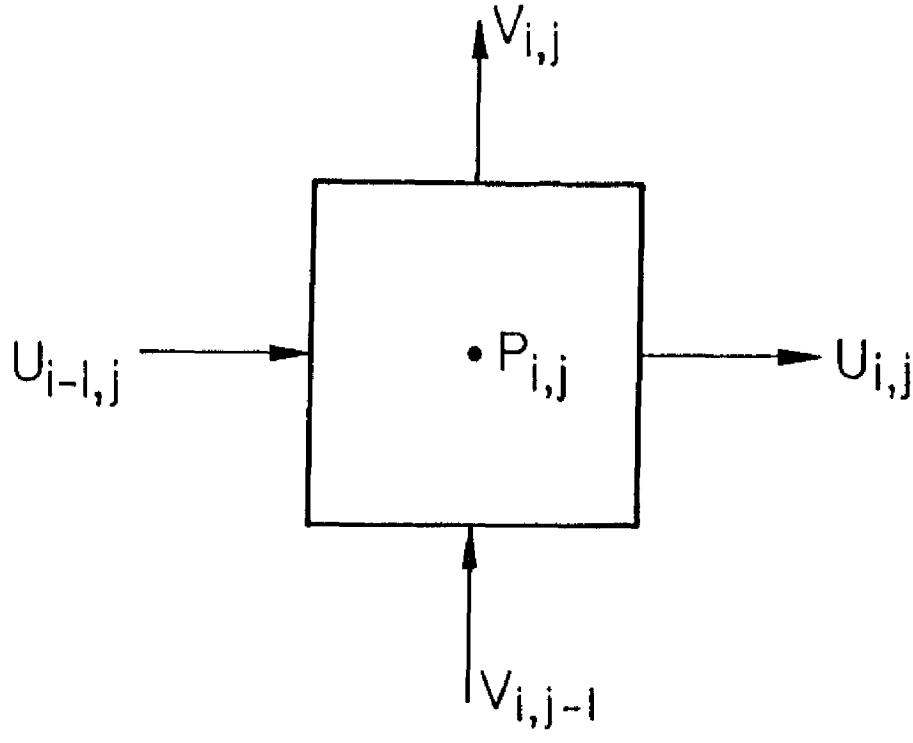

Fig.4.3 Location of the velocity components and pressure on a staggered grid

divergence in each cell. In the subsequent second fold, adjustment of pressure and velocity is done by a iterative process in order to ensure mass conservation in each cell. This iterative correction of explicitly advanced velocity field through implicit continuity equation is equivalent to the solution of a Poisson equation for pressure [130]. The convective terms of the equations (4.2) and (4.3) are discretized by a weighted average of an upwind and central differencing scheme [21,131,132]. Here, the formal first-order accuracy $O(\Delta X)$ of the upwind differencing scheme retains something of the second order accuracy of the advection field [16]. Runchal and Wolfstein [133] used a similar kind of upwind scheme to compute driven cavity flows. Their results compare favorably with those due to second-order schemes.

A concise description of the mathematical methodology for pressure-velocity iteration is described herein. The divergence of velocities D is calculated in each cell from equation (4.1). If the magnitude of D is greater than a prescribed small value ε, the pressure in each cell is adjusted proportional to the negative of velocity divergency by

$$\delta P^{n}_{i,j} = - \omega D^{n}_{i,j} \qquad (4.5a)$$

where ω is defined as

$$\omega = \omega_{o} / \left(2\delta\bar{t} \left(\frac{1}{\delta X^{2}} + \frac{1}{\delta Y^{2}} \right) \right) \qquad (4.5b)$$

The factor ω_{o} is an over relaxation factor. After $\delta P_{i,j}$ has been added to the cell pressure, the velocities are consequently changed in the following way:

$$P^{n+1}_{i,j} = P^{n}_{i,j} + \delta P^{n}_{i,j} \qquad (4.6)$$

$$U^{n+1}_{i,j} \rightarrow U^{n+1}_{i,j} + (\delta\bar{t} \cdot \delta P^{n}_{i,j})/\delta X \qquad (4.7)$$

$$U^{n+1}_{i-1,j} \rightarrow U^{n+1}_{i-1,j} - (\delta\bar{t} \cdot \delta P^{n}_{i,j})/\delta X \qquad (4.8)$$

$$V^{n+1}_{i,j} \rightarrow V^{n+1}_{i,j} + (\delta\bar{t} \cdot \delta P^{n}_{i,j})/\delta Y \qquad (4.9)$$

$$V^{n+1}_{i,j-1} \rightarrow V^{n+1}_{i,j-1} - (\delta\bar{t} \cdot \delta P^{n}_{i,j})/\delta Y \qquad (4.10)$$

This scheme of solution is continued until a steady or periodic flow is obtained. The procedure automatically adjusts the pressure level during each time cycle and thus avoids the need to prescribe pressure boundary conditions during the solution of the Poisson equation for pressure [111].

In order to set the initial condition for tangential velocities, $U_{i,j}$ at each cell is taken equal to unity, i.e., $\frac{u}{U_{av}}=1$. Consequently, the transverse component of velocity $V_{i,j}$ at each cell is taken as zero.

The conditions necessary to prevent numerical instabilities are determined from the Courant-Friedrichs-Lewy (CFL) condition and the restriction on grid-Fourier number.

According to the Courant-Friedrichs-Lewy conditions , the distance the fluid travels in one time increment must be less than one space step. Therefore,

$$\delta\bar{t} < \min\left[\frac{\delta X}{|U|} , \frac{\delta Y}{|V|}\right] \qquad (4.11)$$

When the viscous diffusion terms are more important, the

condition necessary to ensure stability is dictated by the restriction on the grid Fourier numbers, which results in

$$\nu\delta\bar{t} < \left[\frac{1}{2} \frac{(\delta X^2 \quad \delta Y^2)}{(\delta X^2 + \quad \delta Y^2)} \right] \qquad (4.12)$$

Final $\delta\bar{t}$ for each time increment is minimum of the $\delta\bar{t}$'s obtained from (4.11) and (4.12).

4.5 Results and Discussion

4.5.1 Selection of Numerical Grid and Computational Parameters:

For these computations with MAC algorithm 200x34 and 396x66 grids have been used . The computational results for 200 x 34 and 396 x 66 grids show an average difference of 3% in the peak value of $C_f Re_B$ on the channel walls. However, the computation time with 396 x 66 grids is nearly 9 times larger than with 200 x 34 grids. It was found that for all practical purposes 200 x 34 grids can produce grid independent results, although for some calculations 396 x 66 grids were used. Uniform grids are deployed throughout the calculation domain. Computations have been carried out in a channel of length L / H = 6.125. The geometrical centre of the square cylinder is located at a distance X_R = 2.125 from the inlet. The channel and cylinder axes are aligned (Fig.4.1). The aspect ratio (A / B) of the cylinder is 1 . The influence of different blockage ratios (B/H), namely, 0.125, 0.25, 0.3125 and 0.375 on vortex-shedding was studied. Reynolds number was used as an input parameter.

4.5.2 Validation of Computed Results and Comparison Between the Predictions of MAC and EXTRA-FLAG

The structure of the wake and its functional relationship with Reynolds number can be observed in (Fig.4.4) and (Fig.4.5). In Fig.4.4 a computed steady solution for B/H = 0.25 and Reynolds number Re_B= 37 is shown. The recirculating wake is extended to nearly twice the obstacle width in the downstream, but it is steady (symmetrical) and vortex shedding has not started. At Re_B = 85 the wake loses its original symmetry and the flow becomes periodic in the near wake (Fig.4.5).The periodicity is suppressed in the downstream of the square cylinder by the channel walls and the flow at the exit of the channel tends towards steady parabolic. Davis, Moore and Purtell [127]observed periodicity in computations with the same geometrical configuration as ours, at $Re_B \approx$ 100. Okajima [124] found periodicity in the wake behind a rectangular cylinder in an infinite medium (blockage being negligibly small) at Re_B = 70 . Shair et al [120] report a critical Reynolds number of 130 for the wake to become periodic in their experiments with a circular cylinder in a channel.The blockage ratio was 0.33 and the Reynolds number was defined in terms of a maximum velocity U which would exist at the same location as that of the centre of the cylinder under flow conditions identical with those of the experiment but in absence of the cylinder. However, their transition Reynolds number describing the onset of periodicity, based on a definition similar to ours, would be 87 (the average velocity is two-third of the maximum velocity). It can be said that our Reynolds number for

= Uav

Wake stagnat on po nt

B/H 0 25

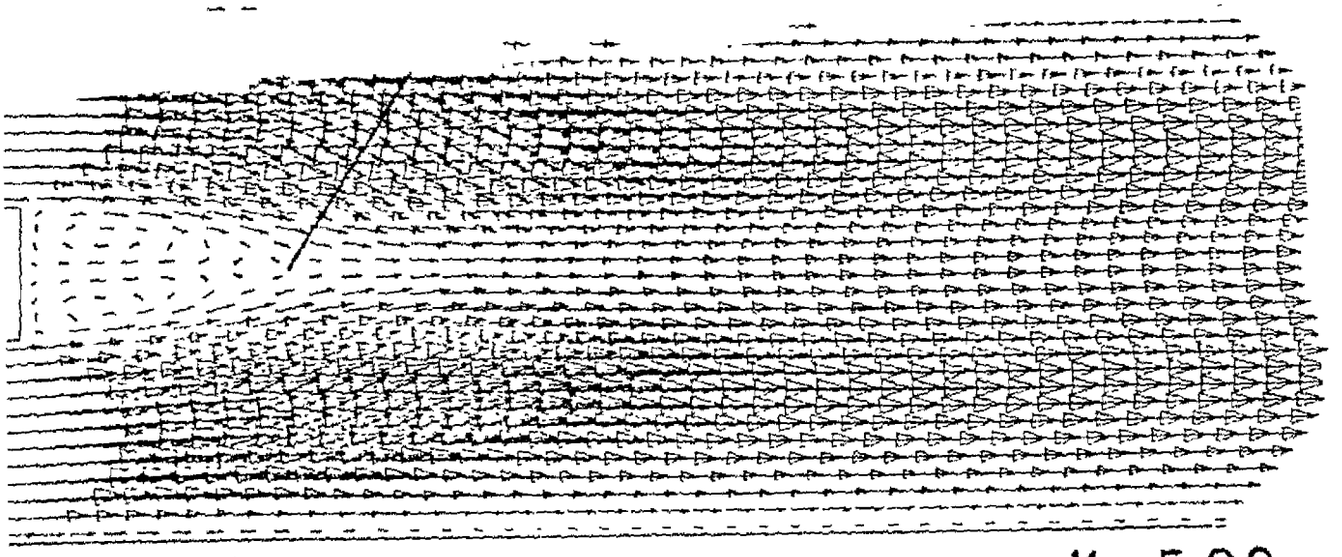

= 2·1875

X = 5·00

.4.4 Attached vortices behind the cylinder in the duct :
$Re_B = 37$

—— = Uav

B/H = 0.25

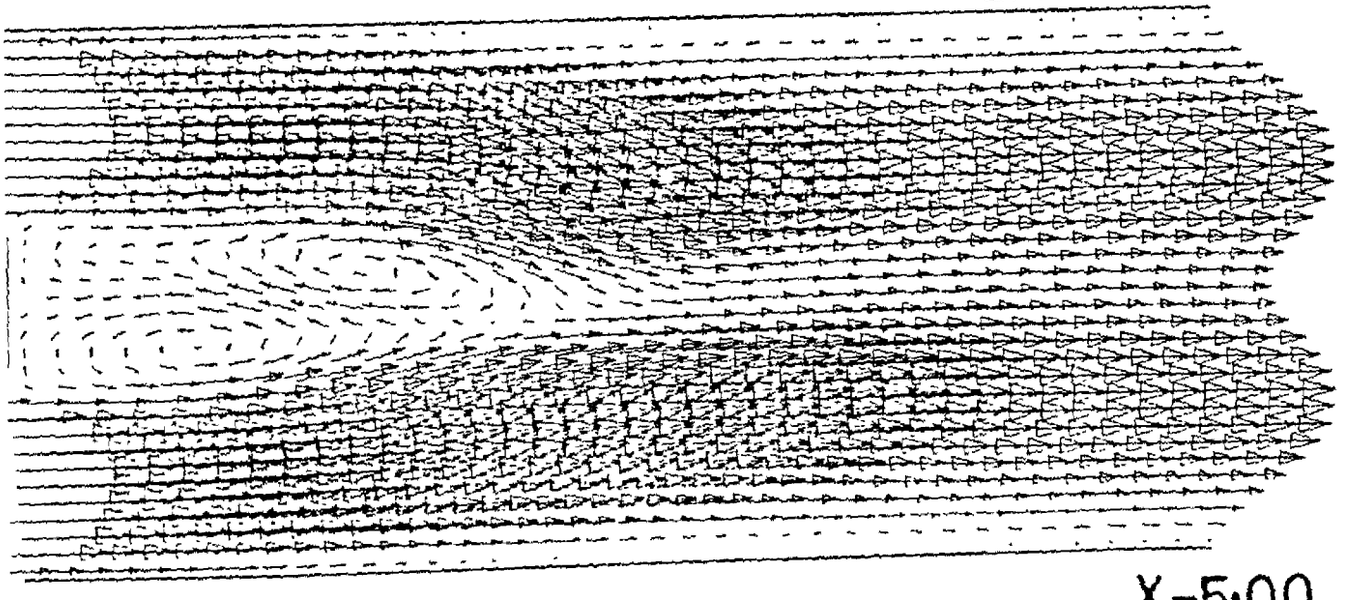

= 2·1875

X = 5·00

ig.4.5 The wake has lost original symmetry and begining to shed vortices into the stream : $Re_B = 85$

the onset of periodicity lies well within the range of critical Reynolds numbers obtained by other researchers. Finally, we may mention that the Figure 4.4 and 4.5 are not merely qualitative since the scales of the average channel velocity U_{av} are shown in the vector-plots and these can be used for quantitative analysis.

Numerical calculations with higher Reynolds numbers($Re_B > 85$) confirm shedding of vortices into the stream. As such, with increasing Reynolds number (beyond the aforesaid transition Reynolds number), the von Karman vortex street is formed and alternate shedding of vortices into the stream becomes prominent. The vortex shedding and formation of the von Karman vortex street is better understood from the numerical flow visualization of Fig. 4.6. For a Reynolds number of 162, separation is observed at the leading edge followed by rolling up of vortices behind the cylinder. The flow is seen to completely detach itself on the lower surface of the cylinder. A favourable comparison between the experimental and numerical flow-visualization has been reported by Okajima [124]. Our observation (Fig. 4.6) of numerical flow visualization follows a qualitative trend similar to Okajima's study [124] for a Reynolds number of 150. At $Re_B = 375$ formation of von Karman vortex street and its serpentine bends become prominent (Fig.4.7). Flow separates at the leading edge and does not reattach during a period of vortex shedding into the wake. The results discussed so far have been obtained with the help of the MAC algorithm. Similar results were obtained form our EXTRA-FLAG algorithm also. Next, we shall illustrate some of the results due to the EXTRA-FLAG algorithm. Fig.4.8 shows the

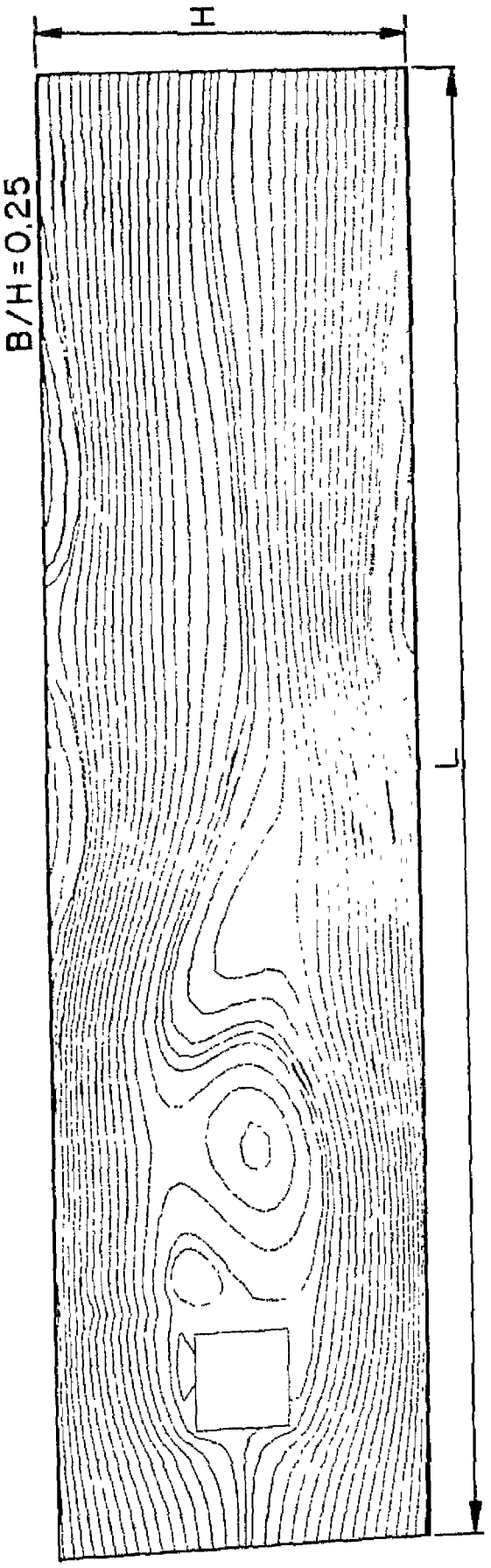

Fig 4.6 Steamlines crossing the cylinder in the duct : $Re_B = 162$

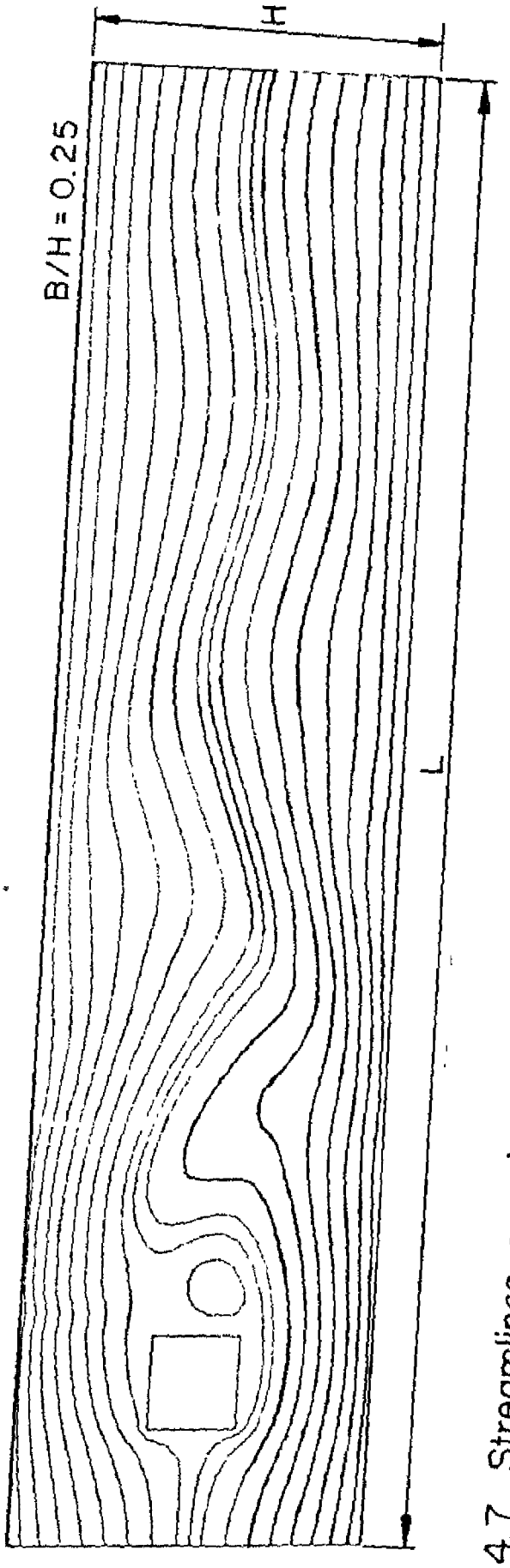

Fig 4.7 Streamlines crossing the cylinder in the duct: $Re_B = 375$

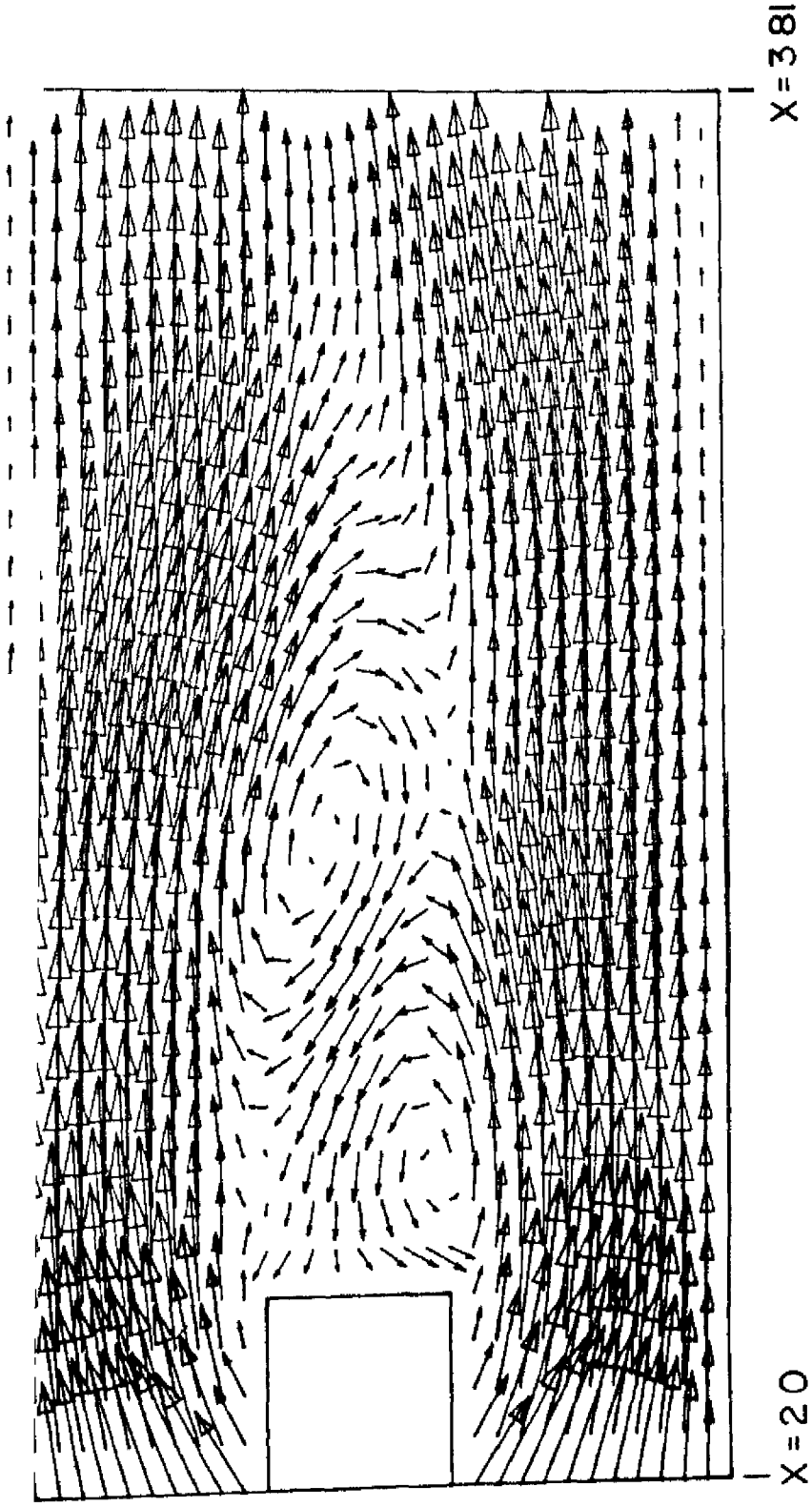
X=381
X=20

asymmetric wake and the onset of formation of the Von Karman Vortex street. Fig.4.9 shows a typical vortex street behind a cylinder for a Reynolds number of Re_B = 125. Fig.4.10 shows the velocity vectors in a channel where the entire wake zone and downstream undulates from side to side. However this undulation and the von Karman vortex street extends upto the end of the channel which is evident from the streamline plot (Fig.4.11).

The proposed EXTRA-FLAG algorithm has not only shown the correct trend of the Wake-zone aerodynamics, it has also predicted quantitative values which are very close to the predictions by MAC algorithm. In the subsequent section, we shall discuss some more intricate physical aspects of partially confined wakes behind a square cylinder. The discrepancy between the quantitative values obtained from two different numerical methods, namely, MAC and EXTRA-FLAG are so insignificant that we are only highlighting the physical phenomena without mentioning the methods deployed for the results.

4.5.3 Lift and Skin Friction Characteristics

Fig.4.12, (a) and (b), show the time evolution of the lift coefficient for two different Reynolds numbers. In each case, periodic flow field is observed after a short transient flow. The vortex shedding frequency can be determined from the time-evolution plot of lift coefficient distribution. Time period T can be calculated computationally by observing the nondimensional time when the lift coefficient is just crossing the mean value. The difference between two such alternate time values (also shown in Fig.4.12) gives the time period T. Once the time

X = 3.81
X = 2.0

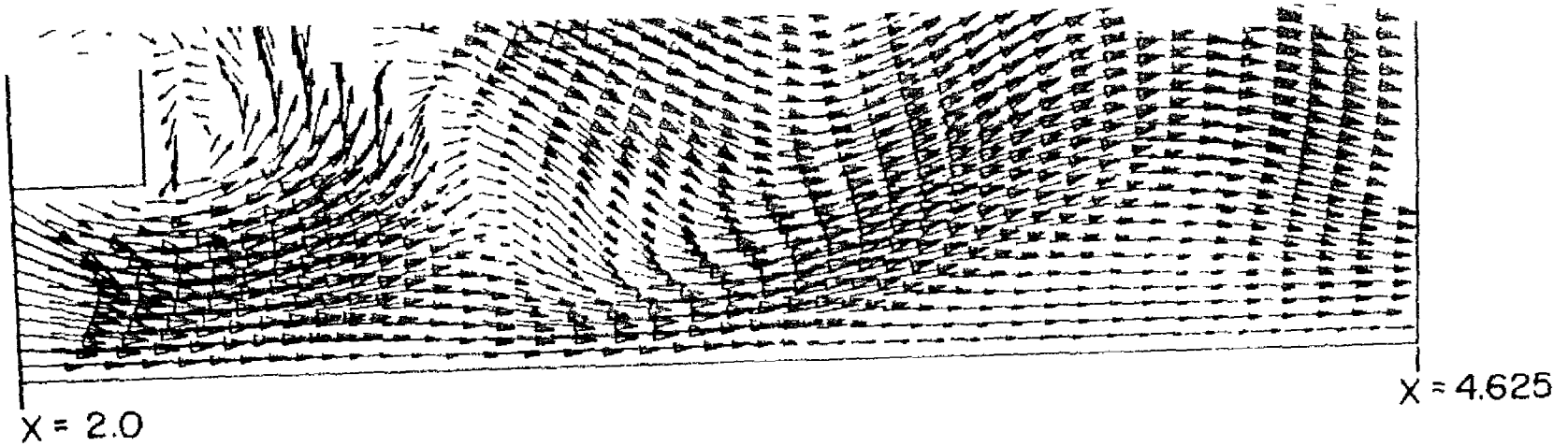

Fig.4.10 Undulation of the flow field at a high Reynolds number

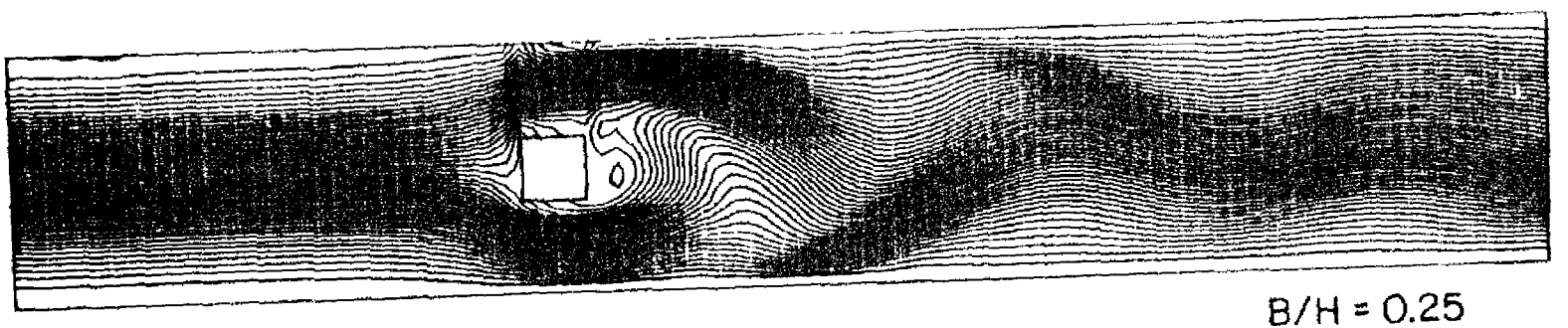

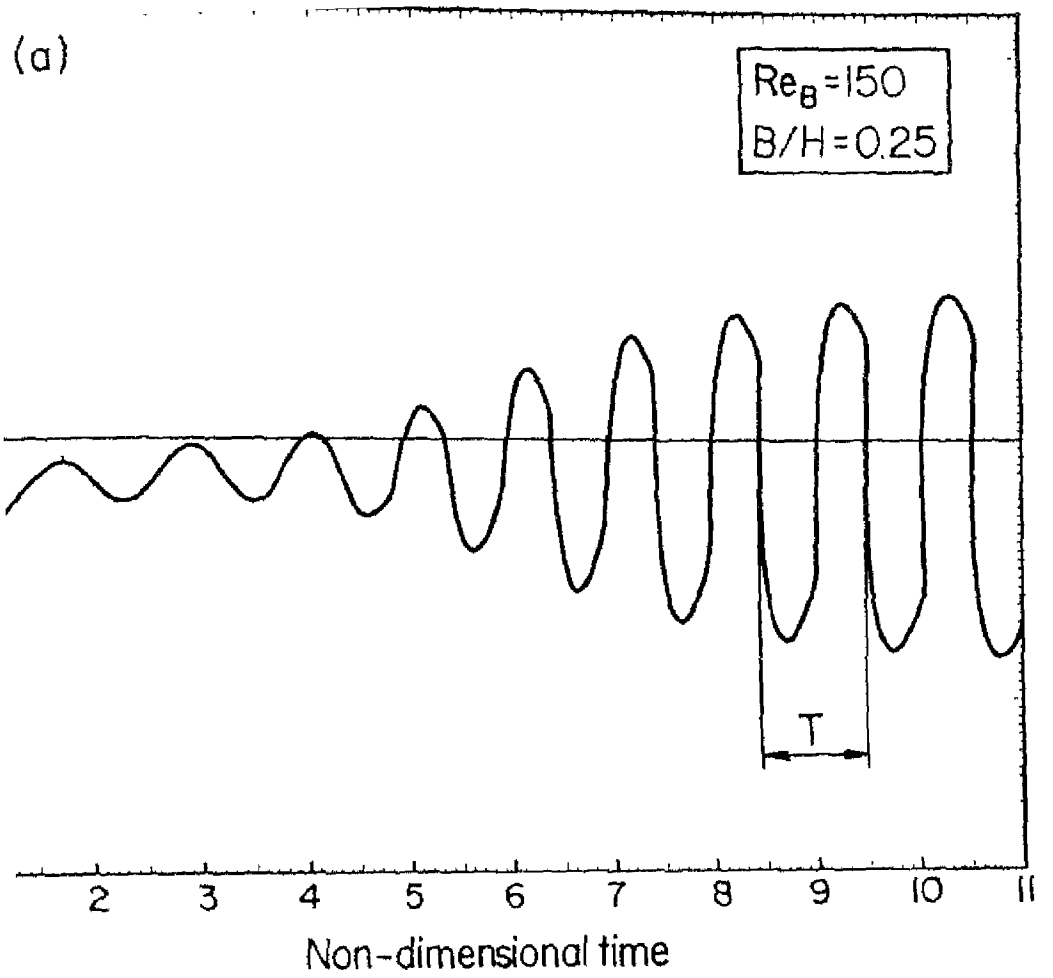

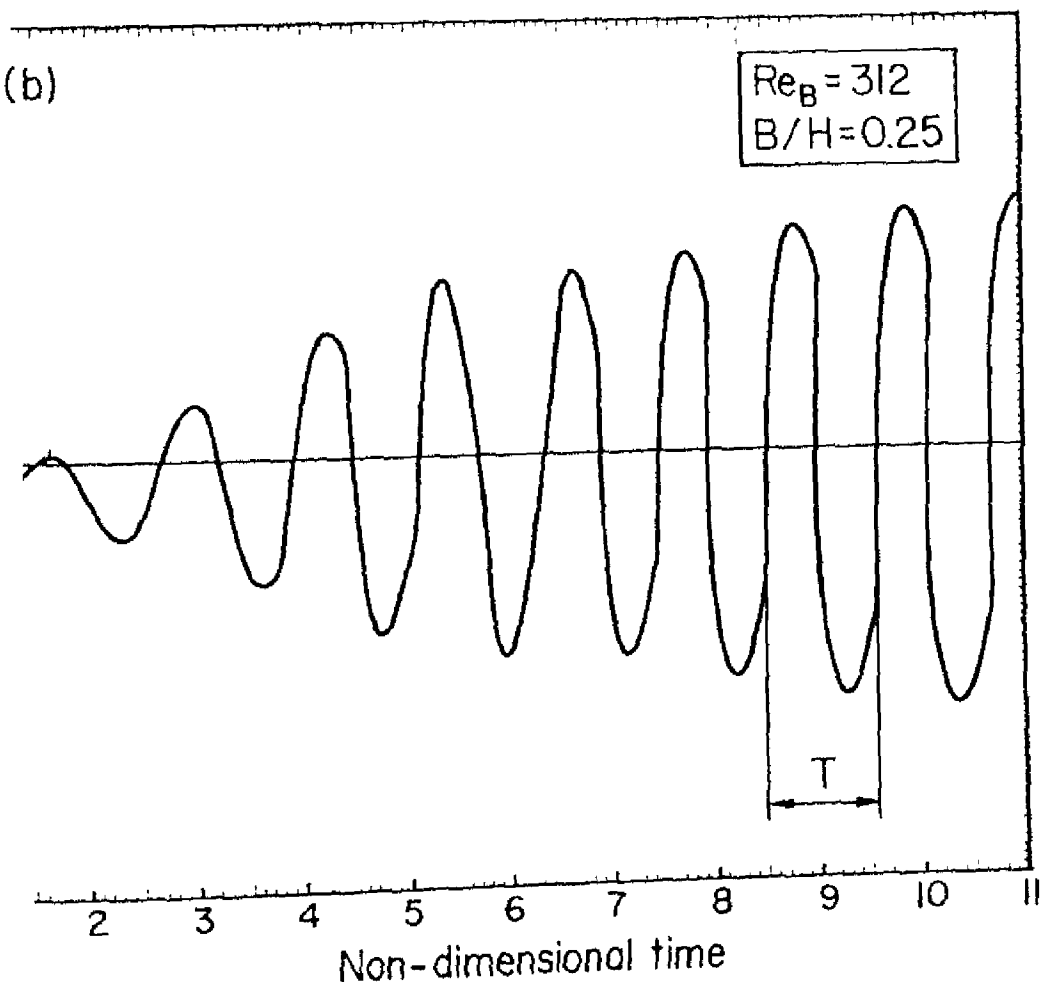

Fig 4.2 Time evolution of lift coefficient

period is known, the corresponding frequency (f = 1 / T) and the Strouhal number (S = fB / U_{av}) can be evaluated. The periodicity is characterized by the vortex shedding frequency, or so to speak, by the dimensionless Strouhal number. Variation of the Strouhal number over a large range of Reynolds number is discussed subsequently.

Flow field in front of the cylinder seems to be nearly independent of the structure of the wake [134]. Influence of the location of the obstacle in the channel (X_R) is not of great significance with respect to wake structure. However, for a uniform entry-profile the effect of flow development will come into play. The effect of periodicity on shear stress distribution is shown in Fig.4.13 (a and b). It is evident that the local skin friction coefficient C (= $C_f Re_B$) on the walls at the channel entrance is equal to 12 (the value of the fully developed laminar flow in a 2-D channel) and tends to this value far downstream of the cylinder. The deviation of skin friction coefficient from 12 in front of the cylinder (nearly at a distance of 2.5 B upstream of the cylinder) shows the upstream influence of the obstacle. It is also seen that the distribution of the skin friction C (= $C_f Re_B$) is same on both the channel walls for a Reynolds number of Re_B= 25 (steady flow). However, for unsteady periodic flow, the situation differs considerably. For a Reynolds number of 125, we can see some remarkably changed trend in the distribution of the skin friction coefficient on the channel walls at the rear of the cylinder. Where the upper plate has a very high value of shear stress (at X ≈ 3.38), a minimum value of shear stress is

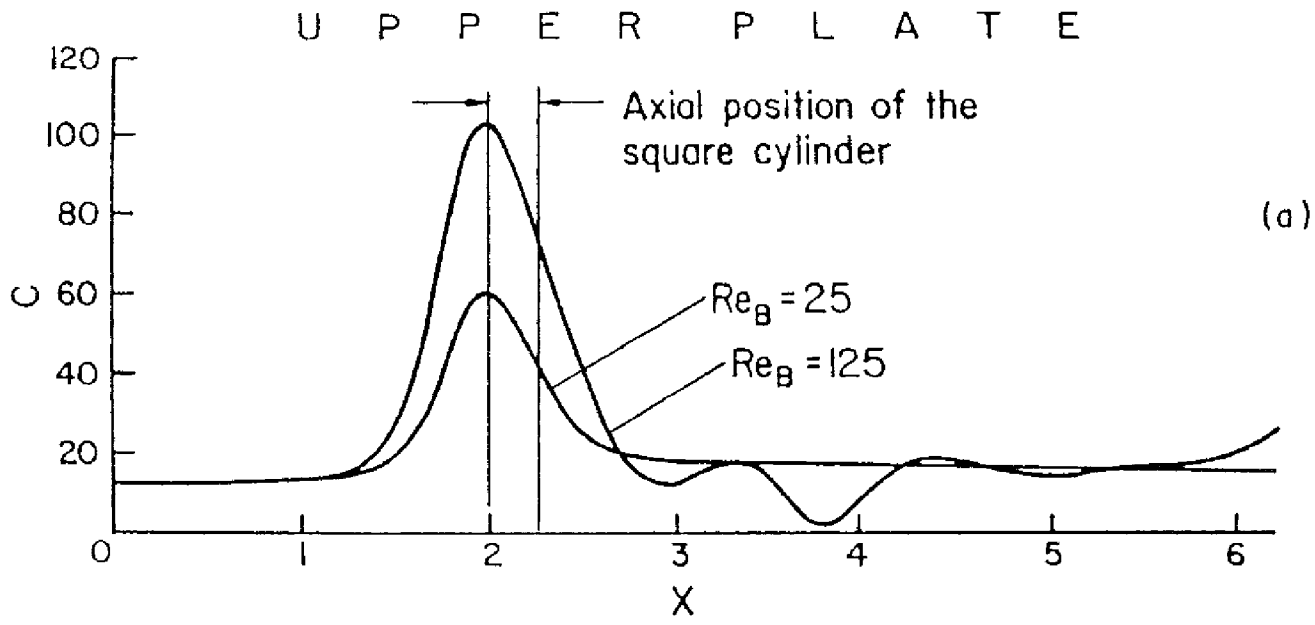
U P P E R P L A T E
120
100
80
C 60
40
20
0
1
2
3
4
5
6
X
Axial position of the square cylinder
(a)
$Re_B = 25$
$Re_B = 125$

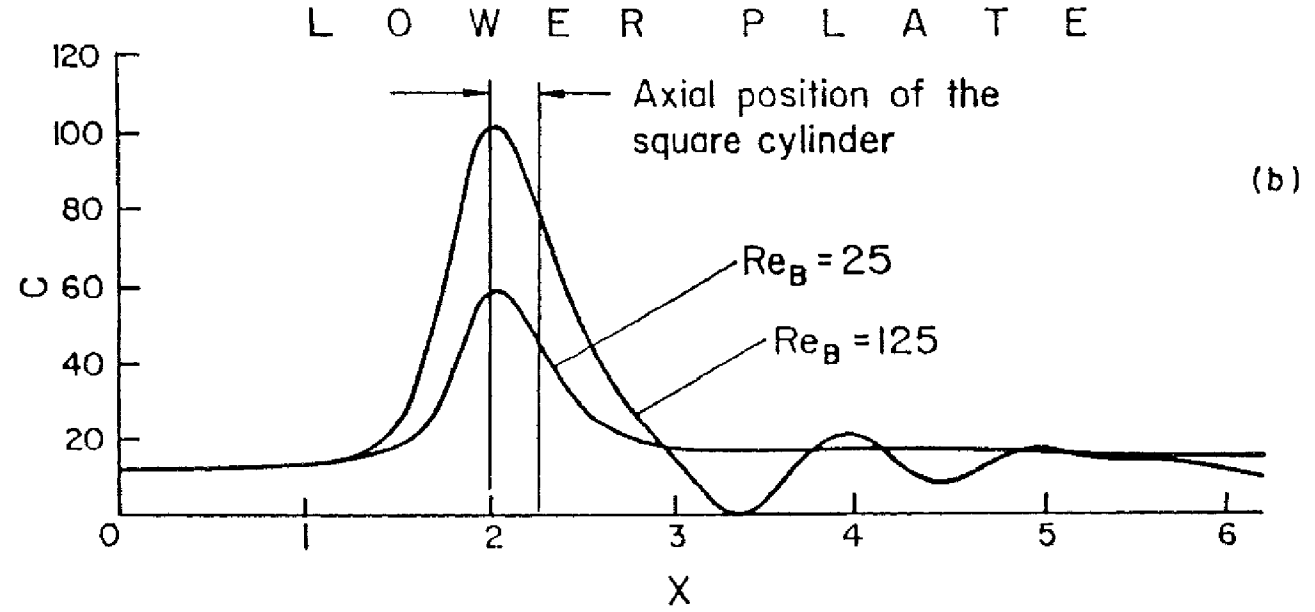
L O W E R P L A T E
120
100
80
C 60
40
20
0
1
2
3
4
5
6
X
Axial position of the square cylinder
(b)
$Re_B = 25$
$Re_B = 125$

observed on the lower plate. However, the trend may be vice-versa at another location (say, X ≈ 3.73) . This oscillating structure is damped gradually in the downstream of the cylinder.

4.5.4 Frequency (Strouhal Number) Characteristics of Vortex Shedding

Frequency (f) of vortex shedding was also measured by another technique. This technique borrows some idea from the measurements of Okajima [124]. We recorded the normal component of velocity at a position of 6 B behind the cylinder at y/H = 0.5 in the wake. For the steady flow, the flow smoothly divides and reunites around the cylinder. As a consequence, the normal component of velocity at the aforesaid location will be zero. However, for an unsteady periodic flow (so to speak, for high Reynolds numbers), the normal velocity component at the same location fluctuates. It is evident from Fig. 4.14(a) that the recorded signal of the fluctuating velocity in the wake results in a sinusoidal wave. The time period T can be calculated from such signal traces and the corresponding frequency f (= 1/T) and the Strouhal number S (= fB/Uav) can also be found out. Fig. 4.14(b) shows the oscillation of the lift coefficient for the same Reynolds number and geometrical configuration as those of Fig.4.14(a) . Strouhal numbers obtained in both the cases completely agree with each other (S = 0.164) .

Effect of blockage ratio on the variation of Strouhal number with Re_B is shown in Fig. 4.15. With increasing blockage ratio the value of Strouhal number increases. In all the cases, the Strouhal number undergoes a slight change with increasing Reynolds number.

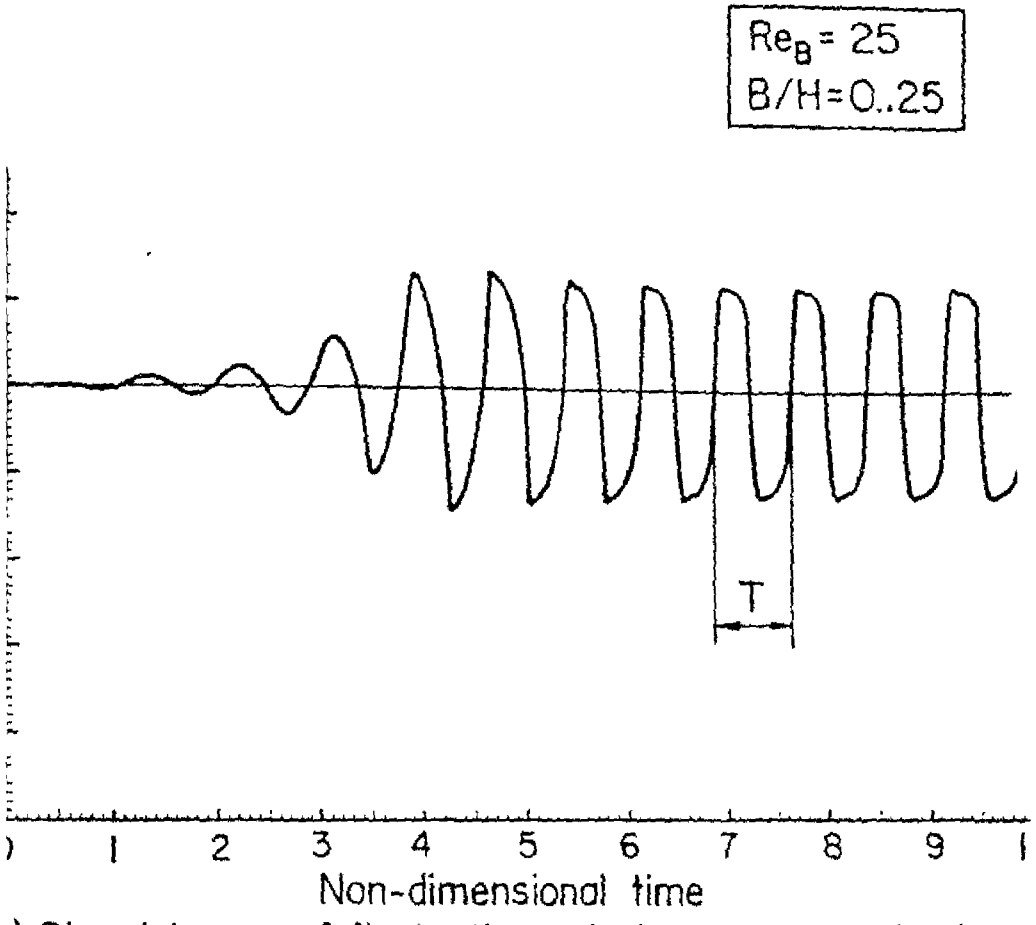

) Signal traces of fluctuating velocity component in the v

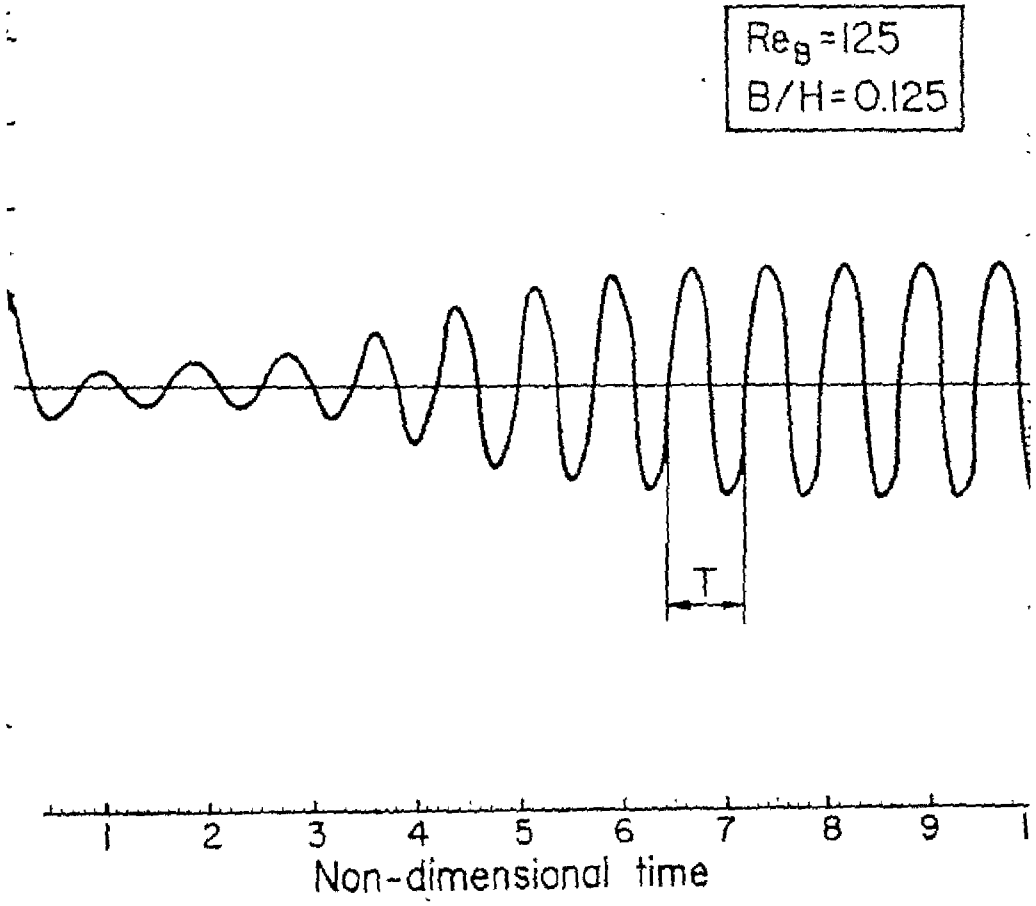

ig 4 14 (b) Time evo'ut'on of ft coeff c ent

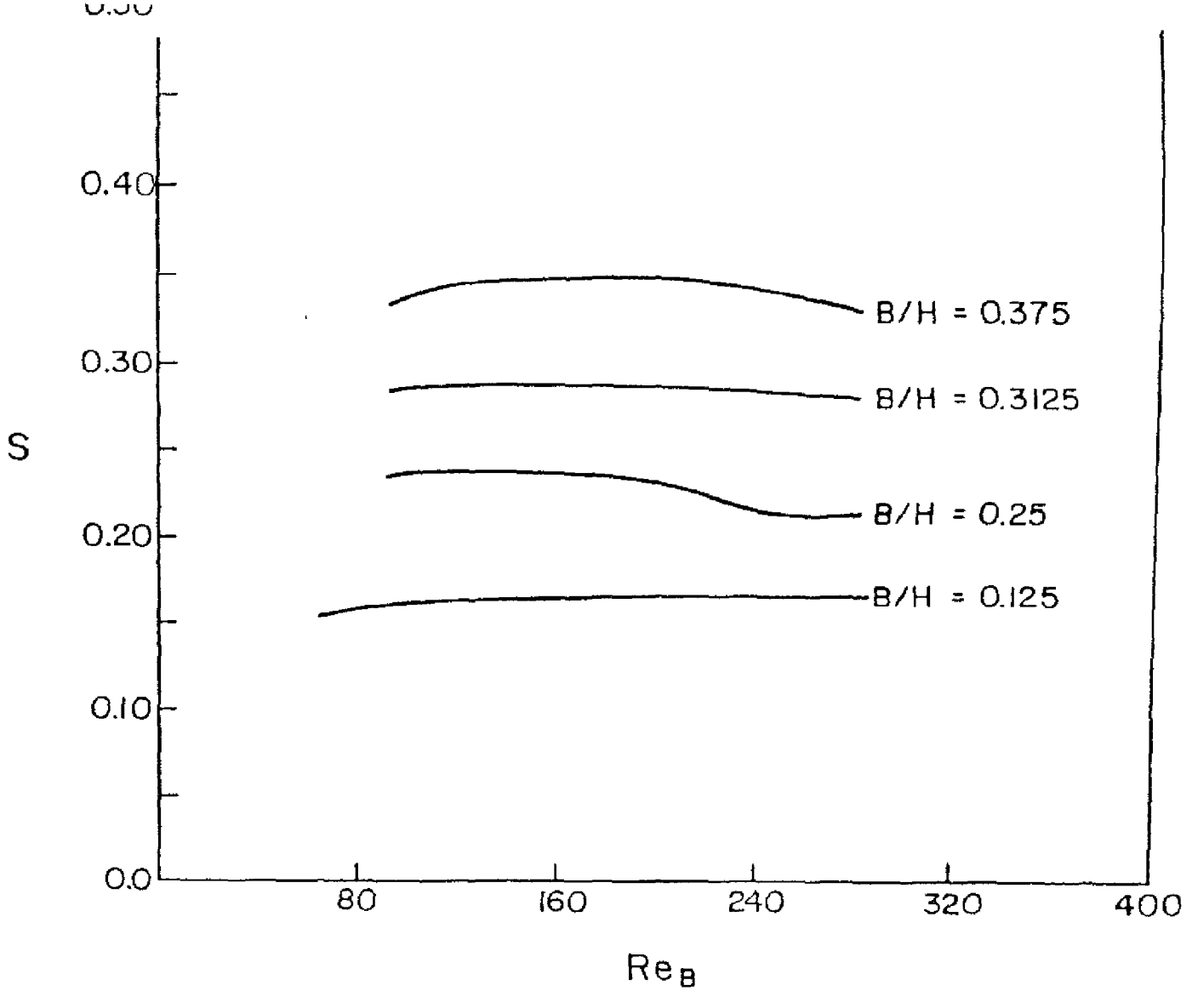

Fig 4.15 Effect of blockage ratio on variation of Strouhal number with Re_B

At a low Reynolds number, there is a steady reattachment behind the leading edge and the flow finally separates at the trailing edge which results in symmetrical vortices. At somewhat higher Reynolds number, after the separation at leading edge, the flow reattaches on either the upper or lower surface of the obstacle during alternate shedding of vortices into the stream. Further increase in Reynolds number, makes the separated flows detached from both the surfaces which eventually widens the wake accompanied by a relatively sharp change in Strouhal number. However, the range of Reynolds number at which the above-desired changes in the wake structure occur, depends upon the blockage ratio (see Figs. 4.6, 4.7, 4.15 and Table 4.1).

Table 4.1 also shows the Strouhal number calculations from two methods, namely, the signal traces of the fluctuating velocity components and the time-evolution of lift coefficients. The calculated values from both the methods agree with one another.

TABLE 4.1:

Strouhal number at different Reynolds number and Blockage Ratio

Obser No.	$Re_B = \frac{U_{av}B}{\nu}$	B/H	Strouhal Number (S=fB / Uav)	
			from time-evolution of lift-coefficient	from signal traces of fluctuating velocity
1	60	0.125	0.1521	0.1520
2	70	0.125	0.1551	0.1556
3	80	0.125	0.16	0.159
4	100	0.125	0.1623	0.162
5	125	0.125	0.164	0.164
6	200	0.125	0.1668	0.1669
7	300	0.125	0.167	0.167

Obser No.	$Re_B=\frac{UavB}{\nu}$	B/H	Strouhal Number (S=fB / Uav)	
			from time-evolution of lift-coefficient	from signal traces of fluctuating velocity
8	400	0.125	0.1672	0.1676
9	500	0.125	0.1672	0.1676
10	600	0.125	0.1674	0.1674
11	800	0.125	0.1651	0.1654
12	87	0.25	0.236	0.237
13	112	0.25	0.238	0.238
14	150	0.25	0.2384	0.2384
15	200	0.25	0.235	0.235
16	250	0.25	0.212	0.210
17	312	0.25	0.22	0.22
18	375	0.25	0.212	0.211
19	500	0.25	0.217	0.216
20	625	0.25	0.213	0.2128
21	87	0.3125	0.2845	0.2853
22	112	0.3125	0.2875	0.2887
23	150	0.3125	0.2913	0.2897
24	200	0.3125	0.2914	0.2886
25	250	0.3125	0.2885	0.2859
26	312	0.3125	0.2842	0.2778
27	87	0.375	0.3317	0.3316
28	112	0.375	0.3452	0.3454
29	150	0.375	0.3488	0.3489
30	200	0.375	0.3506	0.3511
31	250	0.375	0.3566	0.3423
32	312	0.375	0.3337	0.3203

Fig.4.16 compares the Strouhal number distribution with the experimental results of Okajima [124]. Strouhal numbers show continuous but slight change with Reynolds number . The present solution yields a somewhat higher Strouhal number for the entire

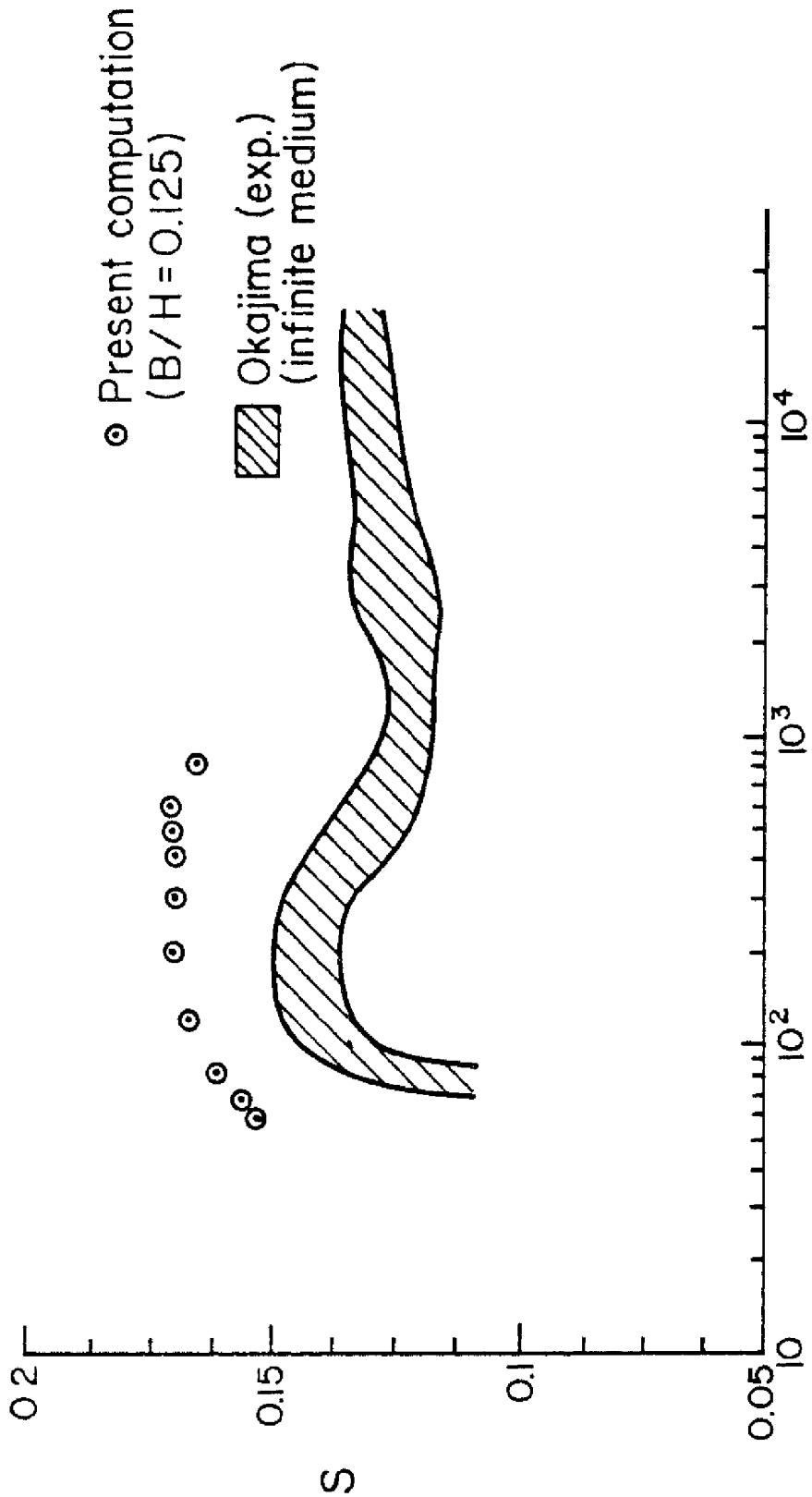

Fig 4.16 Variation of Strouhal number with Reynolds number for a square cylinder

range of Reynolds numbers. This discrepancy between the experimental and calculated results can be explained by noting that the experiments were done for a negligibly small blockage ratio. Although our predictions were done for a very small blockage ratio (B/H = 0.125), one may conjecture that the influence of side walls could not be completely ignored. The finite blockage might have brought about some change in Strouhal number.

The predicted fluctuating velocity signals were monitored at various other locations in the duct. The frequencies of oscillation for a particular situation (for a fixed Reynolds number and blockage ratio) at different spatial locations were found to agree with one another. In the far downstream the amplitude becomes so low that the oscillation becomes insignificant. Possibly because of this reason, in a long duct, von Karman vortex street is gradually damped out and a steady parabolic profile reappears near the exit.

Chapter-5

5. Study of Confined Wakes Behind a Circular Cylinder in a Channel

5.1 Introduction

The vortex structure in the wake of a circular cylinder in an infinite medium has been the subject of numerous theoretical investigations. These studies include semi-analytic solutions of Navier-Stokes equations for flow past a cylinder due to Patel [135,136], numerical studies of Thoman and Szewczyk [121], Lin et al [137], Fornberg [138] and Tuann and Olson [139]. Experimental investigations have also been undertaken to identify the structure of wake behind circular cylinder for different ranges of Reynolds number by Acrivos et al [119], Shair et al [120] and West and Apelt [140]. Coutanceau and Bouard [141,142] used a visualization method to obtain the main features of the flow field behind a circular cylinder in a tank. The change in the geometrical parameters describing the eddies with Reynolds number as well as the ratio between the diameters of the cylinder and the tank are presented. Their study also predicts the range of Reynolds numbers for which a closed wake exists and adheres stably to the cylinder. Braza et al [143] have computed the wake - zone - aerodynamics for incompressible flow past a circular cylinder using a second order accurate velocity-pressure formulation. They have discussed the interaction between the pressure and velocity fields over a range of Reynolds numbers, $100 \leq Re \leq 1000$. The method used is a predictor-corrector pressure scheme, similar to

that proposed by Amsden and Harlow [2] in SMAC. The vortex shedding was initiated by applying a physical perturbation imposed numerically for a short time. However, it has been recognized that there is very little information on the wake-structure when the cylinder is partially enclosed by side walls. Taneda et al [144] presented some observations of the flow past a circular cylinder towed through water near a plane wall. For a very small gap between the wall and the cylinder, they observed a single row of vortices are shed at a Reynolds Number of 170. Kiehm, Mitra and Fiebig [134] have solved full two and three dimensional Navier-Stokes equations behind a circular cylinder in a channel at different Reynolds numbers and blockage ratios. They have found the development of helical vortex tubes in the wake of a circular cylinder for three dimensional flows.

However, the primary purpose of our study is to see how our EXTRA-FLAG algorithm performs in a multiply connected complex geometry involving a rectangular channel with a circular cylinder kept in the middle. We also aim at determining the influence of channel walls on the wake flow behind the cylinder.

5.2.1 Flow Model

From the knowledge of flow past a cylinder in an infinite medium, it can be said that the existence of a wake bubble (Fig.5.1) behind the cylinder is usually observed for Re>5. The length of the wake bubble X_L grows with increasing Reynolds number. In an infinite medium, beyond a Reynolds number of 40, the wake loses it symmetry and vortex shedding starts. Although information on partially confined wake is limited, Shair et al [120] and Kiehm et al [134] have shown that the critical Reynolds

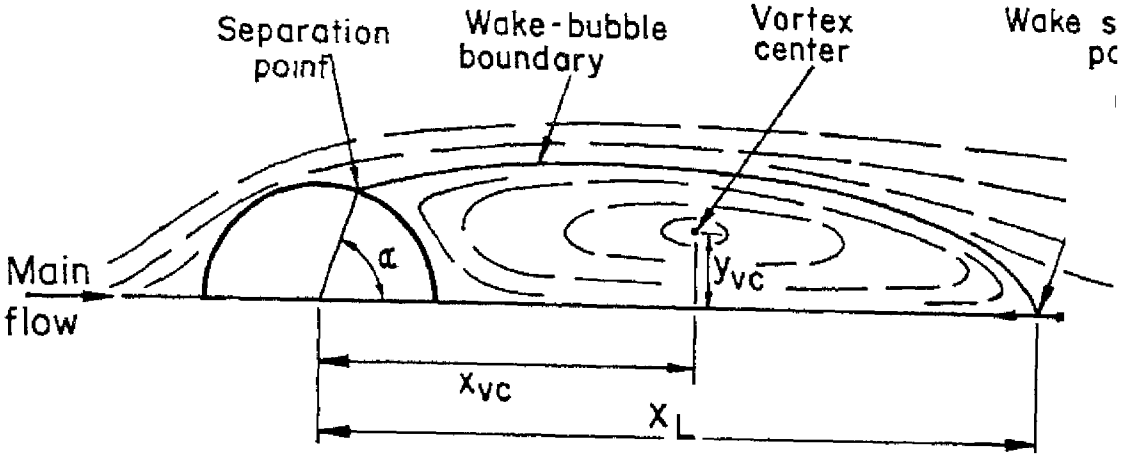

5.1 Steady separated flow past a circular cylinder

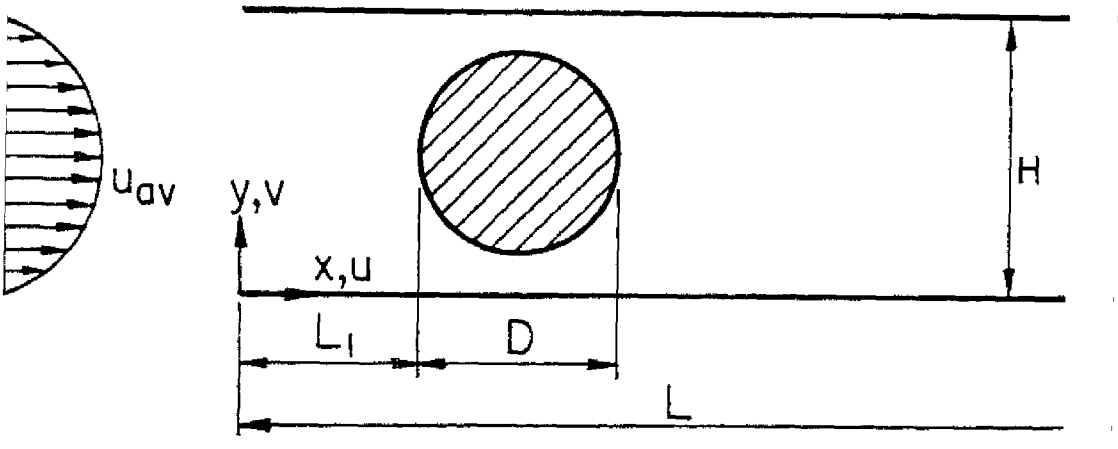

5.2 Configuration definition for 2-D flow in a cha
with built-in circular cylinder.

number at which periodicity starts, grows with increasing blockage ratio (which is defined by the ratio of diameter of the cylinder to height of the channel).

Arising out of the above mentioned observations and the existing knowledge from open literature we recognize that the flow field around a circular cylinder in a channel is characteized by the following parameters

- the Reynolds number
- the blockage ratio (D/H), and
- the velocity profile at the channel inlet.

Consequently, a computational domain which consists of two solid walls with no-slip conditions and a circular cylinder between these walls, is selected as shown in Fig.5.2. No-slip and impervious boundary conditions are applied on the whole surface of the circular cylinder. At the inlet of the channel, parabolic profile for the axial velocity has been deployed and the transverse component of the velocity has been taken as zero. At the exit of the channel, second derivatives of the velocity components in the flow direction have been set equal to zero. This ensures smooth transition of flow through the outflow boundary.

5.2.2 Basic Equations

The basic equations to be solved for the calculation of the laminar incompressible flow are the mass-conservation and the time-dependent Navier-Stokes equations with primitive variables. In nondimensional form these are expressed as equations (2.47), (2.48) and (2.49) [see chapter-2]. The Reynolds number is defined by $Re_D = \frac{\rho U_{av} D}{\mu}$ where U_{av} stands for the average velocity at the

channel inlet and D denotes the cylinder diameter.

5.2.3 Method of Solution

EXTRA-FLAG algorithm is employed to obtain numerical solutions of the flow equations. For the implementation of numerical solution, the computational domain (Fig.5.2) is divided into a number of cells (see Fig.5.3(a)). Fig.5.3(b) shows an enlarged portion of the mesh highlighting the zone surrounding the cylinder.A (99x33) grid is used for computation. The velocity components are collocated and they are defined at the vertices of the cells while the pressure has been defined at the centre of the cell. The details of solution procedure have been outlined in chapter-2. Upwinding was used in the evaluation of convection terms. However, our way of handling convective kinematics has already been mentioned in Chapter-4. We are not mentioning anything more on the algorithm for brevity.

5.3 Results and discussion

Computations were performed at Reynolds numbers of 87, 112 and 625 for the blockage ratio of 0.25. It may be mentioned that for none of the above mentioned cases steady state solution could be obtained. However, the solutions were identified as unsteady periodic. Periodicty was characterized by the vortex shedding frequency which was obtained from the signal tracing of the transverse velocity components at a location 6D behind the cylinder on the centre-line of the channel. As pointed out in chapter-4, this technique borrows the idea from the experimental frequency-determination technique of Okajima [124]. However, for

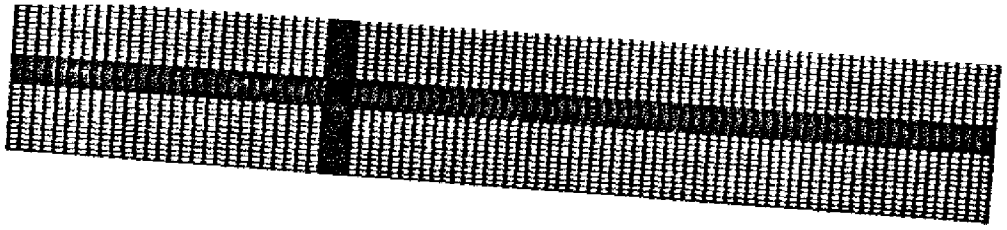

(a)

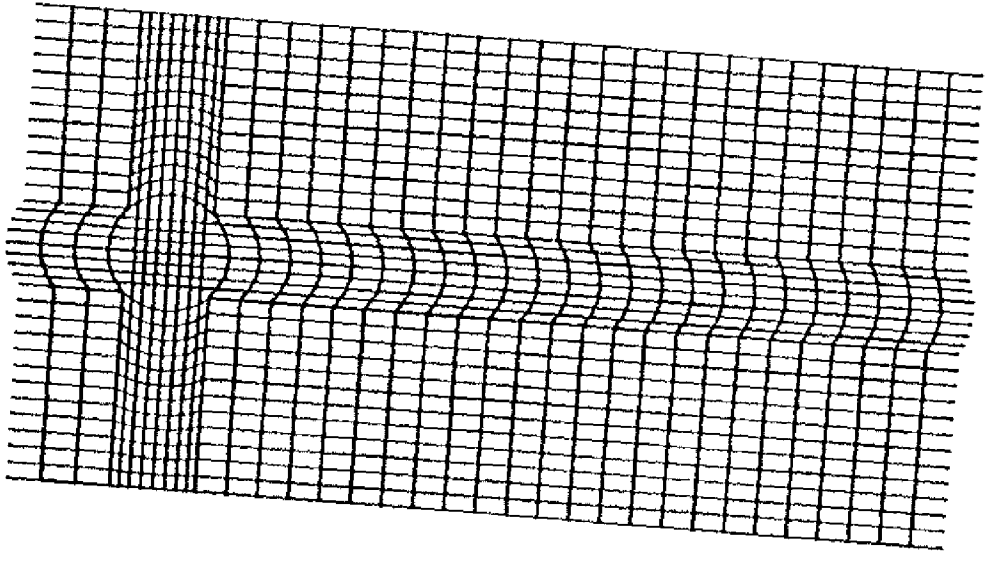

(b)

Fig.5.3 Mesh grid in the computational domain

the first two circumstances (Re_D = 87 and 122), the Strouhal numbers (non-dimensional frequency) were very close to each other with a magnitude of 0.2341 while for Re_D = 625 the Strouhal number was 0.2409.

Fig.5.4 shows the velocity vectors in a channel with built-in circular cylinder for a Reynolds number of 122. The flow has become periodic in the near wake. The periodicity is suppressed in the downstream of the cylinder by the channel walls and the flow at the exit of the channel again assumes an almost parabolic profile.

Fig.5.5 shows the streamlines crossing the cylinder in a duct at a Reynolds number 112. Alternate shedding of vortices and initiation of von Karman vortex street is quite evident from the figure.

Fig.5.6 shows the streamlines in a channel with built-in circular cylinder for a Reynolds number 625. Formation of von Karman vortex street is clearly seen in this figure. With an increase in Reynolds number, the periodicity of the wake becomes more prominent. It can also be appreciated that despite the damping influence of side walls, the undulation of the wake is not completely suppressed in the downstream.

However, the primary purpose of taking up this problem was to test the capability of EXTRA-FLAG algorithm. After analyzing the presented results, possibly it can be said that in the range of Reynolds number studied in this problem, the algorithm works satisfactorily. The study of wake structure for flow past a circular cylinder is indeed a difficult problem. As far as flow physics is concerned, we do not intend to draw any conclusion from

D/H = 0.25

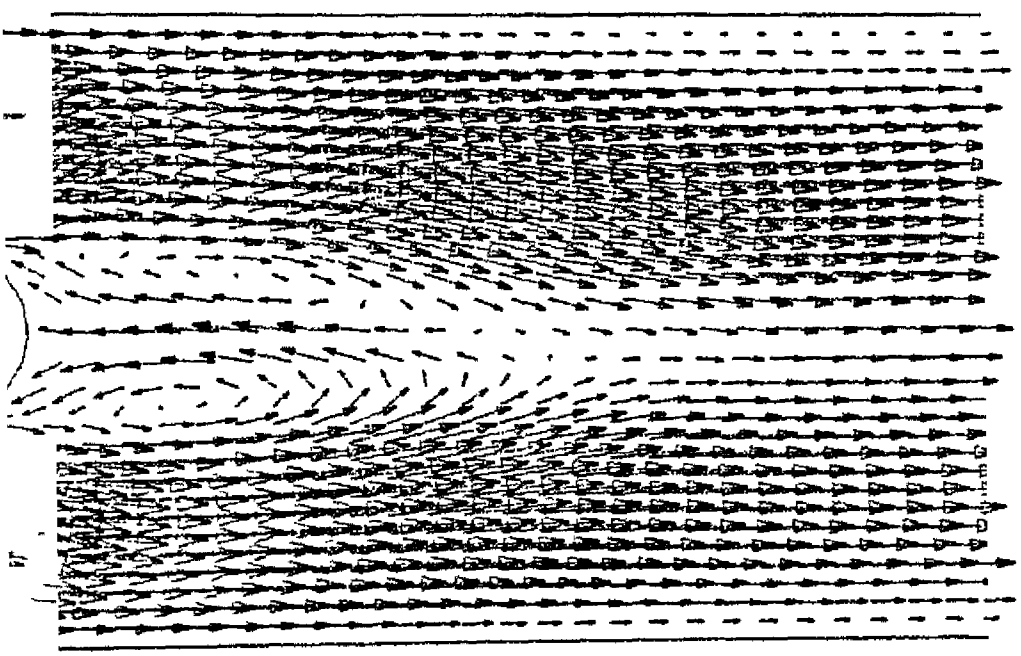

Velocity vectors in a channel with built in circular cylinder, $Re_D = 112$

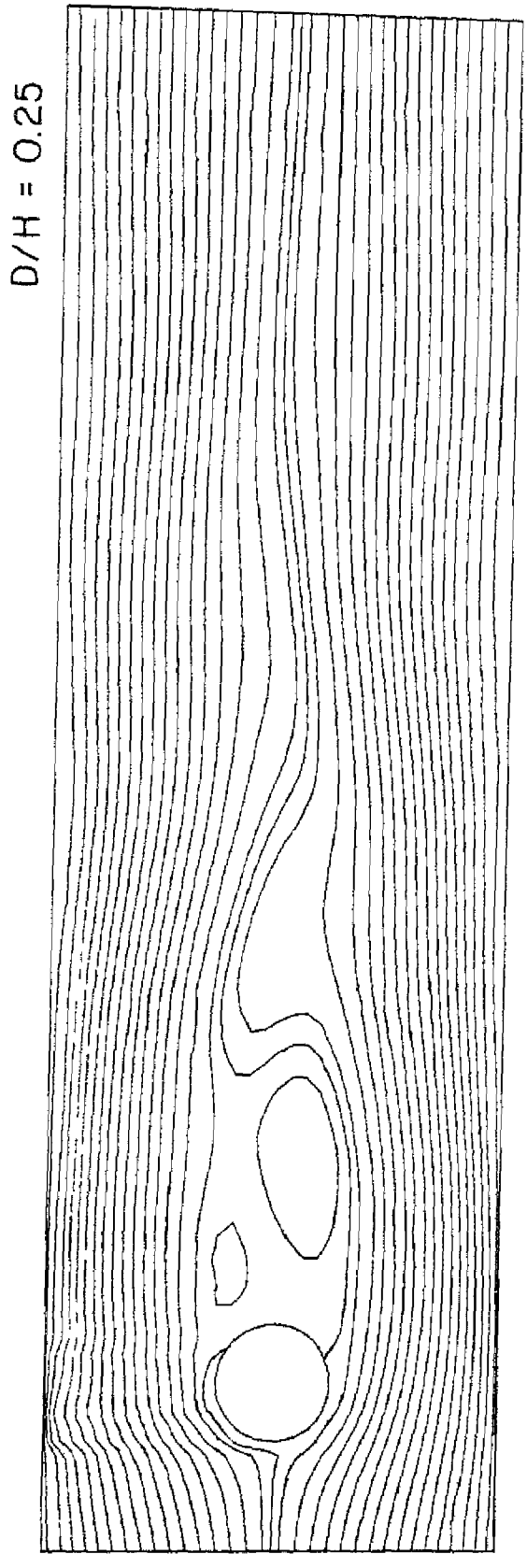

Fig5.5 Streamlines crossing the cylinder in a duct, $Re_D = 112$

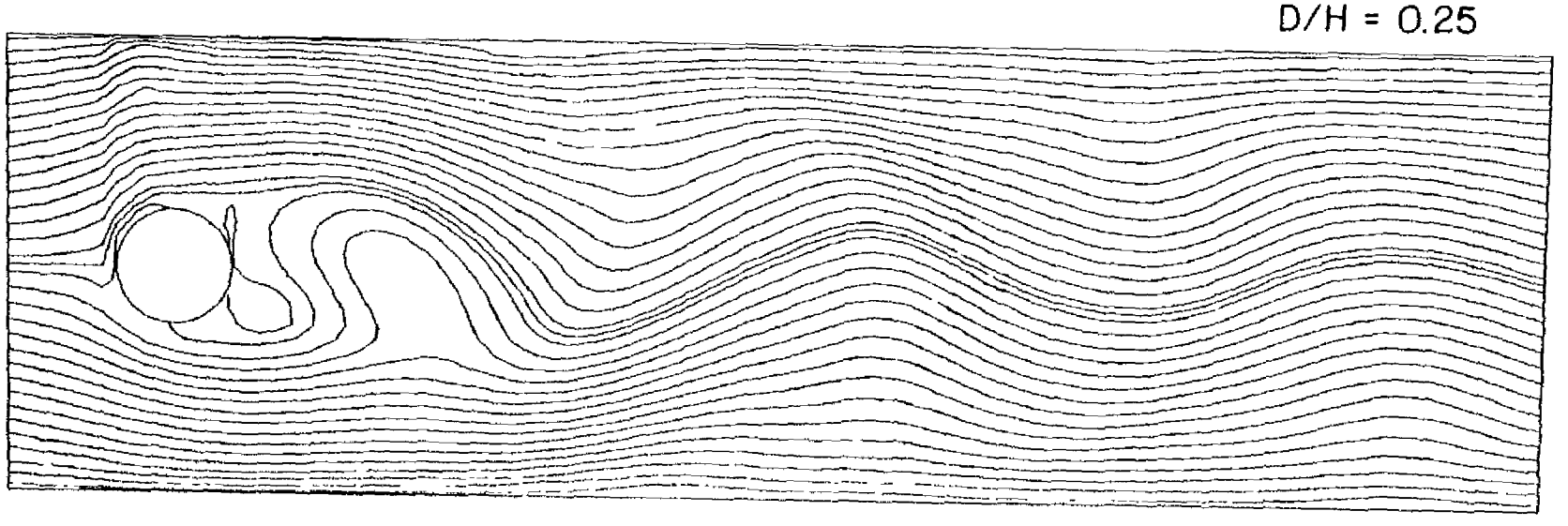

Fig5.6 Streamlines crossing the cylinder in a duct, $Re_D = 625$

our brief study. The formidable task of the detailed simulation of this complex problem may be identified as the scope for future extension.

1. Harlow F.H. and Welch J.E.,"Numerical Calculation of Time-Dependent Viscous Incompressible Flow of Fluid with Free Surface",The Phys Fluids, vol 8,pp 2182-2188,1965.

2. Harlow F.H. and Amsden A.A., "The SMAC Method: A Numerical Technique for Calculating Incompressible Fluid Flows",Los Alamos,Scientific Lab. Rept LA 4370, 1970.

3. Chorin A.J., "A Numerical Method for Solving Incompressible Viscous Flow Problems",J. Comp.Phys., vol 2, pp 12-26, 1967.

4. Viecelli J.A., "A Computing Method for Incompressible Flows Bounded by Moving Walls", J. Comp. Phys. vol 8, pp 119-143,1971.

5. Hirt C.W. and Cook J.L., "Calculating Three Dimensional Flows Around Structures and Over Rough Terrain", J. Comp. Phys., vol 10,pp 324-340, 1972.

6. Patankar S.V. and Spalding D.B.,"A Calculation Procedure for Heat Mass and Momentum Transfer in Three Dimensional Parabolic Flows ",Int. J. Heat Mass Trans, vol 15, pp 1787-1806, 1972.

7. Patankar S.V. , Numerical Heat Transfer and Fluid Flow, Hemisphere, Washington D.C., 1980.

8. Patankar S.V.,"A Calculation Procedure for Two Dimensional Elliptic Situations",Numerical Heat Transfer, vol 4, pp 409-425,1981.

9. VanDoormaal J.P. and Raithby G.D.," Enhancements of the SIMPLE Method for Predicting Incompressible Fluid Flows, Numerical heat Transfer, vol 7,pp 147-163, 1984.

10. Jang D.S., Jetli R. and Acharya S.," Comparison of PISO, SIMPLER and SIMPLEC Algorithms for the Treatment of the Pressure Velocity Coupling in Steady Flow Problems", Numerical Heat transfer, vol 10, pp 209-228, 1986.

11. Issa R.I.,Gosman A.D. and Watkins A.P.,"The Computation of Compressible and Incompressible Recirculating Flows by a Non-iterative Implicit Scheme", J.Comp.Phys., vol 62, pp 66-82, 1986.

12. Thom A. and Apelt C.J.,"Field Computation in Engineering and Physics", Van Nostrand, London, 1961.

13. Burggraf O.R.,"Analytical and Numerical Studies of the Structure of Steady Separeted Flows",J.Fluid Mech.,vol 24,pp 113-151,1966.

14. Courant R., Isaacon E. and Rees M., "On the Solution of Nonlinear Hyperbolic Differential Equations by Finite Differences", Comm. Pure Appl. Meth., vol 5, pp 243-255 1952.

15. Torrance K.E., "Comparison of Finite Difference Computations of Natural Convection",J. Res. N.B.S., vol 72b, pp 281-301, 1968.

16. Roache P.J., "Computational Fluid Dynamics", Hermosa Publ., Albuquerque,New Mexico, 1972.

17. Roache P.J.,"On Artificial Viscosity", J. Comp.Phys., vol 10, pp 169-184,1972.

18. Roberts K.V. and Weiss N.O.,"Convective Difference Schemes",Math. Comp., vol 20,pp 272-299,1966.

19. Bozeman J.D. and Dalton C., "Numerical Study of Viscous Flow in a Cavity",J.Comp. Phys., vol 12, pp 348-363, 1973.

20. De Allen N. G. and Southwell R.V., "Relaxation Methods Applied to Determine the Motion, in two Dimensions, of a Viscous Fluid, Past a Fixed Cylinder", Q.J. Appl. Math., vol 8,pp 129-145, 1955.

21. Spalding D.B.,"A Novel Finite Difference Formulation for Differential Expressions Involving Both first and Second Derivatives",Int. J. Numer Methods Eng., vol 4, pp 551-559, 1972.

22. Raithby G.D. and Torrance K.E., "Upstream Weighted Schemes and Their Application to Elliptic Problems Involving Fluid Flow", Comput Fluids, vol 2, 191-206, 1974.

23. Vanka S.P., Chen B.C.J. and Sha W.T., "A Semi Implicit Calculation Procedure for Flows Described in Boundary-Fitted Coordinate Systems", Numerical Heat Transfer, vol 3, pp 1-19, 1980.

24. Prakash C., "An Improved Control Volume-Finite-Element Methodfor Heat and Mass Transfer and For Fluid Flow Using Equal Order Velocity-Pressure Interpolation", Numerical Heat Transfer, vol 9, pp 253-276, 1986.

25. Prakash C. and Patankar S.V., "A Control Volume-Finite-Element Method for Predicting Flow and Heat Transfer in Ducts of Arbitrary Cross Sections,Part I - Description of The Method", Numerical Heat Transfer, vol 12, pp 389-412, 1987

26. Prakash C. and Patankar S.V., "A Control Volume-Finite-Element Method for Predicting Flow and Heat Transfer in Ducts of Arbitrary Cross Sections,Part II - Application to Some Test Problems", Numerical Heat Transfer, vol 12, pp 413-437, 1987.

27. Baliga B.R., Pham T.T. and Patankar S.V., "Solution of Some Two Dimensional Incompressible Fluid Flow and Heat Transfer Problems, Using a Control Volume-Finite-Element Method",Numerical Heat Transfer, vol 6, pp 263-282, 1983.

28. Raithby G.D., "A Critical Evaluation of Upstream Differencing Applied to Problems Involing Fluid Flow", Comput Methods Appl. Mech. Eng., vol 9, pp 75-103, 1976.

29. Raithby G.D., "Skew Upstream Differencing Schemes for Problems Involving Fluid Flow", Comput Methods Appl. Mech. Eng., vol 9, pp 153-164, 1976.

30. Schneider G.E. and Raw M.J., "A Skewed Positive Influence Coefficient Upwinding Procedure for Control Volume Based Finite Element Convection Diffusion Computation", Numerical Heat Transfer, vol 9 , pp 1-26, 1986.

31. Hassan Y.A., Rice,J.G., and Kim J.H., "A Stable Mass Flow Weighted Two Dimensional Skew Upwind Scheme", Numerical Heat Transfer, vol 6, pp 395-408, 1983.

32. Runchal A.K., "CONDIF : A Modified Central Difference Scheme for Convective Flows", Int. J. Numer Methods Eng., vol 24, pp 1593-1608, 1987.

33. Galpin P.F. and Raithby G.D., "Treatment of Nonlinearities in The Numerical Solution of the Incompressible Navier Stokes Equations", Int. J. Numer Methods Eng., vol 6, pp 409-426, 1986.

34. Pollard A. and Siu L.W.A., "The Calculation of Some Laminar Flows Using Various Discretization Schemes", Comput Methods Appl. Mech. Eng., vol 35, pp 293-313, 1982.

35. de Vahl Davies,G., and Mallinson G.D., "An Evaluation of Upwind and Central Difference Approximations by Study of Recirculating Flows", Comput Fluids, vol 4, pp 29-43, 1976.

36. Leonard B.P., "Newsflash : Upstream Parabolic Interpolation ", Proc of 2nd GAMM Conf on Numer Methods in Fluid Mech. , Koln, Germany, 1977.

37. Leonard B.P., "A Stable and Accurate Convective Modelling Procedure Based On Quadratic Upstream Interpolation", Comput Methods Appl. Mech. Eng., vol 19, pp 59-98, 1979.

38. Leonard B.P., "A Survey of Finite Differences with Upwinding for Numerical Modelling of Incompressible Convective Diffusion Equation", Recent Advancaes in Numer Methods in Fluids, vol 2, Ed. C. Taylor, Pineridge Press, England , 1981.

39. Ham T., Humphrey J.A.C. and Launder B.E., "A Comparison of Hybrid and Quadratic Upstream Differencing in High ReynoldsNumber Elliptic Flow", Comput Methods Appl. Mech. Eng., vol 29, pp 81-95, 1981.

40. Leschziner M.A. and Rodi W., "Calculation of Annular and Twin Parallel Jets Using Various DiscretizationSchemes and Turbulence Model Variants", ASME J.of Fluids Eng.,vol 103, pp 352-360, 1981.

41. Shyy W., "A Study of Finite Difference Approximations to Steady State ,Convection Dominated Flow Problems", J. Comp. Phys, vol 57, pp 415-438, 1985.

42. Raithby G.D.,Galpin P.F.and VanDoormaal,J.P., "Prediction of Heat and Fluid Flow in Complex Geometries Using General Orthogonal Coordinates", Numerical Heat Transfer, vol 9, pp

125-142, 1986.

43. Tao W.Q.and Sparrow E.M., "The Transportive Property and Convective Numerical Stability of The Steady State Convection Diffusion Finite Difference Equation", Numerical Heat Transfer, vol 11, pp 491-497 , 1987.

44. Patel M.K., Markatos N.C. and Cross M., "A Critical Evaluation of Seven Discretization Schemes for Convection Diffusion Equations", Int J Numer Methods Fluids, vol 5, pp 225-244, 1985.

45. Patel M.K., Markatos N.C. and Cross M., "Method of Reducing False Diffusion Errors in Convection Diffusion problems", Appl. Math. Modelling, vol 9 , pp 302-306, 1985.

46. Vanka S.P., "Second-Order Upwind Differencing in a Recirculating Flow", AIAA J., vol 25, pp 1435-1441, 1987.

47. Wilkes N.S. and Thompson C.P., "An Evaluation of Higher Order Upwind Differencing For Elliptic Flow Problems", Numer Methods in Laminar and Turbulent Flows, Pineridge Press, England, pp 248-257 1983.

48. Atias M., Wolfshtein M. and Israeli M., "Efficiency of Navier Stokes Solvers", AIAA J., vol 15, pp 263-265, 1977.

49. Gresho P.M. and Lee R.L., "Don't Suppress the Wiggles - They are Telling You Something!", Comput Fluids, vol 9 , pp 223-253, 1981.

50. Barrett K., "Super-Upwinding - Elements of Doubt and Discrete Differences of Opinion on The Numerical Muddling of the Incomprhensible Defective Confusion Equation (Title Inspired by B P Leonard)", J Caldwell and A O Moscardini (Eds ,

Numerical Modelling in Diffusion Convection, Pentech Press, London, 1982.

51. Christie I., Griffiths D.F., Mitchell A.R. and Zienkiewicz O.C., "Finite Element Methods for Second Order Differential Equations with Significant First Derivatives", Int. J. Numer Methods Eng., vol 10, pp 1389-1396, 1976.

52. Heinrich J.C. and Zienkiewicz O.C., "Quadratic Finite Element Schemes for Two Dimensional Convective Transport Problems", Int. J. Numer Methods Eng., vol 11, pp 1831-1844, 1977.

53. Huyakom P.A., Taylor C., Lee R.L. and Gresho P.M., "A Comparison of Various Mixed Interpolation Finite Elements in The Velocity-Pressure Formulation of The Navier Stokes Equations", Comput Fluids, vol 6, pp 25-35, 1978.

54. Sani R.L., Gresho P.M., Lee R.L. and Griffiths D.F., "The Cause and Cure(?) of the Spurious Pressures Generated by Certain FEM Solutions of the Incompressible Navier Stokes Equations : Part I", Int.J. Numer Methods Fluids , vol 1, pp 17-43, 1981.

55. Donea J. and Guilliani S., "A Simple Method to Generate High Order Accurate Convection Operators for Explicit Schemes Based on Linear Finite Elements", Int. J. Numer Methods Fluids, vol 1, pp 63-80, 1981.

56. Kato Y.,Kawai H. and Tanahashi T., "Numerical Flow Analysis in a Cubic Cavity by The GSMAC Finite Element Method (In The Case Where The Reynolds Numbers are 1000 and 3200)", JSME Int. J. ,vol 33, pp 649-658, 1990.

57 Hung T K and Brown T D , "An Implicit Finite Difference

Method for Solving the Navier Stokes Equations Using Orthogonal Curvilinear Coordinates", J. Comp. Phys, vol 23, pp 343-363, 1977.

58. Pope S.B., "The Calculation of Turbulent Recirculating Flows in General Orthogonal Coordinates", J. Comp. Phys, vol 26, pp 197-217, 1978.

59. Gosman A.D. and Rapley C.W., "Fully Developed Flow in Passages of Arbitrary Cross-section ", Recent Advances in Numerical Methods in Fluids, C. Taylor and K. Morgan (Eds), Pineridge Press, Swansea, 1980.

60. Rapley C.W., "Turbulent Flow in a Duct with Cusped Corners", Int. J. Numer Methods Fluids, vol 5, pp 155-167, 1985.

61. Habib M.A. and Whitelaw J.H., "The Calculation of Turbulent Flow in Wide Angle Diffusers", Numerical Heat Transfer, vol 5, pp 145-164, 1982.

62. Rastogi A.K., "Hydrodynamics in Tubes perturbed by Curvilinear Obstructions", ASME J. Fluids Engineering, vol 106, pp 262-269, 1984.

63. Lawal A. and Majumdar A.S., "Laminar Flow and Heat Transfer in Power law Fluids Flowing in Arbitrary Cross-sectional Ducts", Numerical Heat Transfer, vol 8, pp 217-244, 1985.

64. Gal-Chen T. and Somerville R.C.J., "Numerical Solution of the Navier Stokes Equations with Topography", J. Comp. Phys, vol 17, pp 276-310, 1975.

65. Faghri M., Sparrow E.M. and Prata A.T., "Finite Difference Solutions of Convection Diffusion Problems in Irregular Domains using a Nonorthogonal Coordinate Transformation",

Numerical Heat Transfer, vol 7, pp 183-209, 1984.

66. Thames F.C., Thompson J.F., Mastin C.W. and Walker R.L., "Numerical Solutions for Viscous and Potential Flow about Arbitrary Two Dimensional Bodies Using Body-fitted Coordinate Systems", J. Comp. Phys, vol 24, pp 245-273, 1977.

67. Thompson J.F.,Warsi Z.U.A. and Mastin C.W., "Boundary Fitted Coordinate System for Numerical Solution of partial Differential Equations - A Review", J. Comp. Phys, vol 47, pp1-108, 1982.

68. Steger J.L. and Sorenson R.L., "Autoamtic Mesh Point Clustering Near a Boundary in Grid Generation with Elliptic Partial Differential Equations",J. Comp. Phys, vol 33, pp 405-410, 1979.

69. Sorenson R.L. and Steger J.L., "Numerical generation of Two Dimensional Grids by The Use of Poisson Equations with Grid control at Boundaries", Numerical Grid Generation Techniques, NASA Conf Pub, 2166 , 1980.

70. Maliska C.R. and Raithby G.D., "A Method for Computing Three Dimensional Flows Using Non-Orthogonal Boundary Fitted Coordinates", Int. J. Numer Methods Fluids, vol 4, pp 519-537, 1984.

71. Shyy W., Tong S.S. and Correa S.M., "Numerical Recirculating Flow Calculation Using a Body Fitted Coordinate System", Numerical Heat Transfer, vol 8, pp 99-113, 1985.

72. Acharya S. and Patankar S.V., "Use of an Adaptive Grid Procedure for Parabolic Flow Problems", Int. J. Heat Mass Trans, vol 28, pp 1057-1066, 1985.

73. Patel N.R. and Briggs D.G., "A MAC Scheme in Boundary Fitted Curvilinear Coordinates", Numerical Heat Transfer, vol 6, pp 383-394, 1983.

74. Karki K.C., and Patankar S.V., " Solution of Some Two-Dimensional Incompressible Flow Problems Using A Curvilinear Coordinate System Based Calculation Procedure",Numerical Heat Transfer, vol 14, pp 309-321, 1988.75. Hsu C.F., "A Curvilinear Coordinate Method for Momentum Heat and Mass Transfer in domains of Irregular Geometry", Ph.D. Thesis, Univ Minnesota, 1981.

76. Prakash C., "A Finite Element Method for Predicting Flow Through Ducts with Arbitrary Cross Sections", Ph.D. Thesis, Univ Minnesota, 1981.

77. Rhie C.M., "A Numerical Study of Flow Past an Isolated Airfoil with Separation", Ph.D. Thesis, Univ Illinois, Urbana-Champaign, 1981.

78. Rhie C.M. and Chow W.L., "Numerical Study of The Turbulent Flow Past an Airfoil with Trailing Edge Separation", AIAA J., vol 21, pp 1525-1532, 1983.

79. Rhie C.M., Delaney R.A.and McKain T.F., "Three Dimensional Viscous Flow Analysis for Centrifugal Impellers",AIAA-84-1296, 1984.

80. Peric M., "A Finite Volume Method for the Prediction of Three Dimensional Fluid Flow in Complex Ducts", Ph.D. Thesis, Univ. of London, 1985.

81. Burns A.D., Wilkes N.S., Jones I.P. and Kightley J. R., "FLOW3D : Body Fitted Coordinates, Atomic Energy Research

Establishment, Harwell, U.K., Report no. AERE-R-12262, 1986.

82. Reggio M. and Camarero R., "Numerical Solution Procedure for Viscous Incompressible Flows", Numerical Heat Transfer, vol 10, pp 131-146, 1986.

83. Bernard R.S. and Thompson J.F., "Mass Conservation on Regular Grids for Incompressible Flow", AIAA-84-1669, 17thFluid Dynamics, Plasma Dynamics and LASER Conference, 1984.

84. Peric M., Kessler R. and Scheuerer G., "Comparison of Finite Volume Numerical Methods with Staggered and Colocated Grids", Comput. and Fluids, vol 16, pp 389-403, 1988.

85. Miller T.F. and Schmidt F.W., "Use of a Pressure-Weighted Interpolation Method for The Solution of The Incompressible Navier Stokes Equations on a Non-staggered Grid System", Num Heat Trans, vol 14, pp 213-233, 1988.

86. Majumdar S., "Development of a Finite Volume Procedure for Prediction of Fluid Flow Problems with Complex Irregular Boundaries", Technical Report, SFB 210/T/29, December,1986.

87. Majumdar S., Rodi W. and Vanka S.P., "On The Use of Non-Staggered Pressure-Velocity Arrangement for Numerical Solution of Incompressible Flows", Technical Report, SFB 210/T/35, November,1987.

88. Majumdar S., "Role of Under Relaxation in Momentum Interpolation for Calculation of Flow with Non-staggered Grids", Numerical Heat Transfer, vol 13, pp 125-132, 1988.

89. Williams M., "Methods for Calculating Incompressible Viscous Flows", Numerical Heat Transfer, vol 20, pp 241-253, 1991.

90. Baliga B.R. and Patankar S.V., "A Control Volume Finite

Element Method for Two Dimensional Fluid Flow and Heat Transfer", Numerical Heat Transfer, vol 6, pp 245-261, 1983.

91. Muir B.L. and Baliga B.R., "Solution of Three Dimensional Convection Diffusion Problems Using Tetrahedral Elements and Flow Oriented Upwind Interpolation Functions", Numerical Heat Transfer, vol 9, pp 143-162, 1986.

92. Oden J.T., "Finite Elements of Non Linear Continua", Mc-Graw Hill, NY, 1972.

93. Olson M.D., "Formulation of a Variational Principle-Finite Element Method for Viscous Flows", Proc. Variational Methods in Engineering, Southampton Univ, pp 5.27-5.38, 1972.

94. Baker A.J., "Finite Element Solution Algorithm for Viscous Incompressible Fluid Dynamics", Int. J. Numer Methods Eng., vol 16, pp 89-101, 1973.

95. Taylor C. and Hood P., "A Numerical Solution of Navier Stokes Equations Using Finite Element Technique", Comput Fluids, vol 1, pp 73-100, 1973.

96. Zienkiewicz O.C., "Constrained Variational Principles and Penalty Function Methods in Finite Element Analysis", in G.A. Watson (Ed), Lecture Notes in Mathematics : Conf on the Num Soln of Diff Eqns, Springer-Verlag, Berlin, pp 207-214, 1974.

97. Reddy J.N., "On Penalty Function Methods in Finite Element Analysis of Flow Problems", Int. J. Numer Methods Fluids, vol 2, pp 151-171, 1982.

98. Zienkiewicz O.C., Taylor R.L. and Too J.M., "Reduced Integration Technique in General Analysis of Plates and

Shells", Int. J. Numer Methods Eng., vol 3, pp 575-586,1971.

99. Reddy J.N., "On The Accuracy and Existance of Solutions to Primitive Variable Models of Viscous Incompressible Fluids", Int. J. Eng. Sci, vol 6, pp 921-929, 1978.

100. Tuann S. and Olson M.D., "A Transient Finite Element Solution Method for The Navier Stokes Equations", Comput Fluids, vol 6, pp 141-152, 1978.

101 Taylor C. and Hughes T.G., "Finite Element Programming of The Navier Stokes Equations", Pineridge Press, Swansea, UK, 1981.

102 Comini G. and Del Giudice S., "Finite Element Solution of the Incompressible Navier-Stokes Equations", Numerical Heat Transfer, vol 5, pp 463-478, 1982.

103 Smith S.L. and Brebbia C.A., "Finite Element Solution of Navier-Stokes Equations for Transient Two-Dimensional Incompressible Flow", J. Comp. Phys., vol 17, pp 235-245, 1975.

104 Hood P. and Taylor C., "Navier-Stokes Equations Using Mixed-Interpolation, in Finite Element Methods in Flow Problems, [Ed. by Oden J.T., Zienkiewicz O.C. et al], pp 57-66, UAH Press, Huntsville, 1974.

105 Kawahara M., Yoshimura N., Nakagawa K. and Ohsaka H., "Steady and Unsteady Finite Element Analysis of Incompressible Viscous Flow", Int. J. Numer Methods Eng, vol 10, pp 437-456, 1976.

106 Baker A.J., "Finite Element Solution Algorithm for Viscous Incompressible Fluid Dynamics", Int. J. Numer Meth. in Eng, vol 6, pp 89-101, 1973.

107 Baker A.J., "Research on a Finite Element Numerical Algorithm

for The Three Dimensional Navier Stokes Equations", USAF Tech Rept, AFWAL-TR-81, 1982.

108 Zienkiewicz O.C. and Godbole P.N., "Viscous Incompressible Flow with Special Reference to Non Newtonian (Plastic) Fluids", in R.H. Gallagher et al(Eds), Finite Elements in Fluids, vol 1 , Wiley-InterScience , London, pp 25-55, 1975.

109 Lohmeyer F., Vornberger O., Zeppenfeld K. and Vornberger A., "Parallel Flow Calculations on Transputers", Int. J. Num. Meth. Heat Fluid Flow, vol 1, pp 159-169, 1991.

110. Ghia U., Ghia K. N.and Shin C. T., "High-Resolutions for Incompressible Flow Using the Navier-Stokes Equations and a Multigrid Method", J. Comp. Phys., vol 48 , pp 387-411 , 1982.

111. Peyret R. and Taylor T.D., "Computational Methods for Fluid Flow", pp 199-207 , Springer-Verlag , New York , 1983 .

112. Guj G.and Stella F., "Numerical Solutions of High-Re Recirculating Flows in Vorticity - Velocity Form", Int. J. Numer Methods Fluids , vol 8 , pp 405-416 , 1988 .

113. Wang Y., He J. and Zhang B. Q., "A Calculation Procedure for Steady Two Dimensional Elliptic Flows", Int . J. Numer Methods Fluids , vol 9 , pp 609-617 , 1989 .

114. Perng C. Y. and Street R. L., "Three Dimensional Unsteady Flow Simulations : Alternative Strategies for Volume-Averaged Calculations", Int. J. Numer Methods Fluids, vol 9 , pp 341-362 , 1989 .

115. Peric M., "Efficient Semi-Implicitly Solving Algorithm for Nine-Diagonal Coefficient Matrix", Numerical Heat Transfer, vol 11, pp 251-279, 1987.

116. Abarbanel S.,Bennett S., Brandt A.and Gillis J., "Velocity Profiles of Flow at Low Reynolds Numbers", J. of Applied Mechanics , vol 37 , pp 2-4, 1970 .

117. Mohanty A. K. and Das R., "Laminar Flow in the Entrance Region of a Parallel Plate Channel", AIChE Journal , vol 28 , pp 830-833 , 1982 .

118. Wang Y.L. and Longwell P.A.,"Laminar Flow in the Inlet Section of Parallel Plates" , AIChE Journal , vol 10 , pp 323, 1964 .

119. Acrivos A., Snowden D.D., Grove A.S. and Petersen E.E.," The Steady Separated Flow Past a Circular Cylinder at Large Reynolds Number",J. Fluid Mech., vol 21, pp 737-760, 1965.

120. Shair F.H.,Grove A.S., Petersen E.E. and Acrivos A., " The Effect of Confining Walls on The Stability of The Steady Wake Behind a Circular Cylinder", J. Fluid Mech., vol 17, pp 546-550, 1963.

121. Thoman D.C. and Szewczyk A.A., "Time Dependent Viscous Flow Over a Circular Cylinder", The Physics of Fluids,Supplement II, vol 12, pp 76-87, 1969.

122. Song C.C.S and Yuan M., "Simulation of Vortex Shedding Flow About a Circular Cylinder at High Reynolds Numbers",J. Fluids Engineering (ASME) , vol 112, pp 155-164, 1990.

123. Van Dyke M., "An Album of Fluid Motion ", published by the Department of Mechanical Engineering , Stanford University, Stanford, California, USA, 1982.

124. Okajima A., "Strouhal Numbers of Rectangular Cylinders", J. Fluid Mech., vol 123, pp 379-398, 1982.

125. Okajıma A., Numerıcal Sımulatıon of Flow Around Rectangular Cylinders", J. Wind Engineering and Ind. Aerodynamics, vol 33, pp 171-180, 1990.

126. Kelkar K.M. and Patankar S.V., "Numerical Prediction of Vortex Shedding Behind a Square Cylinder", Int. J. Numer Methods Fluids, vol.14, pp 327-341, 1992.

127. Davis R.W., Moore E.F. and Purtell .P., "A Numerical and Experimental Study of Confined Flow Around Rectangular Cylinders", Phys. Fluids, vol 27, pp 46-59, 1984.

128. Baba N. and Miyata H., "Numerical Study of The 3D Separating Flow About Obstacles with Sharp Corners", Proceedings of 11th Int. Conf. on Num. Methods in Fluid Dynamics, ed. Dwoyer D. L., Hussaini M.Y.and Voigt R. G., pp 126-130, Springer-Verlag, Berlin-Heideberg, 1989.

129 Biswas G.,Laschefski H., Mitra N.K. and Fiebig M., "Numerical Investigation of Mixed Convection Heat Transfer in a Horizontal Channel with a Built-in Square Cylinder", Numerical Heat Transfer Part-A, vol 18, pp 173-188, 1990.

130. Brandt A., Dendy J.E. and Ruppel H.,"The Multigrid Method for Semi-Implicit Hydrodynamics Codes", J.Comp. Phys., vol. 34, pp 348-370, 1980.

131. Hirt C.W., Nichois B.D. and Romero N.C., "SOLA-A Numerical Solution Algorithm for Transient Fluid Flows", Los Alamos Scientific Lab. Rep. LA-5852, 1975.

132. Raithby G.D. and Torrance K.E., "Upstream-Weighted Schemes and Their Application to Elliptic Problems Involving Fluid Flow", Comp. Fluids, vol. 2, pp 191-206, 1974.

133. Runchal A.K. and Wolfstein M.,"Numerical Inte gration Procedure for the Steady State Navier-Stokes Equations", J. Mech. Engg. Sci., vol. 11, pp 445-452, 1969.

134. Kiehm P., Mitra N.K. and Fiebig M., "Numerical Investigation of Two- and Three- Dimensional Confined Wakes Behind a Circular Cylinder in a Channel", AIAA 24th Aerospace Sciences Meeting, Reno, Nevada, AIAA paper - 86 - 0035, 1986.

135. Patel V.A., "Time-Dependent Solutions of the Viscous Incompressible Flow Past a Circular Cylinder by the Method of Series Truncation", Comput Fluids, vol 4, pp 13-27, 1976.

136. Patel V.A., "Karman Vortex Street behind a Circular cylinder by the Series Truncation Method" Comp. Phys, vol 28, pp 14-42, 1978.

137. Lin, C.L., Pepper, W.W., and Lee, S.D., "Numerical Methods for Separated Flow Solutions Around a Circular cylinder", AIAA J., vol 14, pp 900-906, 1976.

138. Fornberg B., "A Numerical Study of Steady Viscous Flows Past a Circular Cylinder", J. Fluid Mech., vol 98, pp 819-855, 180.

139. Tuann S., and Olson M.D., "Numerical Studies of the Flow Around a Circular Cylinder by a Finite Element Method", Comput Fluids, vol 6, pp 219-240, 1978.

140. West G.S. and Apelt C.J., "The Effects of Tunnel Blockage and Aspect Ratio on the Mean Flow Past a Circular Cylinder with Reynolds Numbers between 10^4 and 10^5", J. Fluid. Mech., Vol 114, pp 361-377, 1982.

141. Coutanceau M. and Bouard R., "Experimental Determination of the Main Features of the Viscous Flow in the Wake of Circular

Cylinder in Uniform Translation. Part-1, Steady Flow", J.Fluid. Mech., vol 79, part 2, pp 231-256, 1977.

142 Coutanceau M. and Bouard R., "Experimental Determination of the Main Features of the Viscous Flow in the Wake of Circular Cylinder in Uniform Translation. Part-2. Unsteady Flow", J.Fluid. Mech., vol 79, part 2, pp 257-272, 1977.

143. Braza M., Chassaing P. and Ha-Minh, H., "Numerical Study and Physical Analysis of the Pressure and Velocity Fields in the Near Wake of a Circular Cylinder", J. Fluid. Mech., vol 165, pp 79-130, 1986.

144. Taneda S., "Experimental Investigation of Vortex Streets", J. Phys. Soc. Japan, Vol 20, pp 1714, 1965.

APPENDIX A

Table for CPU time required on CONVEX c 220 machine for erent flow problems dealt with in chapter 3 4 and 5

PROBLEM	GRID	TIME MONITORED FOR
Square Cavity Problem for Re = 100	21 x 21	steady state solr
square cavity problem for Re = 1000	21 x 21	steady state soln
Oblique cavity problem for Re = 1000	21 x 21	steady state soln
Developing flow in a channel for Re = 40	21 x 11	steady state soln
*Flow over square cylinder placed in a channel solved by EXTRA FLAG for Re = 450	97 x 33	one timestep calculation after stabilization of periodicity
*Flow over square cylinder placed in a channel solved by MAC method for Re = 450	200 x34	one timestep calculation after stabilization of periodicity
*Flow over circular cylinder placed in a channel solved by EXTRA FLAG for Re = 450	97 x 33	one timestep calculation after stabilization of periodicity

The current implementation of the EXTRA FLAG may lack in ization in terms of efficient use of skilled programming. The time and storage requirements are parameters which are very tive to the particular implementation of the algorithm. over, the transient problems fall in the category of impulsive which introduces spatial singularities in continuum or entrated imbalance of mass. Hence the first few time steps may up to several hundreds of 'continuity / pressure-velocity itions '. However, after a few time steps , the mass errors diffused in space and the number of continuity iterations goes to a few tens or even less.

use of uniform grid spacing and effective implementation of ogonality of space and the dependent variables reduce the cpu per time cycle as compared to a general solver which has to e all space variables for the entire domain. In fact, major lon of the excess time required by such solvers are used up ting particular variables in corresponding variable stacks.